# SEISMIC RETROFITTING OF REINFORCED CONCRETE BUILDINGS USING STEEL BRACES WITH SHEAR LINK

A THESIS SUBMITTED TO
THE GRADUATE SCHOOL OF NATURAL AND APPLIED SCIENCES
OF
MIDDLE EAST TECHNICAL UNIVERSITY

BY

CENGİZHAN DURUCAN

IN PARTIAL FULFILLMENT OF THE REQUIREMENTS
FOR
THE DEGREE OF MASTER OF SCIENCE
IN
ENGINEERING SCIENCES

SEPTEMBER 2009

Approval of the thesis:

**SEISMIC RETROFITTING OF REINFORCED CONCRETE BUILDINGS USING STEEL BRACES WITH SHEAR LINK**

submitted by **CENGİZHAN DURUCAN** in partial fulfillment of the requirements for the degree of **Master of Science in Engineering Sciences Department, Middle East Technical University** by,

Prof. Dr. Canan Özgen
Dean, **Graduate School of Natural and Applied Sciences** _____

Prof. Dr. Turgut Tokdemir
Head of Department, **Engineering Sciences** _____

Prof. Dr. Murat Dicleli
Supervisor, **Engineering Sciences Dept., METU** _____

**Examining Committee Members**

Prof. Dr. Turgut Tokdemir _____
Engineering Sciences Dept., METU

Prof. Dr. Murat Dicleli _____
Engineering Sciences Dept., METU

Prof. Dr. M. Polat Saka _____
Engineering Sciences Dept., METU

Assoc. Prof. Dr Ahmet Yakut _____
Civil Engineering Dept., METU

Assist. Prof. Dr. Ferhat Akgül _____
Engineering Sciences Dept., METU

**Date: 10.09.2009**

**I hereby declare that all information in this document has been obtained and presented in accordance with academic rules and ethical conduct. I also declare that, as required by these rules and conduct, I have fully cited and referenced all material and results that are not original to this work.**

Name, Last Name: Cengizhan DURUCAN

Signature:

## ABSTRACT

SEISMIC RETROFITTING OF REINFORCED CONCRETE BUILDINGS USING STEEL BRACES WITH SHEAR LINK

Durucan, Cengizhan
M.S., Deparment of Engineering Sciences
Supervisor: Prof. Dr. Murat Dicleli

September 2009, 194 pages

The catastrophic damage to the infrastructure due to the most recent major earthquakes around the world demonstrated the seismic vulnerability of many existing reinforced concrete buildings. Accordingly, this thesis is focused on a proposed seismic retrofitting system (PSRS) configured to upgrade the performance of seismically vulnerable reinforced concrete buildings. The proposed system is composed of a rigid steel frame with chevron braces and a conventional energy dissipating shear link. The retrofitting system is installed within the bays of a reinforced concrete building frame. A retrofitting design procedure using the proposed seismic retrofitting system is also developed as part of this study. The developed design methodology is based on performance-based design procedure. The retrofitting design procedure is configured to provide a uniform dissipation of earthquake input energy along the height of the reinforced concrete building. The PSRS and a conventional retrofitting system using squat infill shear panels are applied to an existing school and an office building. Nonlinear time history analyses of the buildings in the original and retrofitted conditions are conducted to assess the efficiency of the PSRS. The analyses results revealed that the PSRS can efficiently alleviate the detrimental effects of

earthquakes on the buildings. The building retrofitted with PSRS has a more stable lateral force-deformation behavior with enhanced energy dissipation capability than that of the one retrofitted with squat infill shear panels. For small intensity ground motions, the maximum inter-story drift of the building retrofitted with the PSRS is comparable to that of the one retrofitted with squat infill shear panels. But for moderate to high intensity ground motions, the maximum inter-story drift of the building retrofitted with the PSRS is considerably smaller than that of the one retrofitted with squat infill shear panels.

**Keywords:** Seismic retrofitting, reinforced concrete building, steel frame, steel braces, shear link, performance based design

# ÖZ

BETONARME BİNALARIN KESME BAĞLANTI ELEMENALI ÇELİK ÇUBUKLAR KULLANILARAK DEPREM GÜÇLENDİRMESİ

Durucan, Cengizhan
Yüksek Lisans, Mühendislik Bilimleri Bölümü
Tez Yöneticisi: Prof. Dr. Murat Dicleli

Eylül 2009, 194 sayfa

Yakın geçmişte gerçekleşen şiddetli depremlerin çeşitli ülkelerde altyapıya verdiği büyük zararlar, mevcut olan birçok betonarme binanın deprem etkilerine karşı olan korunmasızlığını ortaya çıkarmıştır. Buna bağlı olarak, bu tez çalışması deprem etkilerine karşı, mevcut zayıf betonarme binaların performansını iyileştirmek üzere yapılandırılmış bir sismik güçlendirme yöntemi üzerine odaklanmıştır. Önerilen yöntem, çelik bir çerçeve sistemi, çapraz çelik çubuklar ve klasik bir enerji sönümleyici olan kesme bağlantı elemanından oluşmaktadır. Önerilen sismik güçlendirme sistemi (ÖSGS) betonarme binanın açıklıkları içine yerleştirilerek uygulanır. Buna ek olarak, bu çalışma kapsamında, bir güçlendirme tasarım metodu da geliştirilmiştir. Geliştirilen tasarım metodu performansa dayalı tasarım esasına dayanmaktadır. Önerilen tasarım metodu, betonarme binaya etkiyen deprem enerjisinin bina yüksekliği boyunca düzgün biçimde sönümlenmesini sağlayacak şekilde yapılandırılmıştır. ÖSGS' nin yanısıra kısa dolgu kesme panellerinin kullanılmasıyla gerçekleştirilen klasik bir güçlendirme yöntemi de mevcut bir okul ve ofis binasına uygulanmıştır. ÖSGS' nin etkinliğini değerlendirmek amacıyla, binaların orjinal ve güçlendirilmiş halleri için doğrusal olmayan zaman tanım analizleri yapılmıştır. Analiz sonuçları, ÖSGS' nin

depremlerin binalar üzerindeki yıkıcı etkisini etkili şekilde azaltabileceğini göstermiştir. ÖSGS' yle güçlendirilen bina, kısa dolgu kesme panelleri kullanılarak klasik şekilde güçlendirilen binaya göre daha kararlı bir yanal kuvvet-deplasman davranışına ve arttırılmış enerji sönümleme kapasitesine sahiptir. ÖSGS' yle güçlendirilen ve kısa dolgu kesme panellerinin kullanılmasıyla klasik şekilde güçlendirilen binaların kat deplasmanları küçük şiddetteki yer hareketleri için karşılaştırılabilir seviyededir. Ancak, orta ve yüksek şiddetli yer hareketleri için, ÖSGS' yle güçlendirilen binaların kat deplasmanları, kısa dolgu kesme panellerinin kullanılmasıyla klasik şekilde güçlendirilen binaların kat deplasmanlarından çok daha küçüktür.

**Anahtar Kelimeler:** Sismik güçlendirme, betonarme bina, çelik çerçeve, çelik çubuklar, kesme bağlantı elemanı, performansa dayalı tasarım

## ACKNOWLEDGEMENTS

I would like to thank my supervisor Prof.Dr. Murat Dicleli for his precious help, invaluable suggestions and support throughout this study.

I also would like to thank my friends Memduh Karalar and Ali Salem-Milani for their technical support with the program ANSYS. In addition, I would like to thank my friends Mehmet Ali Erol, Refik Burak, Taymuş, Ayşe Ruşen Ünsal, Hüseyin Çelik and Hakan Bayrak for their encouragements and support.

Finally, I would like to thank my family for their unlimited moral support.

## TABLE OF CONTENTS

## LIST OF FIGURES

FIGURES

## LIST OF TABLES

TABLES

# CHAPTER 1

# INTRODUCTION

## 1.1 Introduction

The catastrophic damage to the infrastructure due to the most recent major earthquakes around the world demonstrated the seismic vulnerability of many existing buildings. The 1999 Kocaeli- Turkey and 2003 Bam-Iran earthquakes caused a total loss of over 100.000 lives due to building collapses while the one that occurred in Taiwan in 1999 caused the collapse of more than 50.000 buildings. These are the examples of severe earthquakes in recent years that resulted in extensive damage to the building stock and associated loss of lives. In many municipal areas around the world, the number of buildings designed and constructed using codes that are now known to provide inadequate safety are potential hazards. In such areas, the number of buildings constructed prior to 1980 greatly outnumbers those that are built according to the newer codes. Therefore, these structurally deficient buildings should be retrofitted to withstand the design level earthquakes in compliance with the modern building design codes. On the other hand, the financial impact of bringing older buildings up to the current code standards can be huge. If this action is not taken, however, the financial impact of the damage resulting from an earthquake can be even more devastating. For instance, the cost of damage to buildings caused by the Northridge earthquake was $15 billion and $7 billion for Loma Prieta (Beising, 2004). In order to prevent these economical losses and loss of lives, the seismic retrofitting of existing buildings is a clear necessity.

There are many well known seismic retrofitting methods for reinforced concrete structures. These methods can be classified mainly into two groups as; (i) conventional methods, based on improving the strength, stiffness and ductility of

the structure, (ii) innovative response modification methods which aim to reduce the effect of seismic forces on structures.

Conventional methods include techniques such as adding reinforced concrete shearwalls to the structure and jacketing of the reinforced concrete columns. The main advantage of these methods is that they can be easily designed and applied using conventional construction techniques. However, conventional methods have some serious technical and practical disadvantages. Strengthening the reinforced concrete columns and/or adding shearwalls results in an increase in the weight of the structure that produce larger earthquake forces. Furthermore, these methods require heavy demolition and construction work that restricts the use of the structure during the rehabilitation process. Innovative response modification methods include techniques such as installing seismic isolation devices to the base of the building or hysteretic, frictional and fluid viscous dampers to the structural framing system of the building. These devices are intended to modify the seismic response of the structure so as to alleviate the effect of the seismic forces acting on the building. Retrofitting methods based on response modification techniques have significant advantages with respect to the conventional seismic retrofitting methods. Response modification methods are very effective for reducing the detrimental effects of the earthquakes. In most cases, these methods do not require heavy demolition or construction work. Nevertheless, these methods also have some economical and practical disadvantages. Their implementation is generally costly. This makes them unsuitable for most cases. Also, in the case of the seismic base isolation technique, a serious modification to the pipe and gas line of the rehabilitated structure has to be made. These modifications are required to allow for large displacements at the foundation level without causing any damage to the pipe and gas lines so as to prevent fire and other hazardous events. Furthermore, most practicing engineers currently lack adequate experience to effectively perform the design of buildings using response modification devices.

In light of the above discussion, it is clear that in addition to the advantages of each retrofitting method, there are numerous disadvantages. Consequently, a

novel seismic retrofitting system that combines the advantages of both conventional and modern retrofitting techniques is required.

Accordingly, this thesis is focused on a proposed efficient energy dissipating steel panel configured to upgrade the performance of seismically vulnerable reinforced concrete buildings by combining the advantages and eliminating most of the disadvantages of conventional and modern response modification retrofitting techniques. The proposed system is composed of a rigid rectangular steel frame with chevron braces and a conventional energy dissipating shear element connected between the braces and the frame. The shear element is designed to yield in shear under the effect of the horizontal components of the brace axial forces before the compression brace buckles. The steel panel is installed within the bay of a reinforced concrete building frame to enhance the stiffness, strength and ductility of the structure. A retrofitting design procedure using the proposed retrofitting technique is also developed as part of this study. The developed design methodology is based on performance based design procedure. The retrofitting design procedure is configured to provide a uniform dissipation of the earthquake input energy along the height of the reinforced concrete building. Furthermore, the performance of two existing reinforced concrete buildings retrofitted using the proposed methodology and a conventional technique involving reinforced concrete shear panels (squat infill shear walls) is also compared as part of this study.

## 1.2 Research Objectives and Scope

The main objective of the proposed research study is to develop an efficient seismic retrofitting technique for reinforced concrete buildings that combine the advantages of both conventional and modern response modification seismic retrofitting techniques.

## 1.3 Thesis Outline

The first chapter of the thesis contains introductory information as well as literature search results on the seismic retrofitting of reinforced concrete buildings.

Chapter two introduces the proposed retrofitting system and contains information about the finite element analyses of a sample, two stories, one bay reinforced concrete frame retrofitted with various configurations of the proposed retrofitting system to study the stress distribution within the reinforced concrete frame members for each panel configuration. From the finite element analyses results the most efficient steel panel configuration is selected for the retrofitting study.

The third chapter contains technical information about two existing reinforced concrete buildings used in this study.

Chapter four describes the development of the site specific response spectra and the selection of appropriate ground motion data for non-linear time history (NLTH) analyses.

Chapter five provides detailed information about the nonlinear structural modeling for the seismic performance assessment of the two buildings used in this study. The structural modeling described in this chapter provides detailed information about the numerical simulation of the non-linear behavior of the beams, columns, brick masonry walls, squat infill shear walls and the nonlinear structural modeling of the steel panels for the seismic performance assessment of the retrofitted buildings. Information about the selected material models that is, concrete, steel and brick, to simulate these nonlinear behaviors is also provided in this chapter.

Chapter six provides information about the retrofitting scheme and the performance based retrofitting design approach.

In Chapter seven, the analyses results for the first building is presented.

Chapter eight presents the analyses results for the second building.

Chapter nine presents a brief summary and conclusions deduced from this research study.

## 1.4 Literature Review

As stated earlier, the main objective of this study is to develop a seismic retrofitting technique which combines the advantages of both conventional and response modification retrofitting techniques. Accordingly, in the following subsections, results of literature review on conventional and innovative seismic retrofitting techniques including those based on response modification is presented.

### 1.4.1. Innovative Seismic Retrofitting Techniques

Innovative seismic retrofitting techniques include those based on modifying the seismic response of the structure as well as those based on enhancing the strength and ductility of the reinforced concrete members. Response modification devices primarily reduce the effect of seismic forces acting on the buildings. Examples of seismic retrofitting techniques based on response modification are seismic base isolation and/or damping devices used within the building's structural system. Some examples of innovative seismic retrofitting techniques based on enhancing the strength and ductility of the reinforced concrete members are carbon fiber reinforced polymer (CFRP) or glass fiber reinforced polymer (GFRP) applications. Innovative seismic retrofitting techniques are more effective with respect to the conventional techniques for enhancing the structural performance of buildings. In general, these techniques will be most applicable to the rehabilitation of buildings whose owners desire superior seismic performance and can afford the higher costs associated with the fabrication and installation of seismic isolators

and/or energy dissipation devices as well as CFRP or GFRP material. Seismic isolation and energy dissipation systems are relatively new and involve sophisticated concepts that require more extensive design and detailed analysis than most conventional rehabilitation schemes do (FEMA-273, 1997). Currently, the lack of common engineering experience in implementing and designing these devices make their application more limited compared to that of conventional retrofitting techniques (Dicleli and Mehta, 2009) A summary of innovative seismic retrofitting techniques is given below.

#### 1.4.1.1. Seismic Base Isolation Techniques

Seismic isolation is a response modification technique that is based on yielding of devices called isolators generally installed between the columns and the foundations at the base of the building. The concept of seismic isolation in buildings is simple. The building is decoupled from the horizontal components of the ground motion by interposing seismic isolators, which have very low horizontal stiffness, at the base of the building. Thus, when the building is subjected to seismic forces, most of the deformation occurs in the isolators rather than in the building as shown in Figure 1.1. This reduces the seismic force and displacement demand on the structural members of the building. A seismic isolator possesses the following three basic features to function properly (i) flexibility to lengthen the period of vibration of the building sufficiently to reduce the seismic force demands, (ii) a built-in energy dissipation mechanism to limit the relative displacement of the isolator, (iii) sufficient rigidity under service load (e.g. wind) levels to limit the vibration of the structure (Dicleli et al, 2004). The low horizontal stiffness of the seismic isolator provides the structure with a fundamental period that is much longer than its original fundamental period without the seismic isolation and the predominant periods of the ground motion. Thus, the earthquake-input energy is deflected by the isolation system and the seismic forces are reduced.

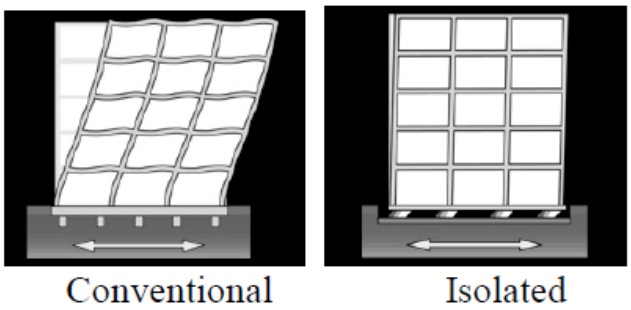


**Figure 1.1** Behavior of base isolated and fixed base buildings

Several retrofitting applications using the seismic base isolation technology exist in the USA, Japan, New Zealand and Italy. The historic San Francisco City Hall in California, USA, which is an outstanding example of classical architecture, was seismically retrofitted in 1998 with lead rubber seismic isolation bearings (Chopra, 2001). The National Museum in New Zealand was retrofitted with 146 lead rubber seismic isolation bearings and 36 Teflon$^{(R)}$ pads (Tezcan and Cimilli, 2002). The historical Utah State Capitol in Salt Lake City is a monumental building which was retrofitted in 2007 using seismic isolation technology. Another example of seismic retrofitting application in the state of Utah in USA is the historical city hall building. This historical masonry building was retrofitted using 208 lead rubber and 239 laminated elastomeric bearings. The U.S. Court of Appeals building in San Francisco (Amin and Mokha, 1995), the Hayward City Hall and the International Terminal of the San Francisco Airport in California, USA were all retrofitted using friction pendulum seismic isolation bearings. Matsumura-Gumi Technical research institute in Japan was seismically retrofitted with high damping natural rubber seismic isolation bearings in 1989(Tezcan and Cimilli, 2002). Administrative building of the Ministry of Defense of Italy in Ancona was seismically retrofitted with high damping rubber seismic isolation bearings in 2000 (Tezcan and Cimilli, 2002). From the review of literature on the seismic retrofitting applications using seismic isolation technology, it is observed that the majority of the retrofitting applications are mainly for important governmental or historical buildings such as museums, airports, city halls and

capitols etc. Special costs associated with the design, fabrication, and installation of seismic isolators limits the use of seismic base isolation technology for ordinary buildings.

#### 1.4.1.2. Passive Energy Dissipating Techniques

Damping is one of many different methods that have been proposed for a structure to achieve optimal performance when it is subjected to seismic forces. Normally, a structure defers the earthquake effects through a combination of strength, flexibility, deformability and energy absorption. The level of damping in a conventional structure is very low, and hence the amount of energy dissipated through damping is also very low. Thus, during strong ground motions, conventional structures usually deform well beyond their elastic limits to absorb the earthquake input energy and remain intact only due to their ability to inelastically deform. Therefore, most of the earthquake input energy is absorbed by the structure itself through localized damage. A damper is an element which can be added to a system to provide forces which are resistive to motion, thus providing a means of energy dissipation. Thus, the concept of added-on dampers within a structure assumes that some of the earthquake energy input into the structure will be absorbed, not by the structure itself, but rather by supplemental damping devices. An idealized supplemental damper would be of a form such that the force being produced by the damper is of such a magnitude and occurs at such a time that the damper forces do not increase the overall stresses in the structure. Properly implemented, an ideal damper should be able to simultaneously reduce both stress and deflection in the structure. There are four basic types of damping devices: viscoelastic, friction, metallic and viscous.

A number of retrofitting applications using damping devices exist in USA and Canada. The Boeing Commercial Airplane Factory in Everett, WA, USA is the world's largest building in volume that was seismically retrofitted with friction dampers in 1996 (Pall et al. 2004). Headquarters of the Canadian Space Agency is a building of national importance. It contains extremely sensitive and costly

equipment. Friction dampers were also used in the seismic retrofitting of this structure in 1992 (Pall et al. 2004). Justice Headquarters in Ottawa, Canada was seismically retrofitted with friction dampers in 1997 (Balazic et al. 2000). Casino de Montreal in Canada that was retrofitted in 1993 is another example of seismically retrofitted buildings with friction dampers. Los Angeles City Hall (Taylor, 2002), Oakland Bay Bridge (Heninger et al. 2003) and San Francisco International Airport that were retrofitted in 1999 are important examples of fluid viscous dampers applications for the seismic retrofit of various structures (Tezcan and Erkal, 2002). From the review of literature on the seismic retrofitting applications using energy dissipation devices (dampers), it is observed that the majority of the retrofitting applications are mainly for important governmental or historical buildings, buildings housing sensitive equipment or major bridges. Higher costs associated with the design, fabrication, and installation of energy dissipation devices limit the use of this technology for ordinary buildings.

#### 1.4.1.4. Fiber Reinforced Polymer

Advanced composite materials such as carbon fiber reinforced polymer (CFRP) is much stronger and lighter than steel. A close up picture of CFRP is demonstrated in Figure 1.2

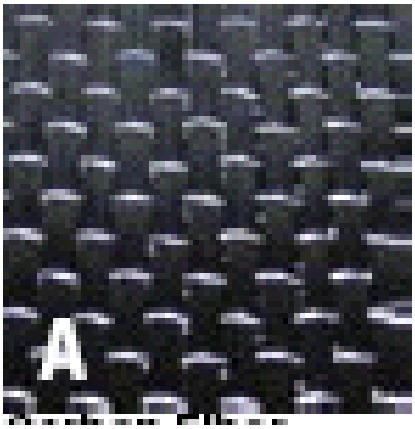


**Figure 1.2** Close up picture of CFRP

Analytical and experimental results have shown that, wrapping structural components (such as columns, beams and walls) with CFRP sheets improve their strength and ductility without adding stiffness to the elements (Ehsani and . Saadatmanesh, 1997; Paterson and Mitchell, 2003; Chang et al, 2004; Chagnon and Massicotte, 2005). The high modulus of elasticity and strength of CFRP makes it suitable for applications as confinement for reinforced concrete columns to enhance their axial strength and ductility. Federal Building in Port Alberni, Canada, a reinforced concrete structure, was built in 1960. Port Alberni is situated in one of the highest seismic zones of Canada. As the columns had adequate shear strength but were weak in flexural strength, the columns were wrapped full-height with one ply of CFRP. The Port Alberni Federal Building was the first application of CFRP for the seismic upgrade of reinforced concrete columns in western Canada (Foo et al. 1996). Ibach Bridge in Lucerne, Switzerland was retrofitted with CFRP in 1991 (Meier 1995) and a highway bridge in Dusseldorf was constructed in 1987 by using GFRP (Clark, 1988). The material cost of FRP systems is relatively high compared to most conventional construction materials (Aboutaha, 2001). Retrofitting with FRP is an expensive way of seismically upgrading buildings. (Aboutaha, 2001). Thus this method is not suitable for seismic retrofitting of ordinary structures such as residential buildings.

### 1.4.2 Conventional Retrofitting Techniques

Conventional seismic design approach intends to dissipate energy under earthquake excitations via the inelastic cyclic deformation of structural components of a building. In this approach, the energy dissipation is usually concentrated at the beam ends where weak beam strong columns approach is used (Rocha et al. 2004). Buildings with inadequate seismic capacity are usually not capable of dissipating such energy. Accordingly, conventional seismic rehabilitation methods mainly focus on upgrading the strength and ductility of the structural system of a building. Conventional rehabilitation of structures can be provided by local and global retrofitting of the lateral load carrying system

(Frosch, 2005; Tankut, 2008 Jirsa, 2006). Local retrofitting is generally used if the number of members to be retrofitted is limited and the structure's drift requirements are satisfied. Global retrofitting methods are generally used when retrofitting of a few members of the building may not be an adequate stand-alone solution particularly due to the structure having insufficient stiffness to satisfy code mandated drift requirements. In such cases, increasing the lateral stiffness of the structure by introducing shear walls or steel braces into the structural system offers a practical solution (Anıl and Altın, 2007). In some cases both local and global retrofitting methods are used together to enhance the seismic performance of a building.

#### 1.4.2.1 Local Retrofitting Techniques

Strengthening of deficient columns is one of the widely accepted techniques used to enhance the seismic performance of moment resisting reinforced concrete frames (Endo et al. 1984). Some conventional techniques of column strengthening, such as concrete jacketing (Bett et al. 1988, Rodriguez and Park, 1994, Abdullah and Takiguchi, 2003) and steel jacketing (Sakino and Ishibashi 1985, Chai et al. 1990, Aboutaha et al. 1999) are available in the literature. Figure 1.3 shows an original and a reinforced concrete jacketed column section. Jacketing with reinforced concrete layers increases the axial and shear load capacity of the columns. Also the flexural capacity can be increased by this method but, it is not an easy process due to the necessity of providing continuity of the longitudinal bars (Tankut, 2008). Providing sufficient bond between the old and new concrete is an important aspect of column retrofitting by concrete jacketing (Julio et al. 2004).

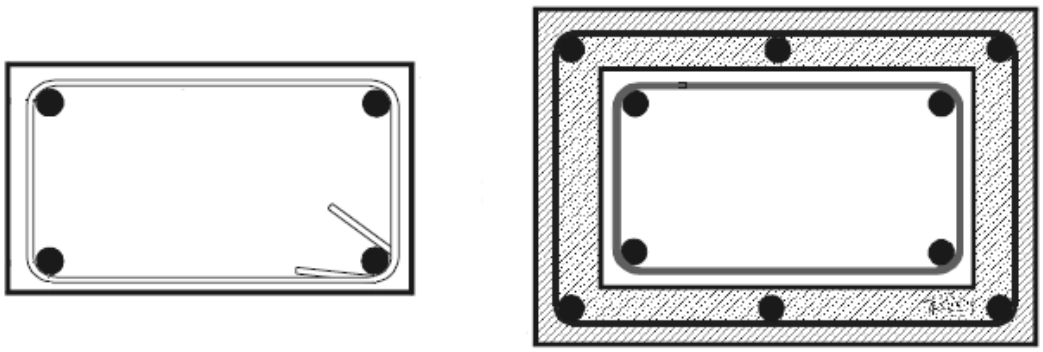

**Figure 1.3** Original and R.C. jacketed column sections

Using steel angles at each corner of a column and connecting these angles with bracing members is another local retrofitting method (Tankut, 2008). This method is generally effective for increasing the axial and shear load capacity of the columns. However, this method is not effective for increasing the flexural capacity of the columns due to the difficulty of providing continuity of the longitudinal steel angles at the corners.

Each strengthening technique has its own advantages and limitations depending on practicability, cost-effectiveness, minimal reduction in useable floor area, and effectiveness in enhancing the desired structural properties (Dipti and Durgesh, 2009). It is a well known fact that the success of the seismic retrofitting with column jacketing technique is dependent on the monolithic behavior of the composite element. (Julip et al. 2003; Bass et al. 1989; Julio et al. 2004). The common practice to achieve this monolithic behavior consists of increasing the roughness of the interface surface and applying a bonding agent. (Alcocer, 1993; Julio et al. 2004). Steel connectors are also occasionally applied to provide this monolithic behavior. (Julio et al. 2004). These construction steps involve specialized workmanship, formwork, time and cost. In summary, long construction times during seismic retrofitting, difficulty of the construction methods and increasing the member sizes by column jacketing are among the significant disadvantages of the local seismic retrofitting techniques (Naderzadeh and Moinfar, 2004; Kelly, 1986; Soong and Dargush, 1997).

#### 1.4.2.2 Global Retrofitting Techniques

Generally global level retrofitting is applied when the entire structural lateral load resisting system is deemed to be deficient. (Thermou and Elnashai. 2005) Adding shear walls, infill walls, steel bracings and wall thickening are the examples of global conventional seismic retrofitting techniques. (Thermou and Elnashai, 2005; Jirsa, 2006) Reinforced concrete shear walls are used to eliminate stiffness eccentricities in a building or to increase the lateral load carrying capacity. The newly added shear walls are usually located within the outer perimeter of the structure thereby reducing interior interference (Jirsa, 2006). However, in some cases, the presence of many windows around the building may create a problem in retrofitting applications with shear walls. Generally, the shear wall reinforcement is made continuous over the height of the building. Holes are bored into the beam or slab to allow for the continuity of the longitudinal reinforcement and to improve the force transfer between the wall and the beam/slab interface (Jirsa, 2006). Reinforced concrete frame of the buildings can also be retrofitted with concrete infill shear panels to increase the lateral strength and stiffness of the structure (Phan et al. 1993; Frosch, 2005; Jirsa, 2006). Rigid infill shear panels act primarily as squat shear walls where pinching and strength degradation of such systems may cause significant disadvantages from the performance point of view (Mansour and Hsu, 2005). Because of the relative rigidity of the infilled bays, the demand on the existing frame is substantially reduced (Phan et al. 1993). This is especially true for buildings with rigid diaphragms (Building Seismic Safety Council, 1992). The advantage of using infill shear panels instead of shear walls is that the continuity of the longitudinal reinforcement throughout the height of the building is not required in the case of the infill shear panels. Figure 1.4 shows the construction of cast in place infill shear panels (Thermou and Elnashai, 2005).

A major drawback of the seismic rehabilitation by adding shear walls or panels is the need for integrating the shear walls/panels with the rest of the structure. (Thermou and Elnashai, 2005). The need for strengthening the existing

foundations to resist the increased overturning moment is another significant drawback of seismic rehabilitation by adding shear walls (Bai, 2003; Thermou and Elnashai, 2005; Frosch, 2005; Pincheira and Jirsa, 2005). Foundation intervention is usually costly and quite disruptive, thus rendering the application of this technique unsuitable for buildings without an existing adequate foundation system (Thermou and Elnashai, 2005; Frosch, 2005). Additionally, the shear wall/panel can obstruct the functional use of the building by impeding access and functional circulation (Binici and Özcebe, 2005; Frosch, 2005). The additional weight of the shear walls/panels added to the weight of the structure is another drawback of retrofitting with shear walls/panels,

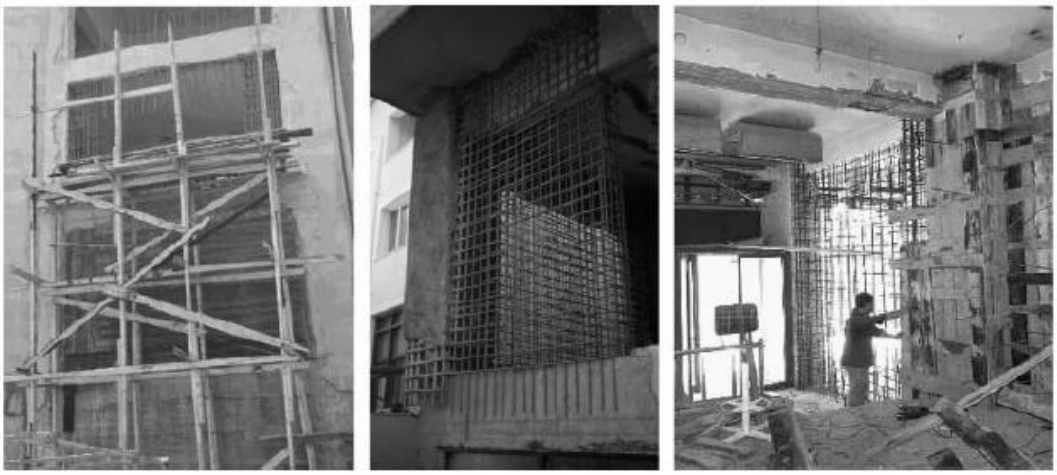

**Figure 1.4** Typical cast in place infill panel

### 1.4.2.3. Steel Bracing Techniques

Concentrically braced frames are among the most efficient structural steel systems for resisting lateral forces because of the complete truss action provided by the frame configuration (Dicleli and Mehta, 2009). Consequently, steel bracings are also used for seismic retrofitting of reinforced concrete buildings. Applications of steel bracing for the seismic retrofitting of ordinary reinforced concrete structures

can be found in the literature. Some applications of steel braces to the seismic retrofitting of regular reinforced concrete structures are the Zaragoza Hospital in Mexico City, (Badoux et al. 1990) and a school in Japan (Kawamata et al. 1980) Nevertheless, very little is known about the effectiveness of steel braces for improving the seismic performance of reinforced concrete structures (Maheri et al. 1997). However, it is a known fact that when subjected to strong ground motions, the buckling of the braces results in a loss of lateral stiffness and strength of the structural system (Dicleli and Mehta, 2009; Khatib et al. 1988). It may also be difficult to achieve well-distributed ductility demands along the height of the retrofitted structure due to the premature buckling of the braces at certain floor levels resulting in soft-story formations, dynamic instability, and hence substantial damage to the reinforced concrete frame members (Tremblay et al. 1996). A buckled bracing system and its hysteretic load-deformation curve are given in Figure 1.5 (a) and 1.5 (b) (Bruneau et al. 1998). The strength and stiffness degradation associated with brace buckling is clearly observed from the figure. Thus, seismic retrofitting of reinforced concrete buildings with braces that may potentially buckle does not seem to be a feasible retrofitting solution. To prevent poor performance characteristics associated with buckling, buckling restrained braces have been developed and are commercially available in the market (Andrews et al. 2009; Victoria and Larry, 2009). Nonetheless, these special braces are categorized as hysteretic dampers (Pollino and Bruneau, 2007). These braces are expensive to use in retrofitting applications of ordinary buildings.

(a)

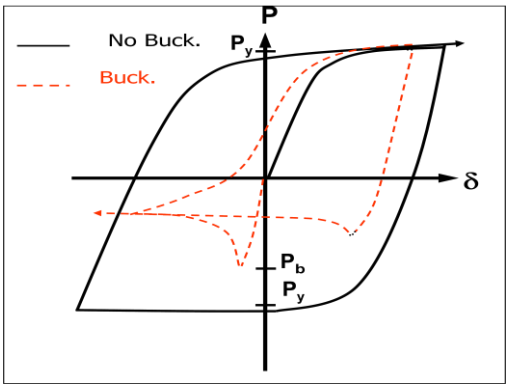


(b)

**Figure 1.5** A buckled CBF and Hysteresis Loop

### 1.4.3. Evaluation of Seismic Retrofitting Techniques

From the review of literature on the innovative response modification and conventional seismic retrofitting techniques, it is clear that, in addition to the advantages of each seismic retrofitting technique, there are numerous disadvantages. As stated earlier, innovative seismic retrofitting techniques which include the application of seismic base isolation technology, energy dissipation devices (dampers) and FRP are too expensive to use for seismic retrofitting of ordinary buildings especially in developing countries (Ahmad et al. 2009; Meftah et al. 2007). Accordingly, response modification technology is applied almost entirely to historical, large and expensive buildings or buildings housing sensitive

internal equipments such as computer centers, chip fabrication factories, emergency operation centers, hospitals, airports, museums, city halls, capitols and so on. In order to apply the advanced technology of response modification techniques in poor countries or in low-cost buildings, a further study for reducing the cost must be carried out (Moon et al. 2002). Conventional seismic retrofitting methods may be used to mitigate the risk that currently exists for seismically vulnerable reinforced concrete structures. Some of these methods are; addition of shear walls or steel braces, column jacketing for weak column strong beam frames and steel jackets for overcoming problems related to poor detailing of reinforcement splice or anchorage in reinforced concrete members (Jirsa, 2006). However, most of these retrofitting methods lead to heavy demolition, lengthy construction time, reconstruction, and occupant relocation (Kelly, 1986; Soong and Dargush, 1997; ATC-17, 1986).

Consequently, a seismic retrofitting system with a philosophy that will concentrate on combining the advantages of both conventional and modern response modification seismic retrofitting techniques is proposed in this thesis.

# CHAPTER 2

# THE PROPOSED RETROFITTING SYSTEM

## 2.1 Introduction

Concentrically braced frames are among the most efficient structural steel systems for resisting lateral forces because of the complete truss action provided by the frame configuration (Dicleli and Mehta 2009). Consequently, steel bracings are also used for seismic retrofitting of reinforced concrete buildings. However, it is a known fact that when subjected to strong ground motions, the buckling of the braces results in loss of lateral stiffness and strength of the structural system (Dicleli and Mehta 2009; Khatib et al. 1988). Thus, seismic retrofitting of reinforced concrete buildings with braces that may potentially buckle does not seem to be a feasible retrofitting solution. Hence, this research study is focused on a proposed braced retrofitting system that is capable of dissipating the earthquake input energy without buckling of the braces. The proposed system is composed of chevron braces and a conventional energy dissipating shear link connected between the braces and the beam (either a steel collector beam connected to the reinforced concrete beam or the reinforced concrete beam itself). Figure 2.1 shows the proposed retrofitting system. Figure 2.2 shows a recent (July 2009) application of the proposed retrofitting system to one of the buildings used in this research study. The shear link is designed to yield in shear under the effect of the horizontal components of the brace axial forces before the compression brace buckles. It is built using a compact steel HP section. HP sections are composed of stocky plates and are generally used for piles due to their ability to sustain high axial impact loads during pile driving. Accordingly, such sections are capable of undergoing large inelastic deformations, as was validated by an earlier research study (Dicleli and Albhaisi, 2004). For seismic retrofitting of reinforced concrete buildings, the proposed system is inserted into the bays of reinforced

concrete frames to improve the stiffness, strength and energy dissipation capacity of the building.

This chapter contains information about the design methodology of the proposed retrofitting system as well as the finite element analyses of a sample, two stories, one bay reinforced concrete frame retrofitted with various configurations of the proposed retrofitting system to study the stress distribution within the reinforced concrete frame members for each configuration. From the finite element analyses results the most efficient configuration is selected for the retrofitting study. The finite element analyses are conducted by using the nonlinear finite element based software ANSYS ver. 10.0. (2009)

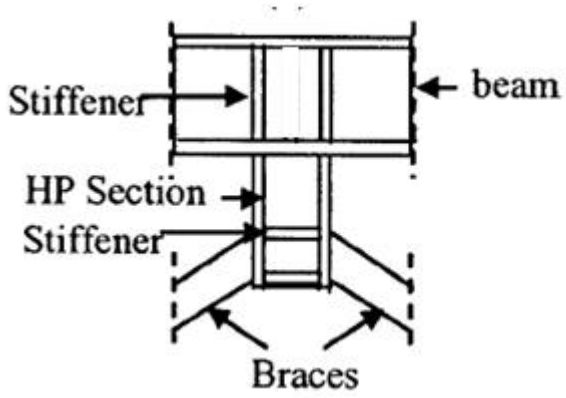


**Figure 2.1** Details of the shear element connections in the proposed retrofitting system (Dicleli and Mehta, 2009).

**Figure 2.2** A recent application of the proposed retrofitting system to Halkbank Eskişehir branch office building

## 2.2 Design Methodology of the Proposed Seismic Retrofitting System

The design methodology of the proposed retrofitting system is taken from Dicleli and Mehta (2009). In the proposed retrofitting system composed of braces and a shear link, the buckling instability of the braces is prevented to achieve a more stable lateral force-deformation behavior of the building and to avoid damage to the braces and other structural members. The buckling instability of the braces is prevented by allowing the shear link to yield in shear before the compression brace buckles. In the shear link, the shear force created by the horizontal components of the brace axial forces is constant along its length. This allows for the development of large plastic deformations without the development of excessive local strains that normally occurs in flexural yielding (Bruneau et al. 1998). Consequently, shear yielding provides more effective energy dissipation than that of flexural yielding (Kasai and Popov, 1986 (a)) and hence, it is adopted for the design of the shear link in the proposed retrofitting method. At the verge of buckling instability of the compression brace, the axial tensile and compressive forces in the tension and compression braces are both equal to the buckling load, $P_b$. Consequently, to prevent buckling instability of the compression brace, the shear link is designed to have a shear capacity, $V_y$, less than twice the horizontal component of the buckling load of the braces (Figure 2.3). Thus;

$$\varphi_s V_y \leq 2P_b \cos\alpha \tag{2.1}$$

In the above equation, $\alpha$ is the angle that the chevron braces make with the horizontal, $\varphi_s$ is an over-strength factor to account for the variations in material strength and strain hardening effect for the shear link and $V_y$ is expressed as (AISC-LRFD, 2001);

$$V_y = 0.6F_y d_w t_w \tag{2.2}$$

where $F_y$ is the yield strength of steel, and $d_w$ and $t_w$ are the depth and thickness of the web.

Furthermore, the length, $h_s$, of the shear link needs to be determined such that yielding occurs in shear before its plastic moment capacity, $M_p$, is reached. For the calculation of $h_s$, a rectangular $V_y$-$M_p$ interaction is assumed based on the experimental test results of Kasai and Popov (1986 (a)). Thus, neglecting the strain hardening effect, the length of the cantilever shear link must be smaller than $M_p/V_y$ to ensure shear yielding. However, due to strain hardening effect, the shear link's plastic base moment, $M_p$, and shear, $V_y$, may increase. The increase in $M_p$ and $V_y$ is accompanied by large flange strains that may result in premature failure of the welded shear link-beam connection due to low cycle fatigue effects. To prevent such a premature failure, an upper bound of $1.2M_p$ and a corresponding shear of $1.5V_y$ have been suggested by Kasai and Popov (1986). Thus;

$$h_s < \frac{1.2M_p}{1.5V_y} = 0.8\frac{M_p}{V_y} \tag{2.3}$$

Designing the shear link based on the above equations will ensure a more efficient energy dissipation based on shear rather than flexural yielding and a more satisfactory performance of the proposed retrofitting system without global buckling instability of the braces.

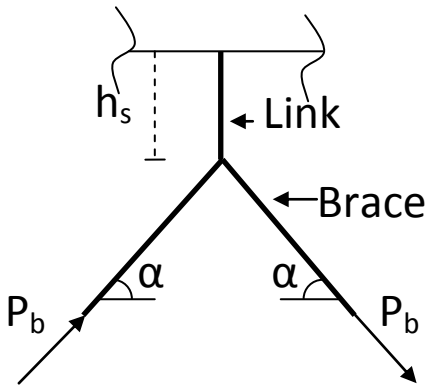


**Figure 2.3** Determination of shear link length

## 2.3 Application of the Proposed Retrofitting System with Various Configurations

The proposed system can be applied in various configurations where (i) the link and the braces are directly connected to the reinforced concrete members via steel plates, bolts and epoxy grouting as shown in Figure 2.4 (a) (Configuration 1), (ii) the link is connected to a collector steel beam attached to the concrete beam and the rest of the members are connected to the reinforced concrete members via steel plates as shown in Figure 2.4 (b) (Configuration 2), (iii) the link and the braces are housed in a steel frame system (steel panel) where the steel frame is connected to the reinforced concrete members by steel bolts and epoxy grouting as shown in Figure 2.4 (c) (Configuration 3).

In the subsequent sections finite element modeling and analyses results for the three configurations introduced above are presented. From the analyses results, the most efficient retrofitting configuration is selected.

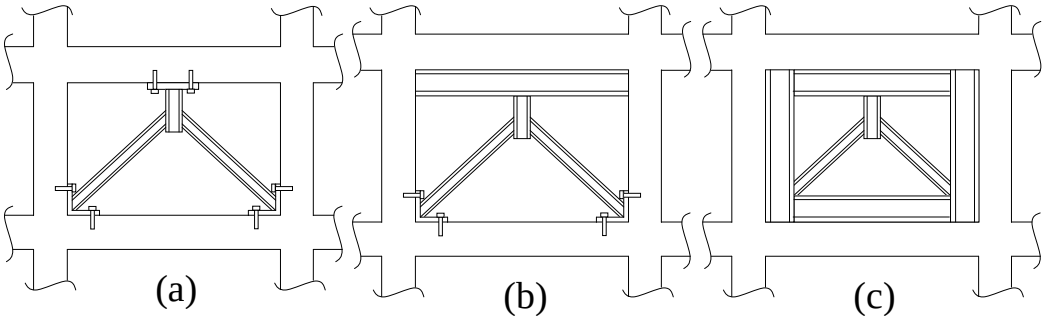


**Figure 2.4** Various configurations of proposed seismic retrofitting system in the reinforced concrete frame (a) Configuration 1, (b) Configuration 2, (c) Configuration 3

## 2.4 Details of the Sample Reinforced Concrete Frame and the Proposed Retrofitting System

This subsection contains information about the details of a two stories, one bay reinforced concrete frame retrofitted with various configurations of the proposed seismic retrofitting system. This frame is used to choose the most efficient configuration of the proposed retrofitting system from the finite element analyses results presented later.

The aforementioned reinforced concrete frame is extracted from the office building used in this study. The dimensions of the structural members of the frame are slightly modified to accommodate the steel retrofitting system configurations used in finite element analyses. Furthermore, a more common 20 Mpa concrete strength is assumed for the frame. An elevation plot of the frame is shown in Figure 2.5. The dimensions of the rectangular columns on the left and right sides of the frame are respectively 0.3 m × 0.6 m and 0.4 m × 0.25 m at the first story level and 0.25 m × 0.40 m and 0.40 m × 0.25 m at the second story level. The beams at both story levels have identical cross sections of 0.25 m× 0.5 m (width×

depth). The dimensions of the steel members used in the proposed retrofitting system of the sample frame are given in Table 2.1.

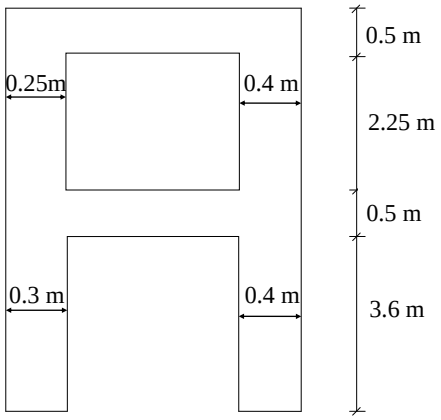


**Figure 2.5** Member sizes of the sample two story one bay reinforced concrete frame

**Table 2.1** Properties of the steel retrofitting system

| Story | Sections | | |
|---|---|---|---|
| | **Shear Link** | **Braces** | **Frame** |
| **1** | HE200M | HE120M | HE220B |
| **2** | HE180M | HE100M | HE220B |

## 2.5 ANSYS Modeling of the Retrofitted Sample Frame

The finite element modeling details of the one bay, two stories reinforced concrete sample frame retrofitted with the proposed seismic retrofitting system are presented in this subsection. The finite element models of the reinforced concrete frame were built in two different levels of complexity. The first set of models is two dimensional while the second set are three dimensional solid linear elastic models. The two dimensional models are built to observe the global distribution

of flexural and shear stresses within the reinforced concrete members of the frame and to assess the stiffness and strength (the strength at the verge of shear link yielding) of the frame associated with the three retrofitting configurations tested as part of this study. The more complicated solid models are used to observe the stress distribution within critical regions of the reinforced concrete frame around the link and at the corners where braces are connected to.

### 2.5.1 Two Dimensional Modeling

Two dimensional (2-D) finite element models of the reinforced concrete frame were built using the nonlinear finite element based software ANSYS (2009). Two different beam elements were used in the finite element modeling of the frame. The reinforced concrete frame members as well as the shear link and steel frame members of the retrofitting system were modeled using the BEAM189 element. In the case of the steel braces of the retrofitting system, BEAM44 is used to account for the moment releases at the ends of the steel braces. In the ANSYS (2009) modeling of the frame, key-points (nodal points) are introduced at the locations where the steel retrofitting system is connected to the reinforced concrete frame by bolts and epoxy grouting (Figure 2.6 (a) and (b)). The mesh sizes of the BEAM189 members connected between the key-points are set equal to the bolt spacing. The rigid joints of the reinforced concrete frame were also modeled using BEAM189 with a large modulus of elasticity. The finite element models of the reinforced concrete frames for the three retrofitting configurations employed in this study are shown in Figure 2.7.

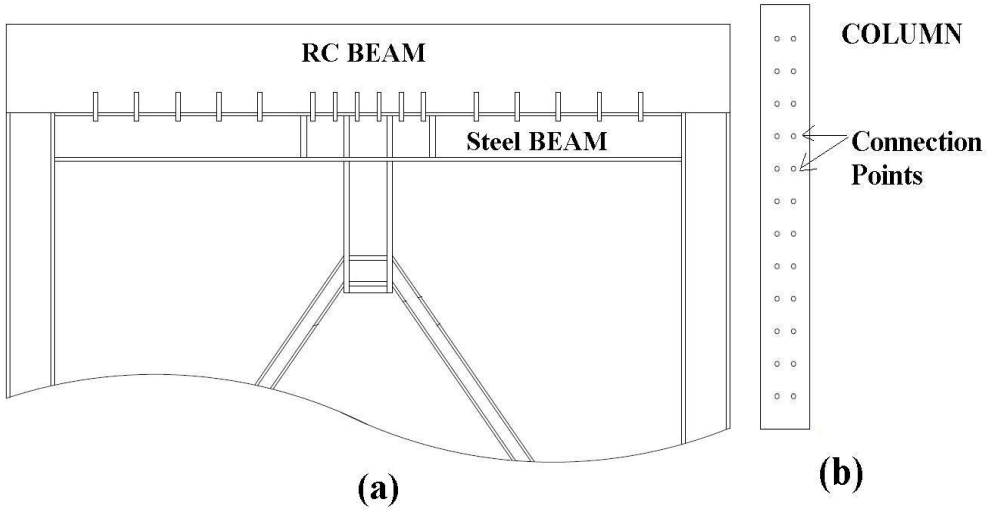


**Figure 2.6** Connection details of the steel and reinforced concrete elements (a) for beam connections, (b) for column connections

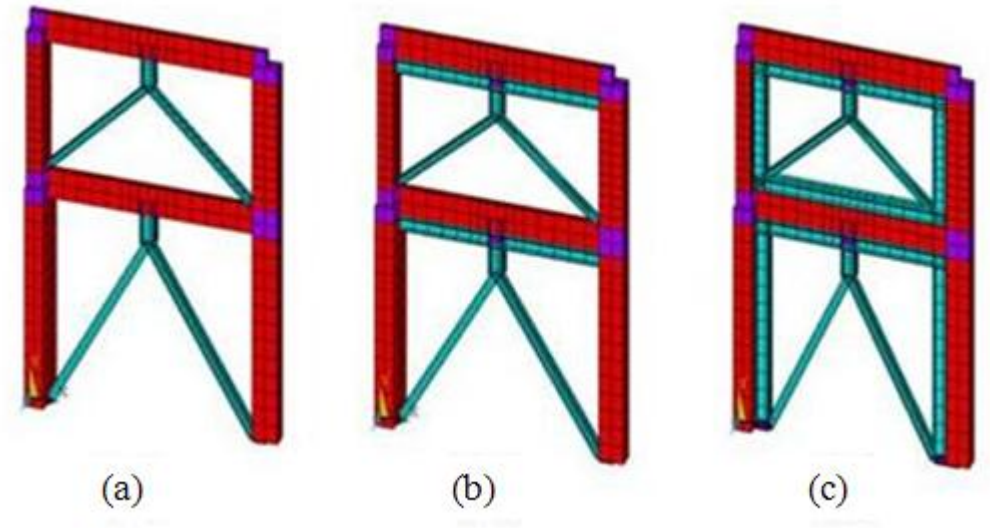


**Figure 2.7** Two dimensional finite element models of the proposed retrofitting system with various configurations. (a) Configuration 1, (b) Configuration 2, (c) Configuration 3

### 2.5.2 Three Dimensional Solid Modeling

Three dimensional (3-D) partial solid models of the critical regions of the reinforced concrete frame around the link and at the corners where the braces are connected were built to more precisely evaluate the stress concentrations at these locations. The partial solid models were built such that the behavior of the overall frame is simulated correctly. This required the structural analyses of the 2-D model of the frame under lateral load before the partial models could be built. For the region around the link, a local T-shaped section of the frame is modeled to investigate the stress distribution within that region as shown in Figure 2.8 by thick solid lines. The length of the beam element where the link is connected to is determined as the distance between the inflection points along the beam obtained from the moment diagram of the 2-D retrofitted reinforced concrete frame model under lateral load. Roller supports are assigned at two ends of the beam to allow for movement under lateral load while a hinge support is assigned at the end of the link to allow for the formation of a similar moment diagram as in the case of the full model as shown in Figure 2.8. A lateral load required to yield the link is then applied at the roller on the left of the link. For the region around the corner where the brace is connected, a rotated T-shaped section of the frame is modeled to investigate the stress distribution within that region as shown in Figure 2.8 by thick solid lines. The length of the column element connected to the joint is determined as the distance between the inflection points along the column obtained from the moment diagram of the 2-D retrofitted reinforced concrete frame under lateral load. The length of the beam element connected to the joint is determined as the distance between the joint and the inflection point along the beam. A roller support is assigned at the end of the beam to allow for movement under lateral load while a hinge support is assigned at the base (at the inflection point) of the lower column to allow for the formation of a similar moment diagram as in the case of the full model as shown in Figure 2.8. A lateral load equal to the shear in the upper column is applied at the top of the upper column to produce the same moment distribution as in the case of the full model. In addition, a lateral load equal to the summation of the shear in the lower column and the

horizontal force of the axial load in the brace minus the shear in the upper column is applied to the joint where all the members are connected to. The brace compressive axial force is also applied at the end of the brace to accurately simulate the actual stress distribution within the frame members.

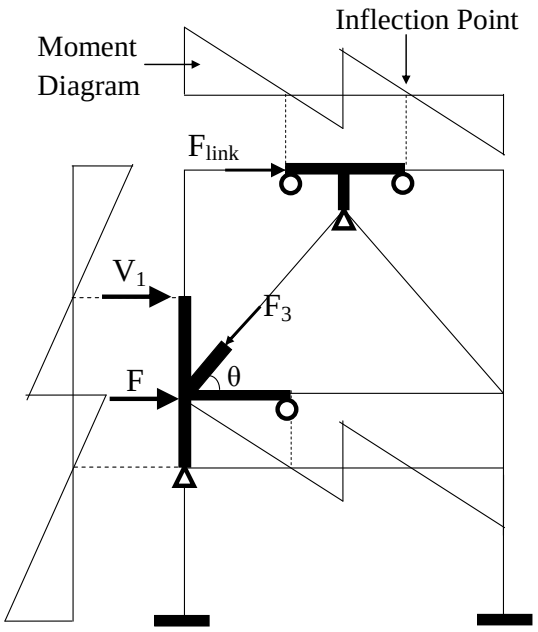


**Figure 2.8** Details of the solid models

The solid models of the critical parts of the frame are built using the program ANSYS (2009). Solid element is used to model the reinforced concrete and steel members. Full composite action is assumed between the reinforced concrete and steel members. For Configuration 1, 25 mm thick steel plates are introduced at the locations where the link and the braces are connected to the reinforced concrete surfaces. The plate elements are also modeled using solid elements in ANSYS. Rigid plate members at the support locations and points of load applications are introduced to ensure a realistic stress distribution within the reinforced concrete members of the frame. The partial ANSYS models corresponding to the cases where steel housing frame is excluded from (Configuration 1) and included in

(Configuration 3) the retrofitting system is shown in Figure 2.9 (a) and (b) respectively. The preprocessor program Solidworks and automatic mesh generation feature of the program ANSYS are used to build the finite element models.

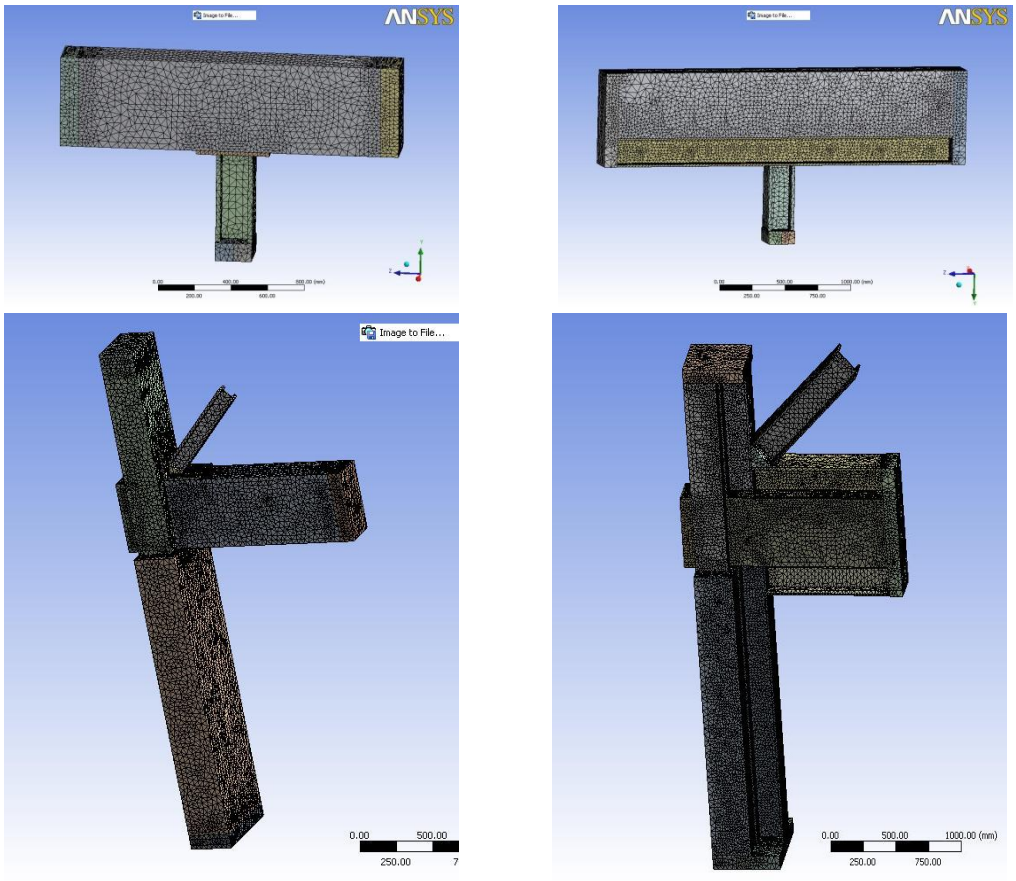


(a) (b)

**Figure 2.9** Solid Models used in the 3-D analyses, (a) steel housing frame is excluded from the model, (b) steel housing frame is included in the model

## 2.6 Analyses Results

Two sets of analyses are conducted. In the first set of analyses (Analyses case 1), for each retrofitting configuration tested, the lateral load pattern was selected to

provide simultaneous yielding of the shear links at the two story levels. This resulted in different lateral load patterns and base shears for each retrofitting configuration. This was done for the comparative assessment of the strength (the strength at the verge of shear link yielding) and associated stress distribution within the members of the reinforced concrete frames retrofitted with various configurations. In the second set of analyses (Analyses case 2), a single load pattern is applied on all the frames (average of the loads applied on the frames retrofitted with Configuration 1 and 2. In this case the base shear is identical for all the cases. This was done to facilitate the comparison of the stress distribution within the reinforced concrete members of the frames for all the retrofitting configurations including the case where no retrofitting was done (no retrofitting case is only for the 2-D analyses).

### 2.6.1 Analyses Results for the Two Dimensional Models

The analyses results obtained from the two dimensional linear finite element analyses were comparatively evaluated for various configurations of the proposed seismic retrofitting method. The analyses results for analyses cases 1 and 2 are given in Table 2.2. and 2.3 respectively. The Configuration 4 given in Table 2.3 is the bare reinforced concrete frame without the retrofitting system. Tables 2.2 and 2.3 compare the stiffness, base shear, top displacement, axial and shear stress distributions within the reinforced concrete members of the frame retrofitted with various configurations of the proposed retrofitting system.

For Analysis Case 1, as observed from Table 2.2, the retrofitting system with the additional steel frame housing the link and the braces (Configuration 3) produces a structural system with a much higher elastic stiffness compared to the retrofitting system with the collector beam (Configuration 2) and the one that includes only the braces and shear link (Configuration 1). Consequently, it is expected that the lateral drift of the frame will be smaller when retrofitting Configuration 3 is used. This, in turn, may result in less damage to the nonstructural and reinforced concrete structural components of the building

during a potential earthquake. Moreover, the presence of the steel frame members in Configuration 3 increased the base shear capacity of the building by around 30% compared to Configurations 1 and 2 (at the verge of yielding of the shear links). This means that the building retrofitted with Configuration 3 may remain within the elastic range at higher seismic loads. The retrofitting Configuration 3 is also useful for providing additional vertical support to the reinforced concrete frame to resist the gravity loads against any potential collapse situation. Table 2.2 also shows the maximum axial and shear stress values within the reinforced concrete members. For all the cases considered the shear stresses are small. The axial stresses are larger for Configuration 1 and comparable for Configurations 2 and 3 although the frame with Configuration 3 is exposed to larger lateral loads (to cause yielding of the link). The distributions of axial stresses are shown in Figures 2.10, 2.11 and 2.12 while the distributions of shear stresses are shown in Figures 2.13, 2.14 and 2.15. As observed from the figures the stresses are more intense around the link, at the joints and support locations. However, all the axial stresses are smaller than the 20 MPa strength of the concrete.

In Table 2.2, an important point to be noted is the slightly smaller base shear force of Configuration 2 in comparison to that of Configuration 1 of the proposed retrofitting system. The reason for the smaller base shear in the case of the frame with retrofitting Configuration 2 is the presence of the collector beam. The collector beam reduces the height of the retrofitted bay and hence that of the braces. Consequently the braces are now inclined at a smaller angle, $\theta$, from the horizontal. Since the yielding of the shear link is controlled by the sum of the horizontal components of the brace axial forces ($2P_b \cos\theta$), a smaller lateral force due to the smaller angle $\theta$ ($\cos\theta$ is larger) is required to yield the link in the case of the frame with a collector beam (Configuration 2).

The analyses results for Analysis Case 2 where all the frames are subjected to the same lateral load are presented in Table 2.3. As observed from the table, retrofitting Configuration 3 produces the smallest axial stresses in the reinforced concrete members. The bare frame (Configuration 4) has a very large concrete

axial and shear stresses when it is subjected to the same lateral load as the other retrofitted frames. This clearly shows the benefits of using the proposed retrofitting system within the elastic range. The distributions of axial stresses are shown in Figures 2.16, 2.17, 2.18 and 2.19 while the distributions of shear stresses are shown in Figures 2.20, 2.21 2.22 and 2.23. As observed from the figures the stresses are more intense around the link, at the joints and support locations.

**Table 2.2** Finite element analyses results for Analysis Case 1

| Configuration | Stiffness (kN/m) | Base Shear (kN) | Displacement (mm) | Axial Stress (MPa) | | Shear Stress (MPa) | |
|---|---|---|---|---|---|---|---|
| | | | | Column | Beam | Column | Beam |
| 1 | 32500 | 455 | 14.0 | 9.5 | 16.4 | 0.9 | 2.0 |
| 2 | 40090 | 445 | 11.1 | 8 | 5.6 | 0.62 | 1.83 |
| 3 | 50609 | 582 | 11.5 | 10 | 7.7 | 1.37 | 2.9 |

**Table 2.3** Finite element analyses results for Analysis Case 2

| Configuration | Stiffness (kN/m) | Base Shear (kN) | Displacement (mm) | Axial Stress (MPa) | | Shear Stress (MPa) | |
|---|---|---|---|---|---|---|---|
| | | | | Column | Beam | Column | Beam |
| 1 | 32500 | 450 | 13.8 | 9.4 | 16.2 | 0.9 | 2.0 |
| 2 | 40090 | 450 | 11.4 | 8.1 | 5.9 | 0.6 | 1.9 |
| 3 | 50609 | 450 | 8.9 | 7.7 | 5.7 | 1.0 | 2.2 |
| 4 | 3125 | 450 | 144.0 | 61.8 | 61.8 | 5.4 | 4.5 |

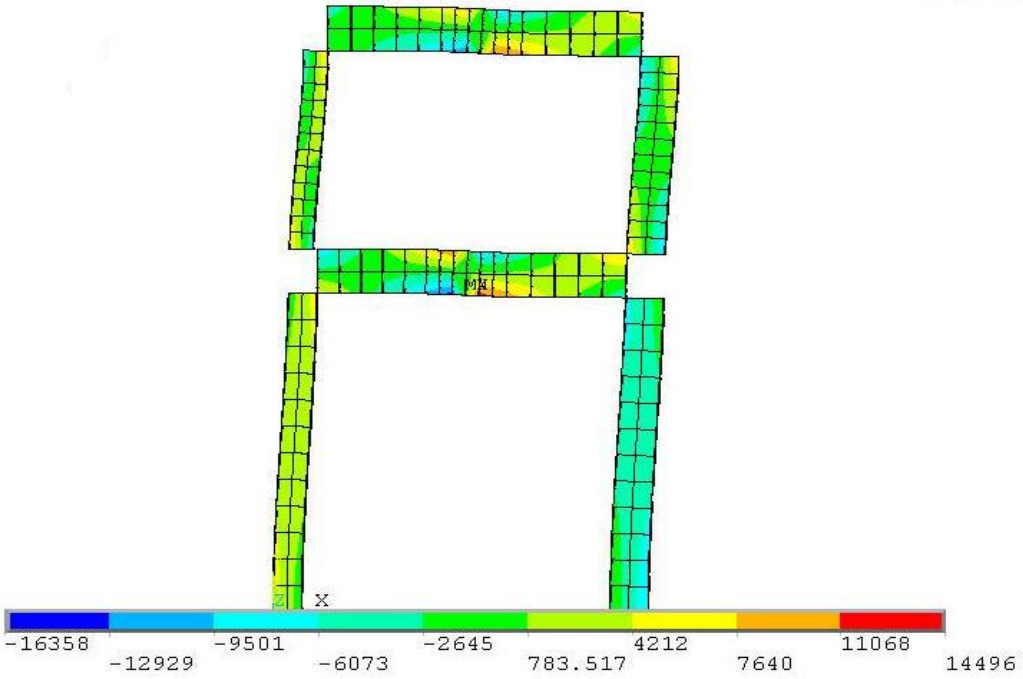


**Figure 2.10** Axial stresses on reinforced concrete elements for the first loading case and the Configuration 1

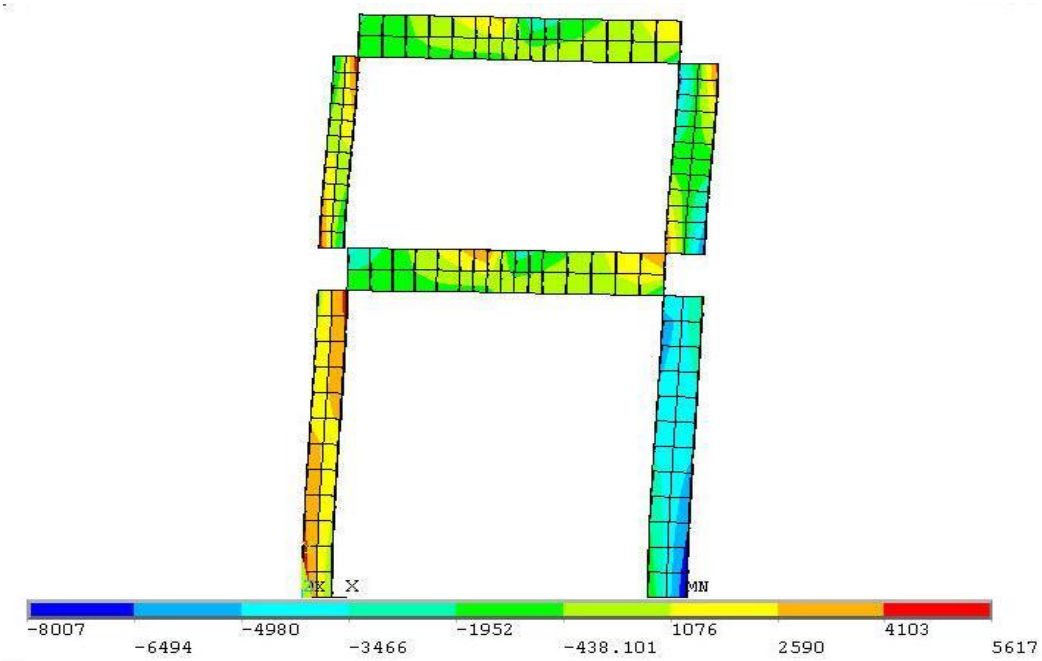


**Figure 2.11** Axial stresses on reinforced concrete elements for the first loading case and the Configuration 2

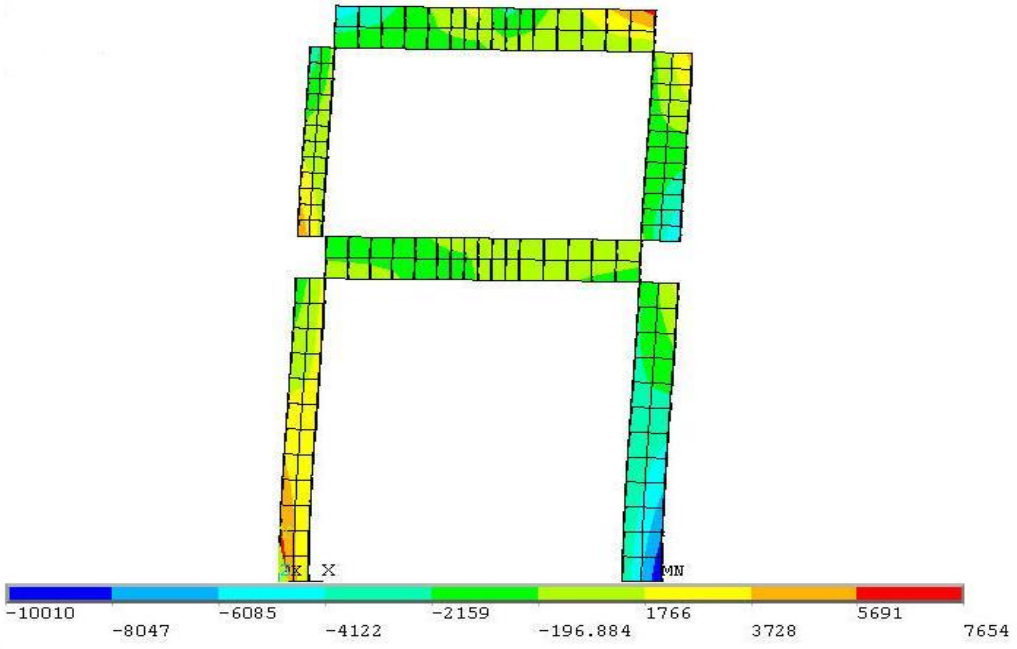


**Figure 2.12** Axial stresses on reinforced concrete elements for the first loading case and the Configuration 3

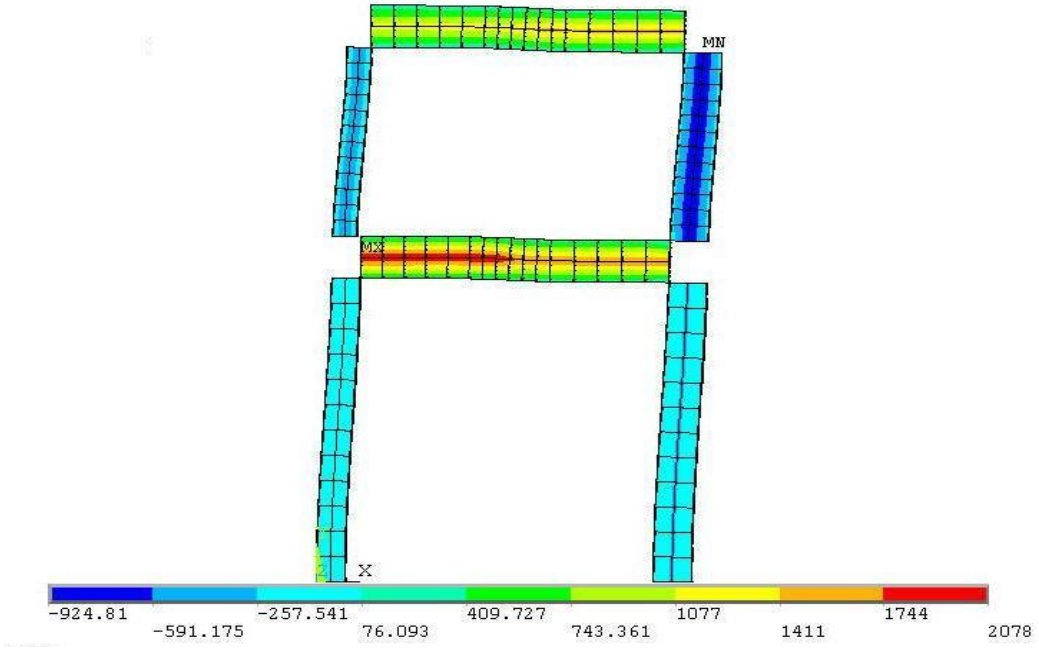


**Figure 2.13** Shear stresses on reinforced concrete elements for the first loading case and the Configuration 1

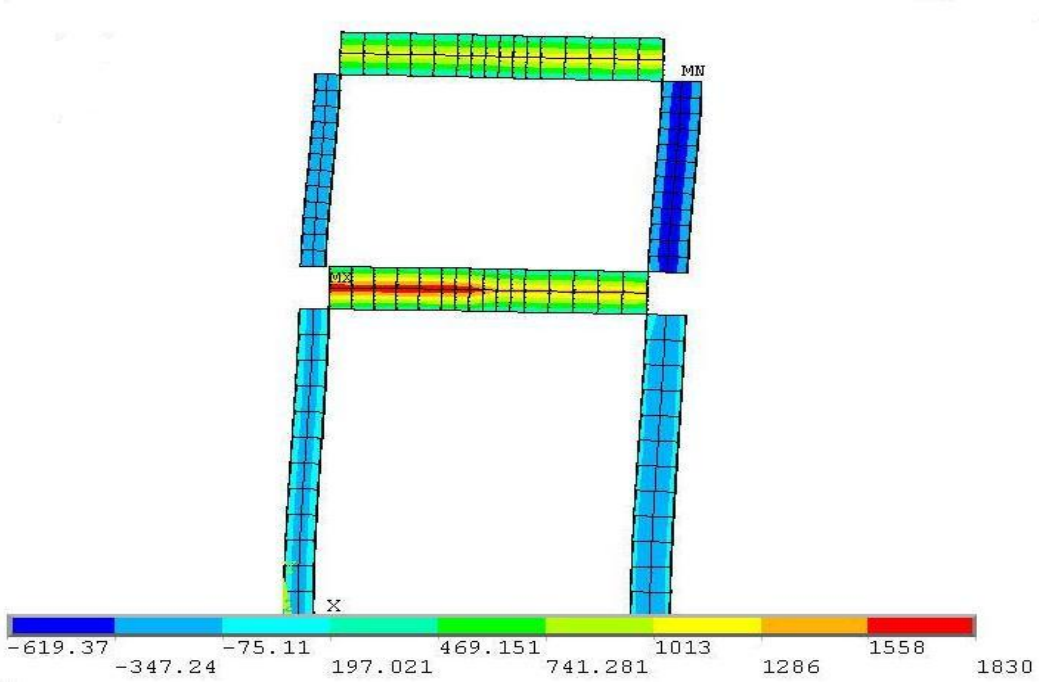


**Figure 2.14** Shear stresses on reinforced concrete elements for the first loading case and the Configuration 2

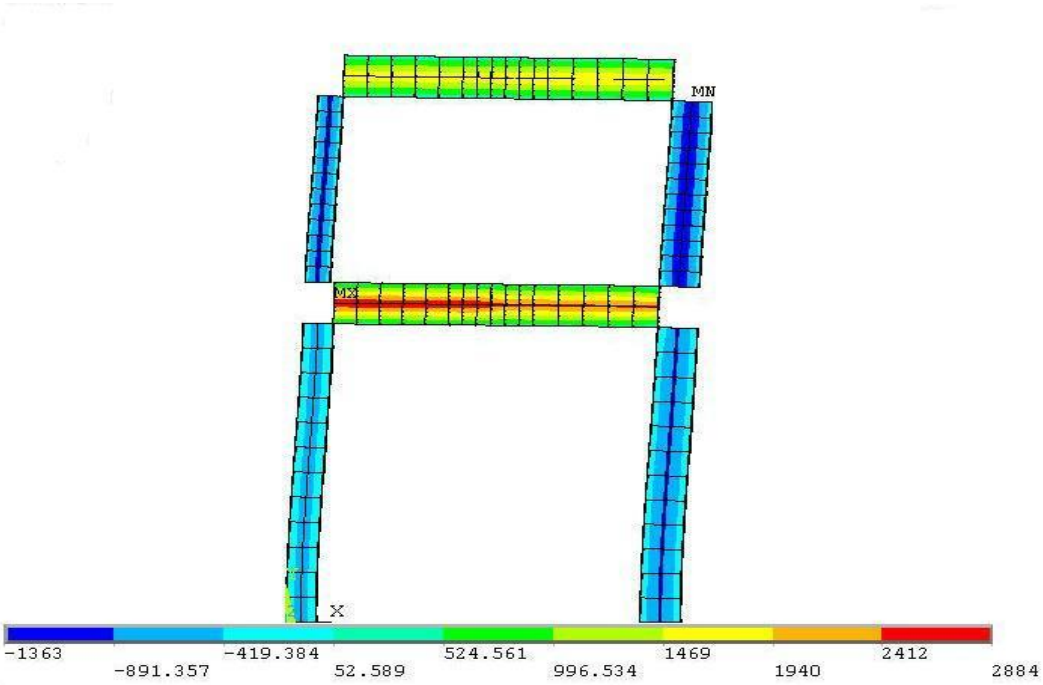


**Figure 2.15** Shear stresses on reinforced concrete elements for the first loading case and the Configuration 3

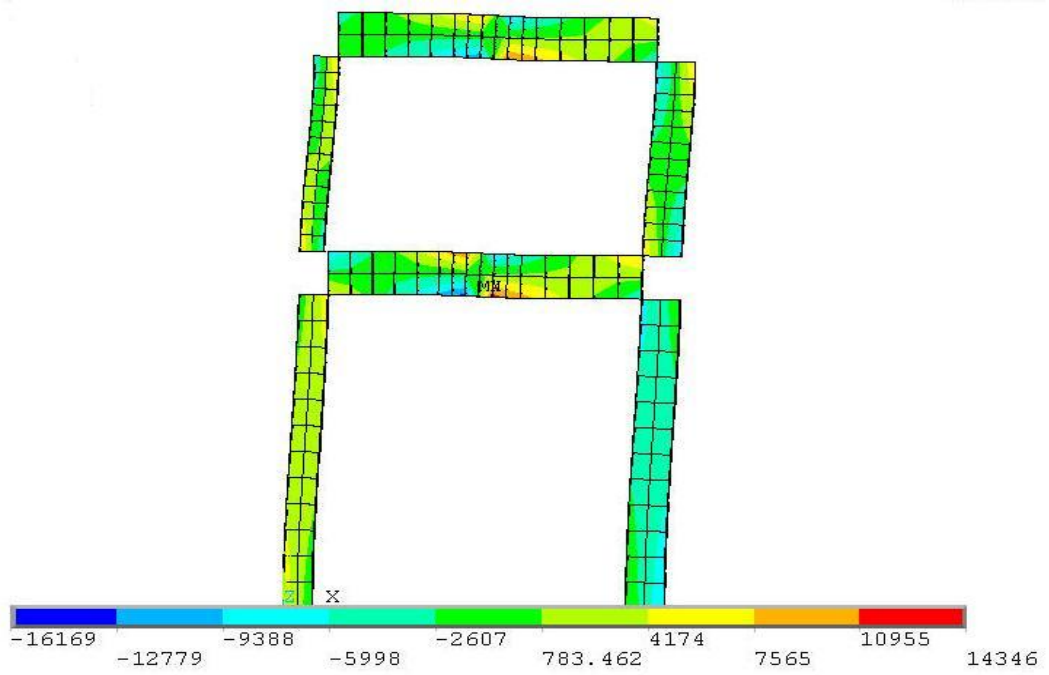


**Figure 2.16** Axial stresses on reinforced concrete elements for the second loading case and the Configuration 1

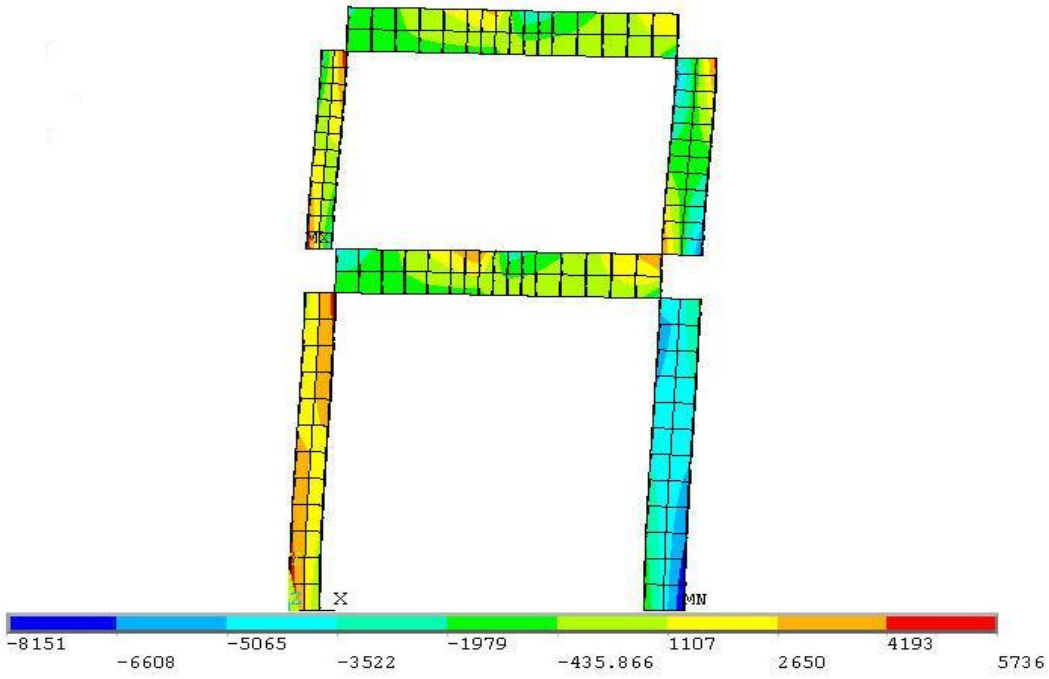


**Figure 2.17** Axial stresses on reinforced concrete elements for the second loading case and the Configuration 2

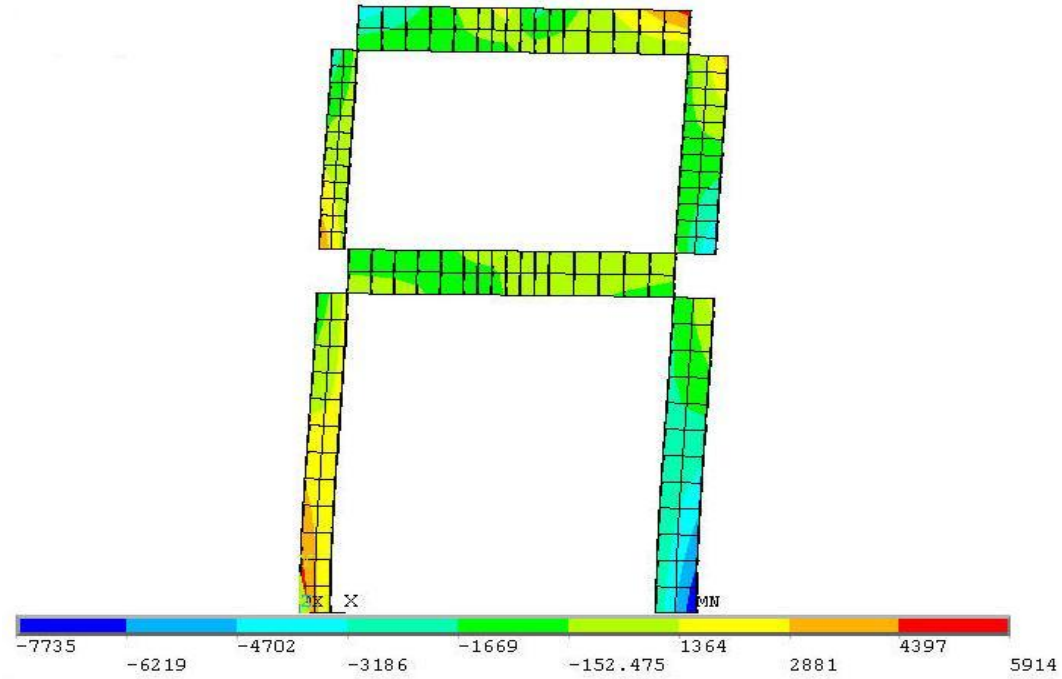


**Figure 2.18** Axial stresses on reinforced concrete elements for the second loading case and the Configuration 3

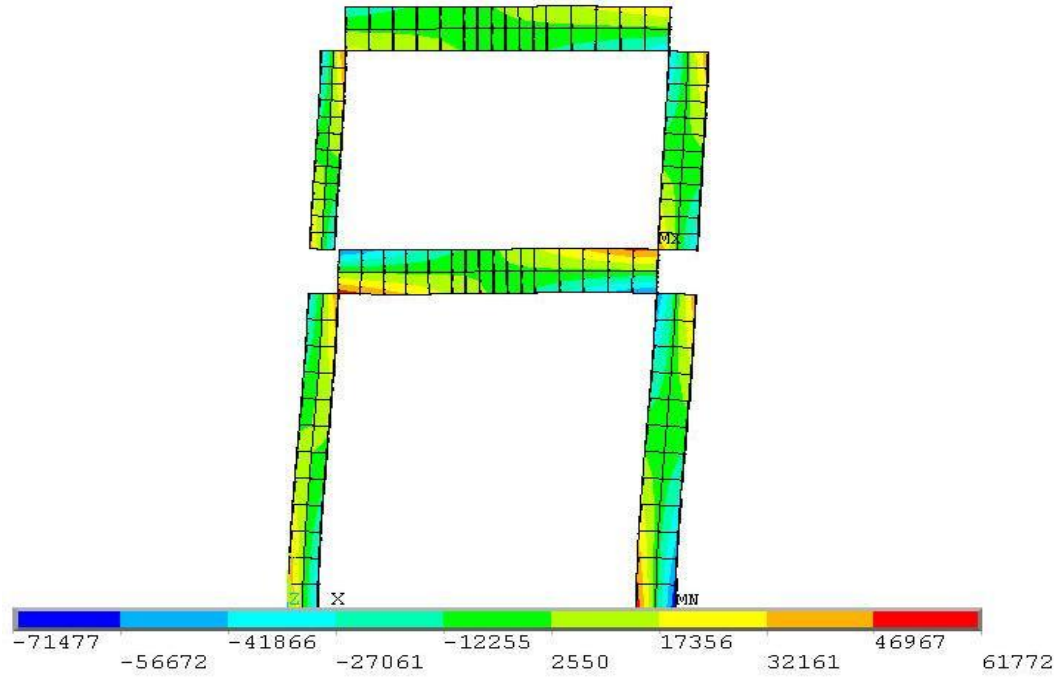


**Figure 2.19** Axial stresses on reinforced concrete elements for the second loading case and the Configuration 4

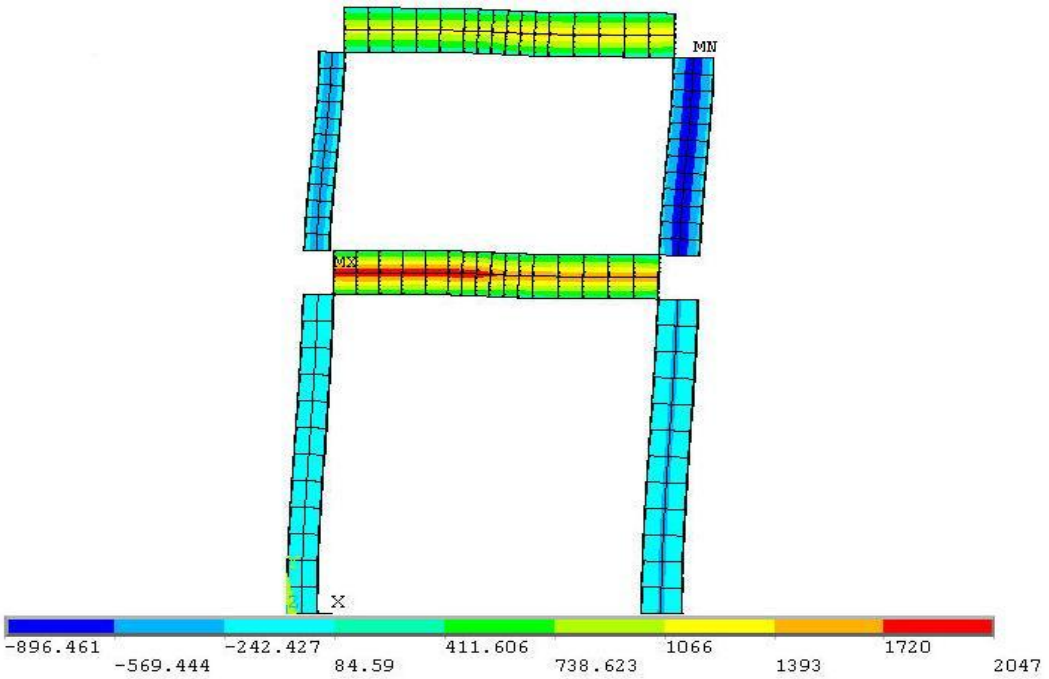


**Figure 2.20** Shear stresses on reinforced concrete elements for the second loading case and the Configuration 1

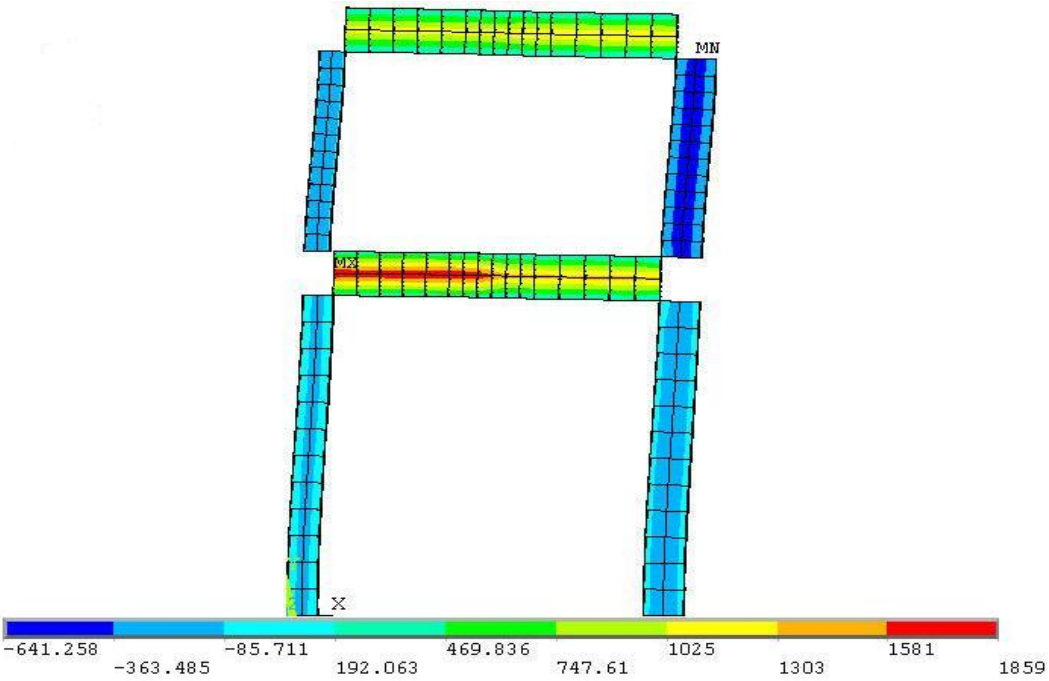


**Figure 2.21** Shear stresses on reinforced concrete elements for the second loading case and the Configuration 2

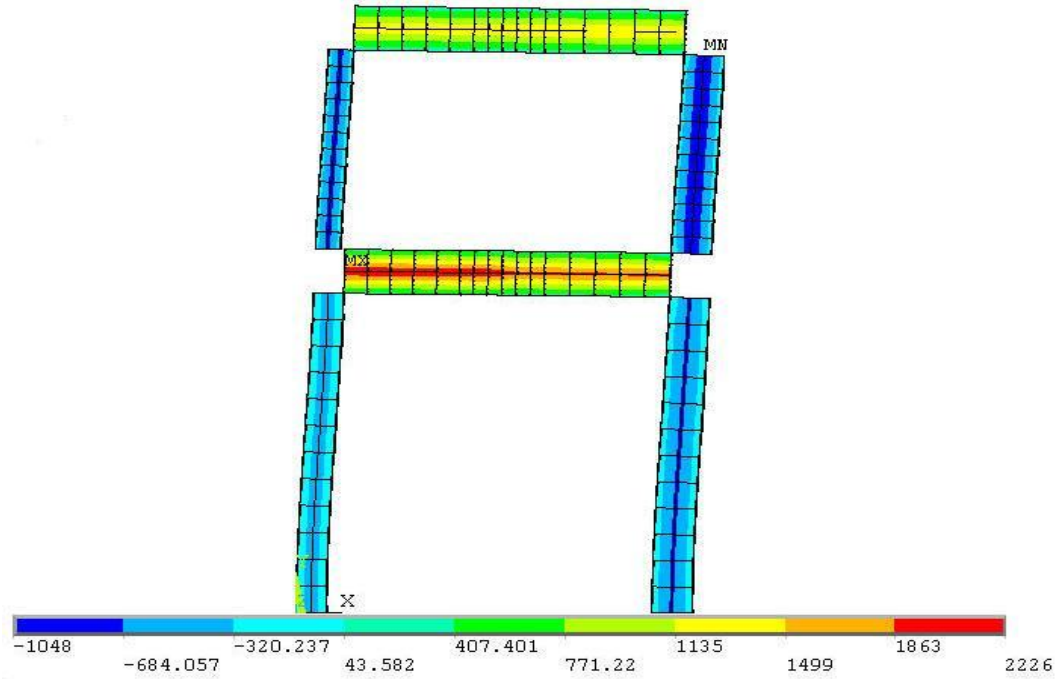


**Figure 2.22** Shear stresses on reinforced concrete elements for the second loading case and the Configuration 3

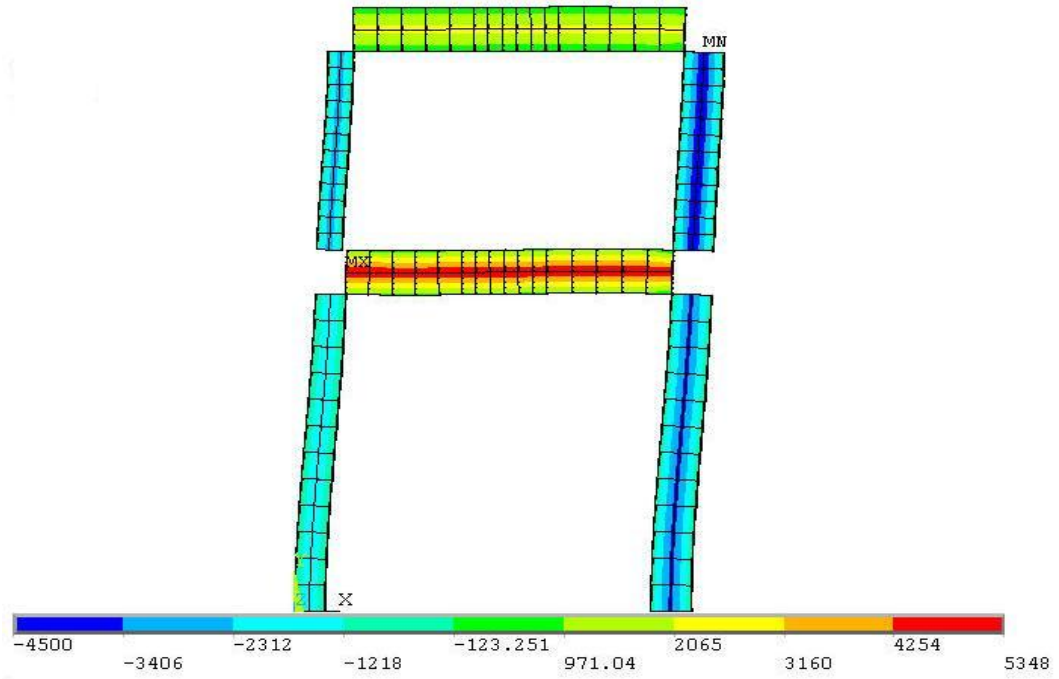


**Figure 2.23** Shear stresses on reinforced concrete elements for the second loading case and the Configuration 4

### 2.6.2 Analyses Results for Solid Models

The results obtained from the linear three dimensional finite element analyses are comparatively evaluated for two Configurations (1 and 3) of the proposed seismic retrofitting method. These results are presented in Tables 2.4, 2.5 and 2.6 for the upper link joint and the lower left joint of the sample frame for the two analyses cases considered. The distributions of the axial stresses are shown in Figures 2.24, 2.25, 2.26 and 2.27 for Analysis Case 1 and in Figures 2.28 and 2.29 for Analysis Case 2. The analyses results revealed that high axial stress concentrations around the connections of the link and the braces to the reinforced concrete frame members occur in the case of Configuration 1. The magnitude of these stresses exceed the compressive resistance of the concrete as noted from the 83 MPa and 47 MPa stresses in Tables 2.4 and 2.5. This is indicative of local damage to the concrete members. Such local damages may be amplified under cyclic loading resulting in loosening of the connections of the steel members to the reinforced concrete members of the frame. In the case of Configuration 3 however, the presence of the housing steel frame results in a more even distribution of forces transferred from the link and braces to the reinforced concrete members of the frame. This results in much lower stresses in the reinforced concrete members as noted from the 5.5 MPa and 10 MPa stresses in Tables 2.4 and 2.5. The findings from the analyses of more refined 3-D solid model are in good agreement with those from the analyses of the 2-D model. Consequently, it is expected that Configuration 3 will offer a better seismic retrofitting solution for reinforced concrete buildings.

**Table 2.4** Finite element analyses results for the upper link joint for Analyses Cases 1and 2

| Configuration | Axial Stress (MPa) |
|---|---|
| | Beam |
| 1 | 83 |
| 3 | 5.5 |

**Table 2.5** Finite element analyses results for the lower left joint for Analysis Case 1

| Configuration | Axial Stress (MPa) | | |
|---|---|---|---|
| | Column (Upper) | Column( Lower) | Beam |
| 1 | 35 | 27 | 47 |
| 3 | 13 | 12 | 10 |

**Table 2.6** Finite element analyses results for the lower left joint for Analysis Case 2

| Configuration | Axial Stress (MPa) | | |
|---|---|---|---|
| | Column (Upper) | Column( Lower) | Beam |
| 1 | 25 | 34 | 20 |
| 3 | 11 | 7 | 9.5 |

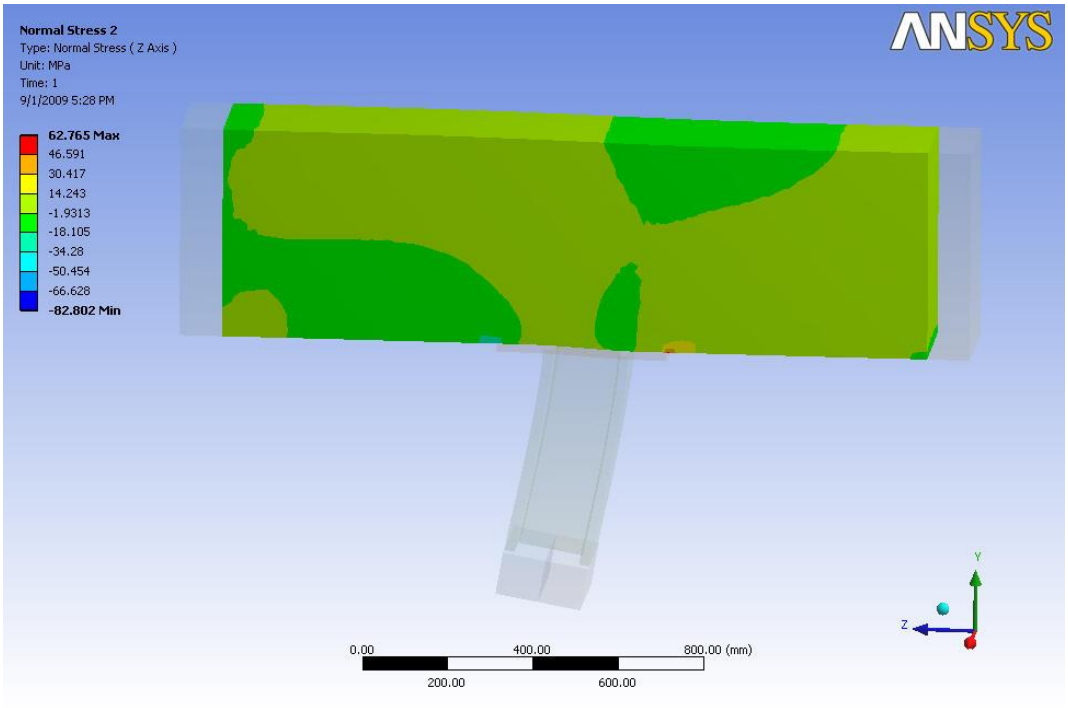


(a)

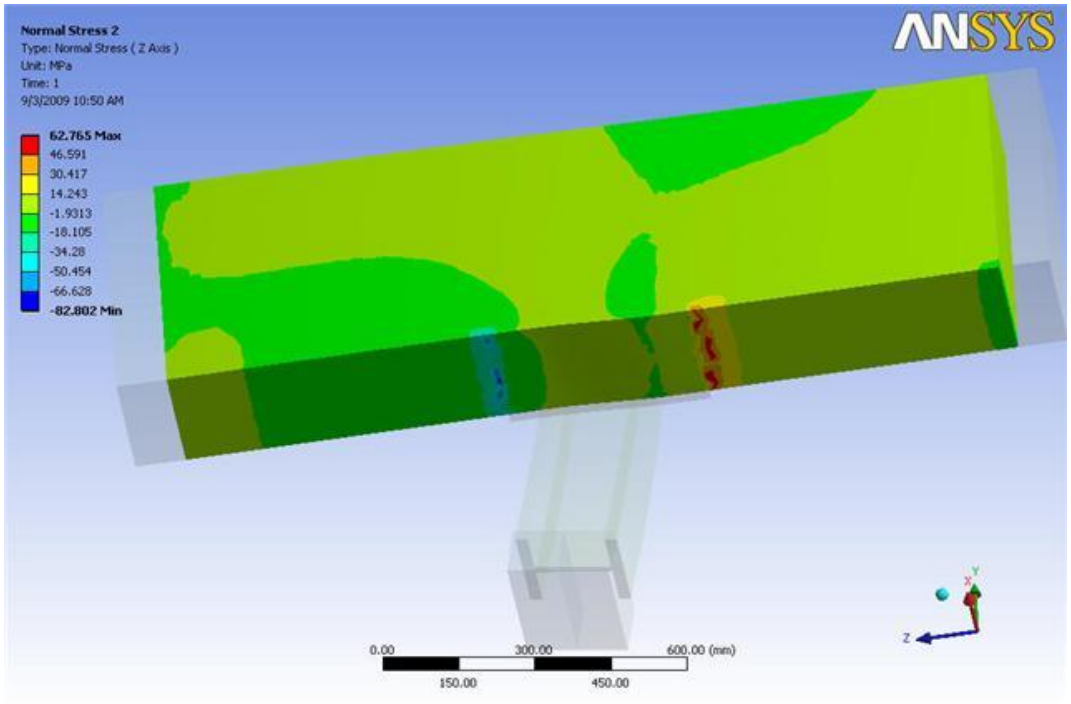


(b)

**Figure 2.24** Axial stresses on reinforced concrete beam element at the location of the link with a maximum stress of 83MPa for Analyses cases 1 and 2 and for Configuration 1;(a) side view, (b) bottom view

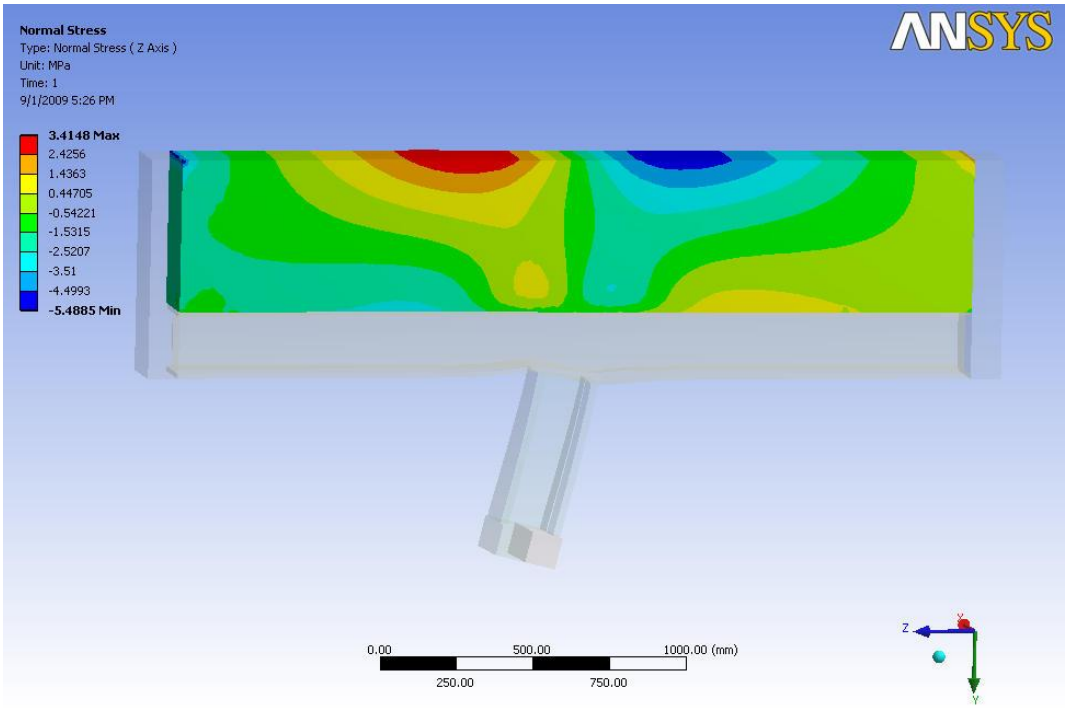


(a)

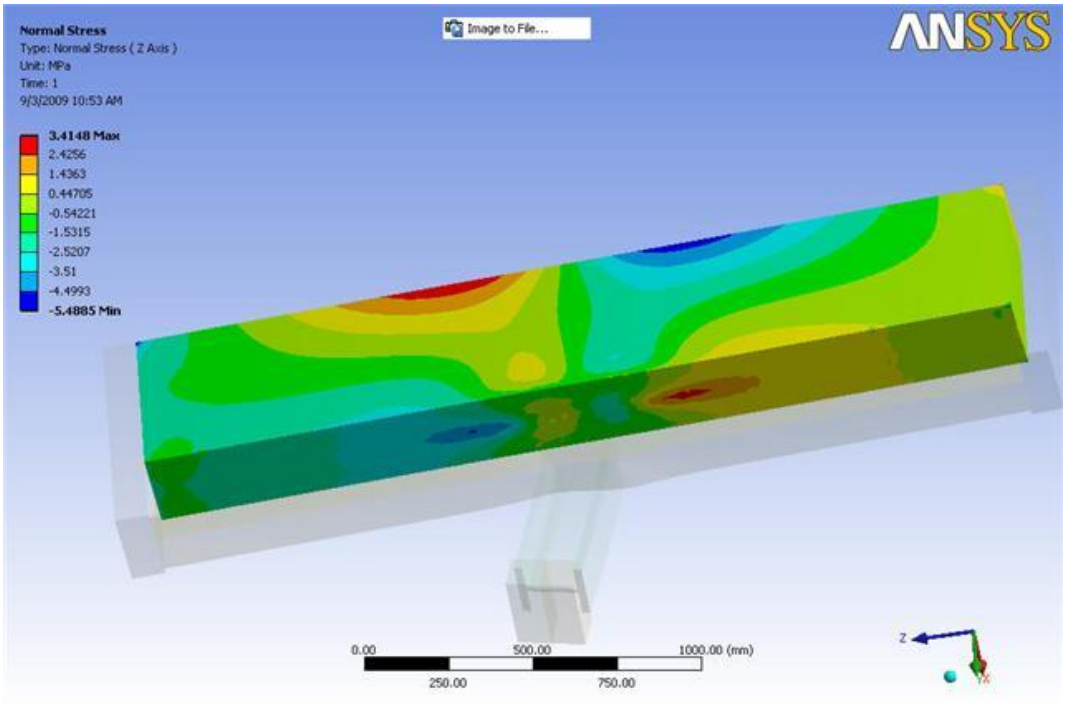


(b)

**Figure 2.25** Axial stresses on reinforced concrete beam element at the location of the link with a maximum stress of 5.5MPa for Analyses Cases 1 and 2 and for Configuration 3; (a) side view, (b) bottom view

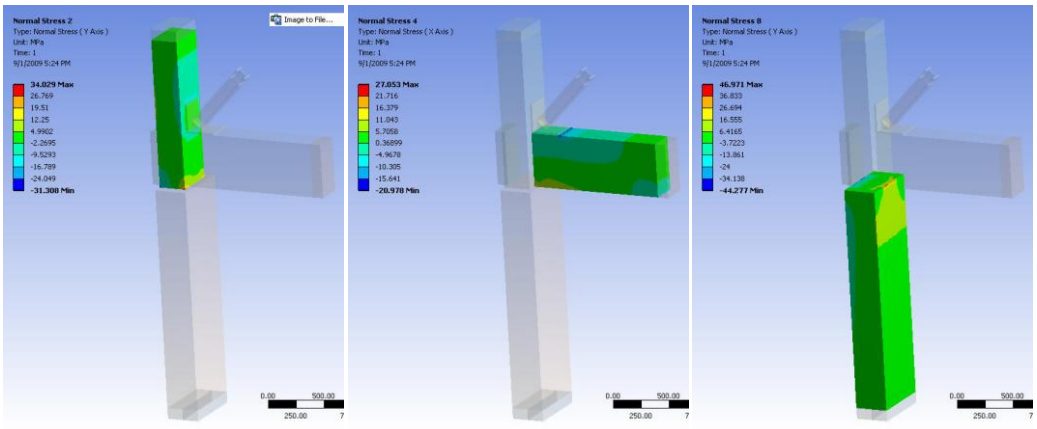


**Figure 2.26** Axial stresses on reinforced concrete elements at the lower left joint of the frame with a maximum stress of 47 MPa for Analysis Case 1 and for Configuration 1.

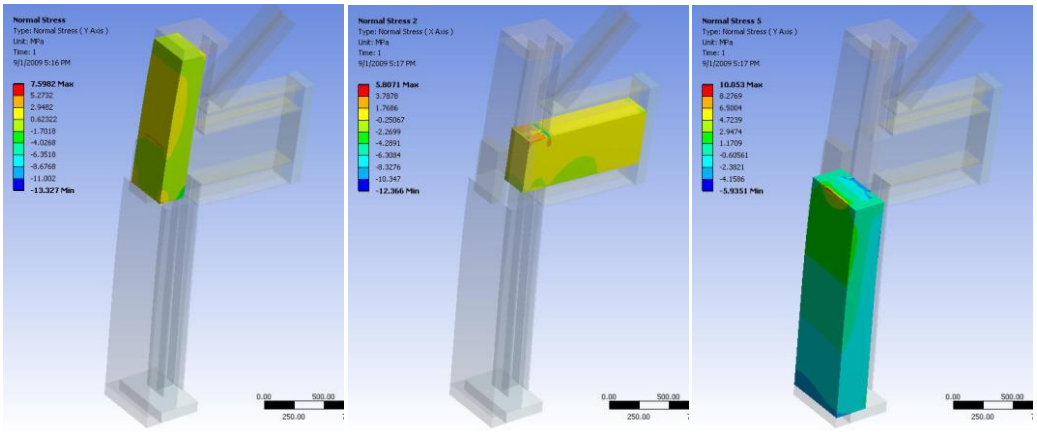


**Figure 2.27** Axial stresses on reinforced concrete elements at the lower left joint of the frame with a maximum stress of 13 MPa for Analysis Case 1 and for Configuration 3.

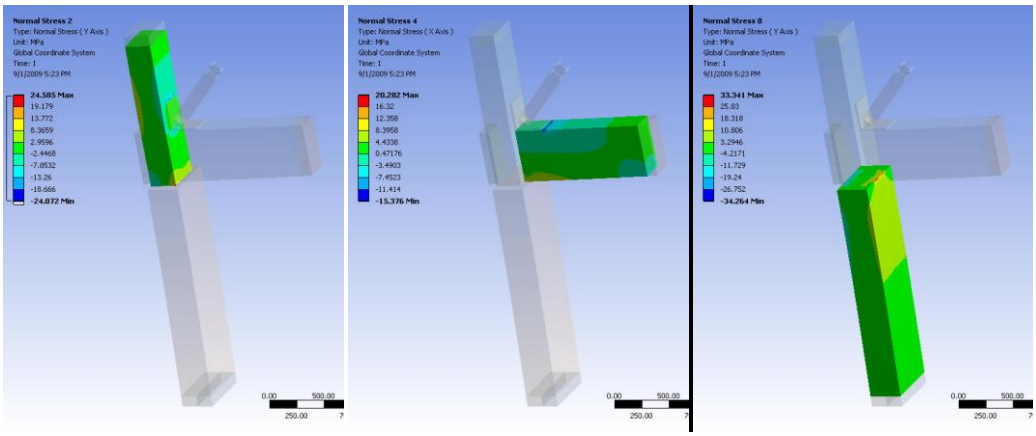

**Figure 2.28** Axial stresses on reinforced concrete elements at the lower left joint of the frame with a maximum stress of 34 MPa for Analysis Case 2 and for Configuration 1.

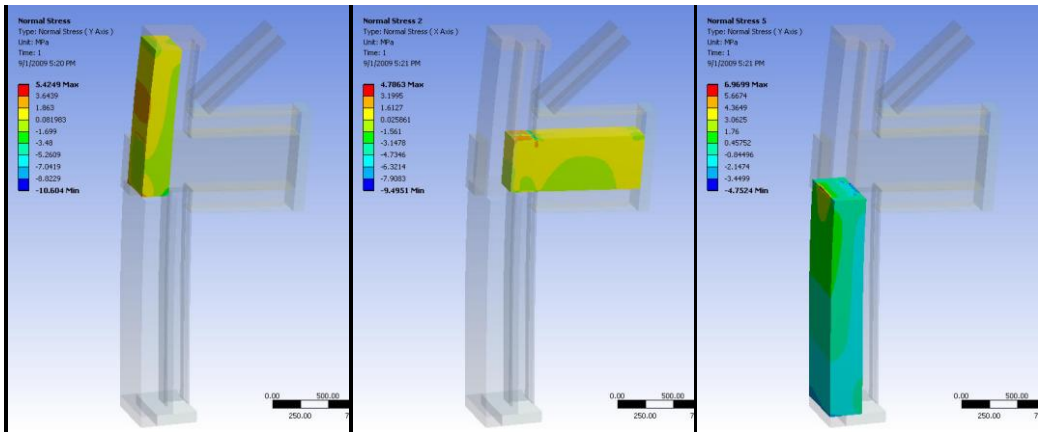

**Figure 2.29** Axial stresses on reinforced concrete elements at the lower left joint of the frame with a maximum stress of 9.5 MPa for Analysis Case 2 and for Configuration 3.

## 2.7 Summary

Comparative finite element analyses of a sample, two stories, one bay reinforced concrete frame retrofitted with various configurations of the proposed retrofitting system are conducted to identify the configuration with the most benefits.

From the 2-D and 3-D finite element analyses results, Configuration 3 where the link and the braces are encased in a steel frame system (Figure 2.4 (c)) was observed to increase the stiffness and strength of the frame while decreasing the stress concentrations within the reinforced concrete members of the frame and providing support to the reinforced concrete structure to prevent potential collapse due to gravitational effects after a potential damaging earthquake. Accordingly, Configuration 3 is selected for the retrofitting of the buildings used in this study.

# CHAPTER 3

# SELECTED BUILDINGS FOR SEISMIC RETROFITTING

## 3.1 Introduction

Two existing buildings are selected to test the efficiency of the proposed seismic retrofitting method. The first building is a two storey school building, located in Çankırı-Ilgaz. The second building is a six storey office building located in Eskişehir. The first building is chosen to represent low-rise buildings while the second one is selected to represent mid-rise buildings. The appropriate selection of the buildings enabled testing the efficiency of the proposed seismic retrofitting technique for the most widely used reinforced concrete structure types in Turkey.

The buildings selected for seismic retrofitting have some common properties. These properties are; nearly symmetrical floor plans, a moment resisting frame system (i.e. no shear walls) and poorly detailed reinforced concrete structural members. Furthermore, both buildings are located in areas with high risk of seismic activity.

## 3.2 School Building

### 3.2.1 General Properties

Fatih Sultan Mehmet Primary School is located in Ilgaz, Çankırı, Turkey. It is a two story reinforced concrete structure. A photograph of the school building is shown in Figure 3.1. The school was built in 1987 in compliance with the 1975 Turkish Seismic Design Code (Turkish Republic Ministry of Public Works 1975). Therefore the seismic capacity of the building is not sufficient according to the

current Turkish seismic design code. (Turkish Republic Ministry of Public Works 2007)

**Figure 3.1** Fatih Sultan Mehmet Primary School

The structural system of the building is composed of reinforced concrete moment resisting frames. In the long direction of the building the frames generally have eight bays (four 3.6 m and four 7.2 m wide) and in the short direction of the building the frames generally have two bays (7.2 m wide). The heights of the first and second stories are 3.2 m. The floor plans of the building are shown in Figure 3.2. The slab thickness is 0.20 m in the first story and 0.15 m in the second story. The first and second story structural member sizes are identical. The dimensions of the most of the rectangular columns are 0.3 m × 0.5 m while the remaining columns near the wider bays have cross sections larger than 0.3 m × 0.5 m and up to 0.55 m × 0.50 m. All the beams supporting the large 7.2x7.2 m slabs are 0.3-0.4 m wide and 0.7 m deep, while the remaining beams are 0.3 m wide and 0.50 m deep. The dimensions of the beams and columns are given in Table A1 in Appendix A. In the table, the beams are labeled as B-s-x(a1-a2) where s is the story number, x is the axis label along the beam and a1 and a2 are the axis labels at the left and right ends of the beam. The columns are labeled as C-s-xy where s

is the story number, and x and y are the orthogonal axes intersecting at the column. The reinforced concrete frame bays of the building are filled with brick masonry walls.

The low compressive strength of the concrete and the smooth reinforcement steel used in the construction of the building are the important deficiencies of the structure. The materials considered in the modeling are a low strength concrete class C16 and the smooth reinforcing steel of class St.220 (Turkish standards). The compressive strength and the modulus of elasticity of the concrete are respectively: $f_c$=16 MPa and $E_c$=18,800 MPa. The yield strength and the modulus of elasticity of the steel are $f_{sy}$=220 MPa and $E_s$=200,000 Mpa respectively.

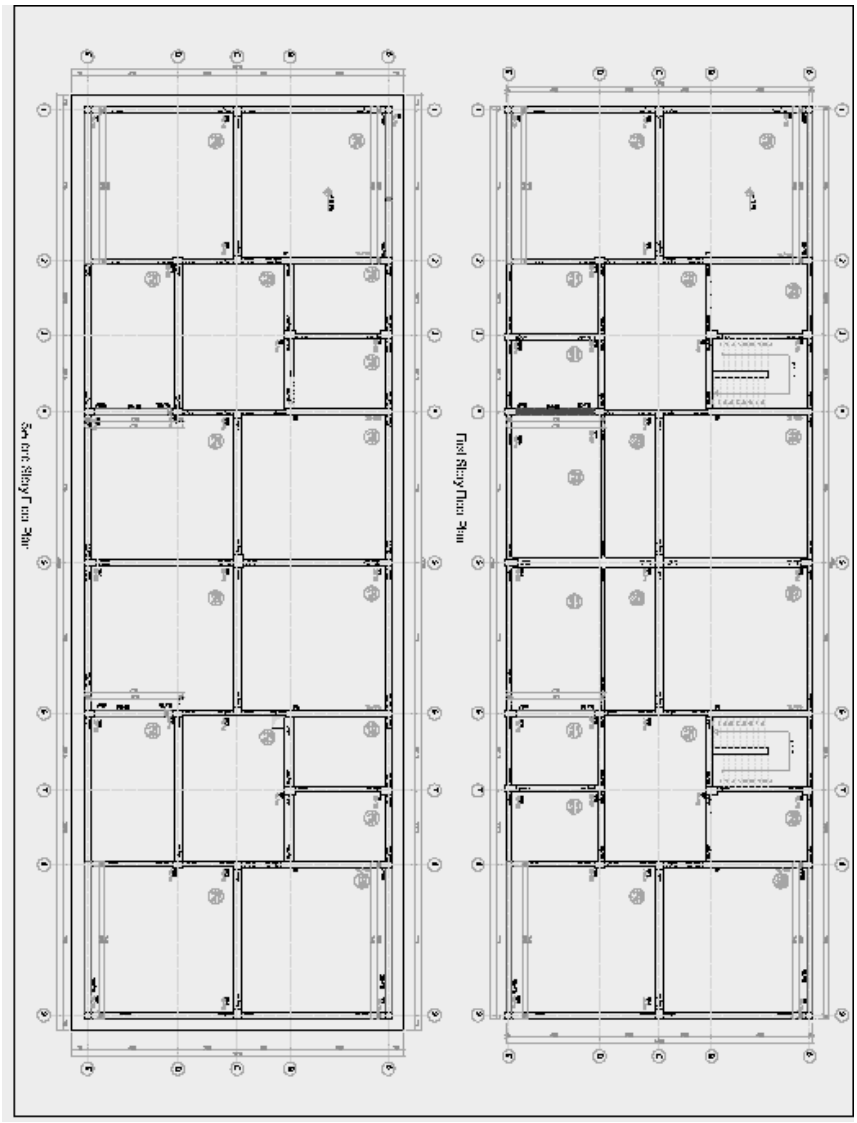

**Figure 3.2** Floor plans of the Fatih Sultan Mehmet Primary School

### 3.2.2 Soil and Seismic Zone Properties

The School is located in an area near the North Anatolia Fault Line. Soil characteristic of the site is a mixture of stiff, clayey and silty sand. Soil type is classified as group C per Turkish Seismic Design Code (Turkish Republic Ministry of Public Works 2007) and Z2 per Turkish Republic Ministry of

Transportation Railways, Harbors and Airports Construction General Directorate (DLH) code.

### 3.2.3 Determination of Shear Critical Members

For the building under consideration the shear end flexural capacities of all the reinforced concrete members are estimated. To determine the reinforced concrete members that may fail in shear (shear critical members) prior to the formation of flexural plastic hinges at the member ends first, the maximum shear that a reinforced concrete member can be subjected to up on formation of flexural plastic hinges is calculated using the following equation;

$$V_{max} = \phi \frac{M_{p1}+M_{p2}}{L} \quad (3.1)$$

where $\phi$ is the over-strength factor taken as 1.30 (FEMA-356, 2000), $M_{p1}$ and $M_{p2}$ are the flexural capacities at each one of the member ends and L is the member length. Next, the calculated shear capacities of the reinforced concrete members are compared with the maximum shear calculated using the equation above. For the building under consideration, it is found that none of the members fail in shear prior to the formation of flexural plastic hinges at the member ends. Therefore, in the nonlinear analyses of this particular building full flexural plastic formation at the member ends is assumed.

## 3.3 Office Building

### 3.3.1 General Properties

Halkbank Eskisehir branch office building is located in Tepebaşı, Eskişehir-Turkey. It is a six story reinforced concrete structure. A photograph of the office building during seismic retrofitting construction is shown in Figure 3.3. The building was built in 1950. Therefore, the seismic capacity of the building is not

sufficient according to the current Turkish seismic design code (Turkish Republic Ministry of Public Works 2007).

**Figure 3.3** Office building under rehabilitation

The structural system of the building is composed of reinforced concrete moment resisting frames. In the long direction of the building the frames generally have four bays and in the short direction of the building the frames generally have two bays. The height of the first story is 2.9 m while the height of the second story is 3.85 m. The heights of the remaining stories are 2.75 m. The floor plan of a typical story in the building is shown in Figure 3.4. The slab thickness is 0.10 m in all the stories. The beam sizes in all the stories are generally identical and the column sizes decrease at the upper storey levels. Dimensions of the rectangular columns are generally 0.5 m × 0.5 m at the lower story levels while the remaining column sizes decrease to 0.2 m × 0.2 m at the uppermost story levels. Generally, the beams are 0.1 m wide and 0.50 m deep. The dimensions of the beams and columns are given in Table A2 in Appendix A. No brick masonry walls exist in the building. Most of the reinforced concrete frame bays are filled with timber window frames and a limited number of them are filled with thin gypsum walls

with negligible structural resistance. The low compressive strength of the concrete and the smooth reinforcement steel used in the construction of the building are the important deficiencies of the structure. The materials considered in the modeling are a low strength concrete class C13 and the smooth reinforcing steel of class St.220 (Turkish standards). The compressive strength and the modulus of elasticity of the concrete are respectively: $f_c$=13 MPa and $E_c$=16,900 MPa. The yield strength and the modulus of elasticity of the steel are $f_{sy}$=220 MPa and $E_s$=200,000 Mpa respectively.

### 3.3.2 Soil and Seismic Zone Properties

The office building is located in an area at a distance of nearly 100km from the North Anatolia Fault Line. Soil characteristic of the site is composed of alluvial ground due to the presence of nearby Porsuk creek. The soil type is classified as group D per Turkish Seismic Design Code (Turkish Republic Ministry of Public Works 2007) and Z4 per Turkish Republic Ministry of Transportation Railways, Harbors and Airports Construction General Directorate (DLH) code.

### 3.3.3 Determination of Shear Critical Members

Similar to the school building the shear and flexural capacities of all the reinforced concrete members of the office building are estimated. The calculated shear capacities of the reinforced concrete members are then compared with the maximum shear calculated using Equation 3.1. It is found that a few columns and one beam do not have adequate shear capacity to allow for flexural plastic hinge formation at the member ends. Obviously, this will dramatically reduce the lateral displacement capacity of the building under earthquake loads. To prevent such a poor seismic performance, these members are retrofitted using steel angles and braces to upgrade the shear capacity while keeping the flexural capacity at the same level (the steel members used to upgrade the shear capacity of the columns are terminated at a distance of 50 mm from the member ends). Following this local retrofitting, none of the members will fail in shear prior to the formation of

flexural plastic hinges at the member ends. Therefore, in the nonlinear analyses of this particular building full flexural plastic formation at the member ends is assumed.

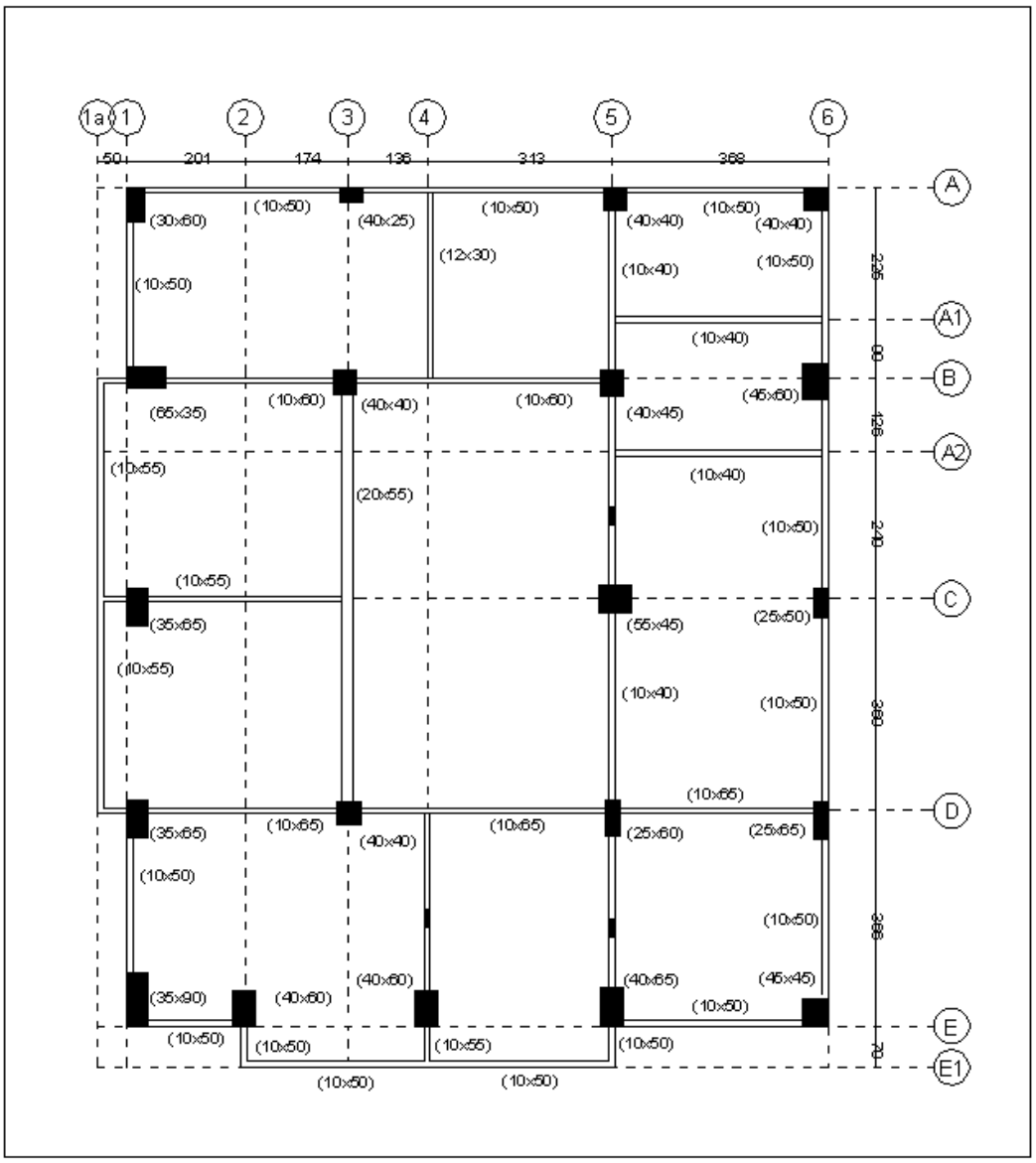


**Figure 3.4** A typical floor plan of the office building

# CHAPTER 4

# SITE SPECIFIC RESONSE SPECTRA AND RESPONSE SPECTRA COMPATIBLE GROUND MOTIONS

## 4.1 Introduction

A number of linear and nonlinear structural analyses were conducted to assess the seismic performance of the original and retrofitted example buildings used in this research study. Response spectrum (RS) analyses were conducted to determine the lateral load patterns along the height of the buildings. These lateral load patterns are used in the nonlinear pushover (NLP) analyses. RS analyses were also used within the iterative procedures for the retrofitting design of the buildings used in this study. These RS analyses necessitate appropriate acceleration response spectra that reflect the site seismic characteristics. The significance of the appropriate selection of the design response spectra originates from the importance of simulating the actual magnitude and pattern of the seismic loads that act on the building. Design seismic loads for reinforced concrete structures rely on the peak ground acceleration (PGA) values and the shapes of the response spectra (Paz, 1994). The PGA values and the shape of the response spectra tightly depend on the earthquake magnitude, the distance from the earthquake source and the local geological conditions. Underestimation of PGA or wrong evaluation of response spectra may lead to severe damages during earthquakes (Sokolov, 2000). Consequently, at present, instead of using standard response spectra available in the design codes, it is crucial to construct site-specific response spectra (SSRS) reflecting the influence from different magnitude events at different distances as well as the variety of local site conditions (Sokolov, 2000). In this study SSRS approach was used to obtain the design response spectra for the analyses and retrofitting design of the buildings under consideration. The procedure used to construct the design response spectra are presented in the following sections. To

accurately simulate the nonlinear behavior of the selected buildings under the effect of ground motions, nonlinear time history (NLTH) analyses were conducted. These NLTH analyses required an accurate estimation of the probable earthquake excitations at the building site. Consequently, SSRS compatible accelerograms were obtained to accurately simulate the effect of the probable earthquakes at the building site. The procedure to obtain the SSRS compatible accelerograms is given in section 4.5.

### 4.2 Procedure to Obtain Site Specific Response Spectra

SSRS were mainly obtained for conducting RS analyses as part of iterative seismic retrofitting design procedure, determining the lateral load pattern along the height of the building for NLP analyses and for obtaining site specific ground motions for NLTH analyses. SSRS were obtained by a method which takes into account the distance of the location of the structure to the fault and local soil conditions. This requires the determination of the approximate global coordinates of the building site. The approximate coordinates of the example buildings were obtained by using the Google Earth software (Google, 2009) which considers the satellite photos of the locations and gives coordinates as latitudes and longitudes.

The formulation for the determination of the SSRS is taken from the Turkish Republic Ministry of Transportation Railways, Harbors and Airports Construction General Directorate (DLH) code (Yüksel Proje, 2007). The procedure for obtaining SSRS curves requires two spectral acceleration parameters, $S_{MS}$ and $S_{M1}$ respectively for short period and one second period of the response spectra. These parameters are given as;

$$S_{MS} = F_a x S_S$$

$$S_{M1} = F_v x S_1$$

$S_s$ and $S_1$ are the spectral acceleration parameters for site specific spectra which are given in the DLH design code as a function of the coordinates of the structure for soil type B (stiff soil). The parameters $F_a$ and $F_v$ in the above equations relate

these $S_s$ and $S_1$values to soil types other than type B. These parameters ($F_a$ and $F_v$) are soil factors for short period and one second period, which are defined in Tables 4.1 and 4.2 respectively.

**Table 4.1** Short period soil factor $F_a$

| Soil Type | Short Period Spectral Acceleration | | | | |
|---|---|---|---|---|---|
| | $S_S \leq 0.25$ | $S_S = 0.50$ | $S_S = 0.75$ | $S_S = 1.0$ | $S_S \geq 1.25$ |
| **A** | 0.8 | 0.8 | 0.8 | 0.8 | 0.8 |
| **B** | 1.0 | 1.0 | 1.0 | 1.0 | 1.0 |
| **C** | 1.2 | 1.2 | 1.1 | 1.0 | 1.0 |
| **D** | 1.6 | 1.4 | 1.2 | 1.1 | 1.0 |
| **E** | 2.5 | 1.7 | 1.2 | 0.9 | 0.9 |
| **F** | [b] | [b] | [b] | [b] | [b] |

**Table 4.2** One second period soil factor $F_v$

| Soil Type | One second period spectral acceleration | | | | |
|---|---|---|---|---|---|
| | $S_1 \leq 0.1$ | $S_1 = 0.20$ | $S_1 = 0.3$ | $S_1 = 0.4$ | $S_1 \geq 0.5$ |
| **A** | 0.8 | 0.8 | 0.8 | 0.8 | 0.8 |
| **B** | 1.0 | 1.0 | 1.0 | 1.0 | 1.0 |
| **C** | 1.7 | 1.6 | 1.5 | 1.4 | 1.3 |
| **D** | 2.4 | 2.0 | 1.8 | 1.6 | 1.5 |
| **E** | 3.5 | 3.2 | 2.8 | 2.4 | 2.4 |
| **F** | [b] | [b] | [b] | [b] | [b] |

The shape of the design response spectrum (Figure 4.1) for various period ranges are defined by the following equations.

$$S_{ae}(T) = 0.4S_{MS} + \frac{0.6S_{MS}}{T_0}T \qquad T \leq T_0 \qquad (4.1)$$

$$S_{ae}(T) = S_{MS} \qquad T_0 \leq T \leq T_S \qquad (4.2)$$

$$S_{ae}(T) = \frac{S_{M1}}{T} \qquad T_s \leq T \leq T_L \qquad (4.3)$$

$$T_s = \frac{S_{M1}}{S_{MS}} \tag{4.4}$$

$$T_0 = 0.2T_s \tag{4.5}$$

where $T_0$ and $T_s$ are defined as the spectrum corner periods and $T_L$ is given as 12s, which is beyond the range of the vibration period interval of the buildings considered in this study.

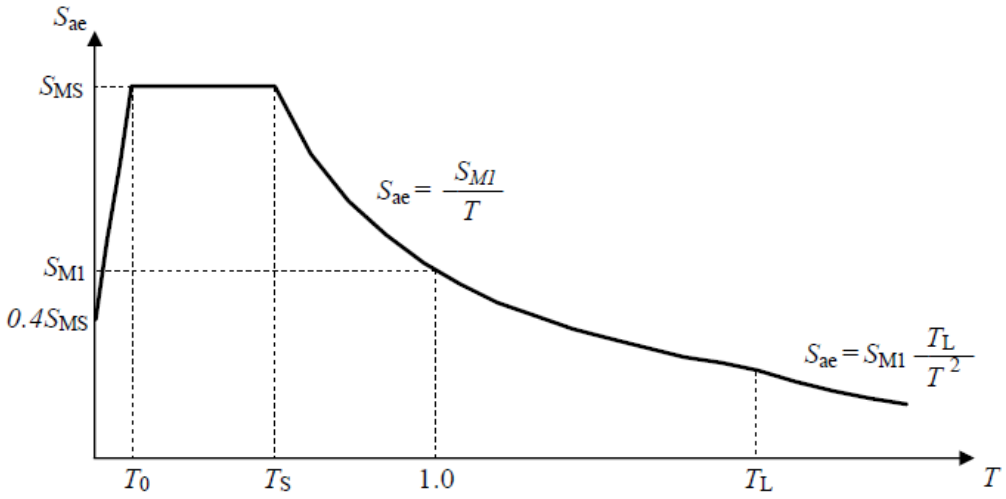


**Figure 4.1** Symbolic shape of response spectrum

SSRS are obtained for three different earthquake levels with different probabilities of being exceeded (50% in 50 years, 10% in 50 years and 2% in 50 years) for the performance based design of the buildings under consideration. Details about the earthquake and expected performance levels used for the performance assessment and retrofitting design of the buildings are given in Chapter 6.

### 4.3 Site Specific Response Spectra for School Building

The school building is located in Çankırı-Ilgaz and its approximate coordinates are; longitude: 33.40N and latitude: 40.60E. Corresponding $S_s$ and $S_1$ values for the three earthquake levels is given in Table 4.3.

**Table 4.3** $S_s$ and $S_1$ values for school building

| **$S_s$** | | | **$S_1$** | | |
|---|---|---|---|---|---|
| **Prob. of being exceeded in 50 years** | | | **Prob. of being exceeded in 50 years** | | |
| 50% | 10% | 2% | 50% | 10% | 2% |
| 0.33 | 0.59 | 0.88 | 0.13 | 0.28 | 0.46 |

The other parameters; $F_a$, $F_v$, $S_{MS}$, $S_{M1}$, $T_s$ and $T_0$ defining the response spectrum are obtained as per the procedure outlined in Section 4.2. These parameters are listed in Table 4.4

**Table 4.4** Necessary parameters to obtain the SSRS for school building

| **Design Parameters** | **Prob. of being exceeded in 50 years** | | |
|---|---|---|---|
| | **50%** | **10%** | **2%** |
| $F_a$ | 1.20 | 1.05 | 1.00 |
| $F_v$ | 1.67 | 1.52 | 1.34 |
| $S_{MS}$ | 0.40 | 0.62 | 0.88 |
| $S_{M1}$ | 0.22 | 0.43 | 0.62 |
| $T_s$ | 0.55 | 0.69 | 0.70 |
| $T_0$ | 0.11 | 0.14 | 0.14 |

Figure 4.2 shows the plot of the SRSS for the three earthquake levels used in the seismic performance assessment and retrofitting design of the school building.

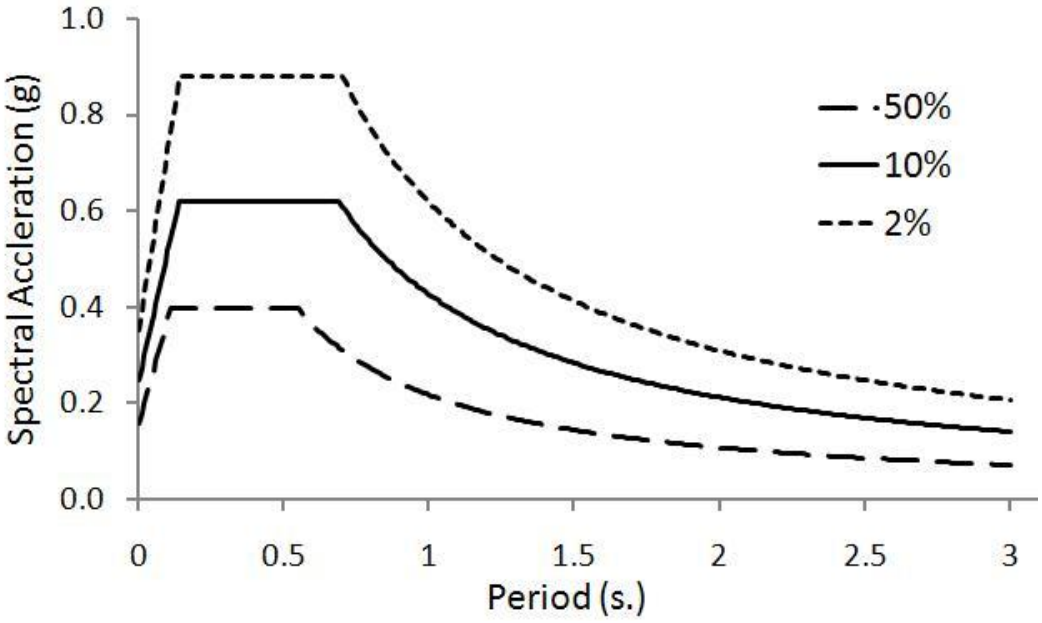


**Figure 4.2** SSRS for school building

### 4.4 Site Specific Response Spectra for Office Building

Halkbank Eskişehir branch office building is located in Tepebaşı-Eskişehir. The approximate coordinates of the structure obtained using the Google Earth software (Goggle, 2009) are; longitude: 30.33E and latitude: 39.45N. A procedure similar to that outlined in Section 4.2 was followed to obtain the SSRS for the office building. The data used in the generation of the SSRS is given in Tables 4.5 and 4.6. Figure 4.3 shows the plot of the SRSS for the three earthquake levels used in the seismic performance assessment and retrofitting design of the office building.

**Table 4.5** $S_s$ and $S_1$ values for office building

| $S_s$ | | | $S_1$ | | |
|---|---|---|---|---|---|
| **50%** | **10%** | **2%** | **50%** | **10%** | **2%** |
| 0.27 | 0.52 | 0.82 | 0.09 | 0.16 | 0.25 |

**Table 4.6** Necessary parameters to obtain the SSRS for office building

| **Design Parameters** | **Prob. of being exceeded in 50 years** | | |
|---|---|---|---|
| | **50%** | **10%** | **2%** |
| $F_a$ | 1.58 | 1.38 | 1.17 |
| $F_v$ | 2.4 | 2.16 | 1.9 |
| $S_{MS}$ | 0.43 | 0.72 | 0.96 |
| $S_{M1}$ | 0.22 | 0.35 | 0.48 |
| $T_s$ | 0.51 | 0.48 | 0.50 |
| $T_0$ | 0.10 | 0.10 | 0.10 |

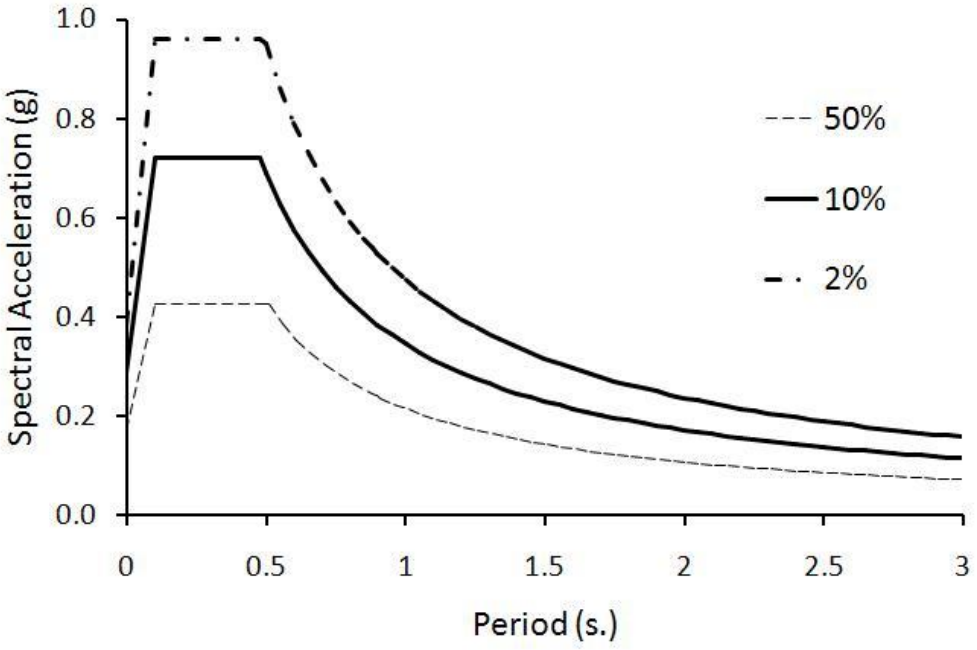


**Figure 4.3** SSRS for office building

### 4.5 Response Spectra Compatible Ground Motions

The NLTH analyses conducted as part of this study requires acceleration time histories which are compatible with the SSRS obtained for the structures under consideration. Based on the requirements of the International Building Code (IBC 2000) SSRS compatible ground motions are selected as follows. First, seven earthquake ground motions whose response spectra are compatible with the SSRS are selected from the PEER (Pacific Earthquake Engineering Research) strong motion database of the University of California, Berkeley. Details of the selected ground motions are given in Table 4.7. The acceleration time histories of the ground motions are shown in Figures 4.4-4.10. The search for these ground motions within the database was conducted by considering PGAs, site conditions and distances to fault line. Each one of these ground motions were first scaled to PGAs of the SSRS for the three earthquake levels with different probabilities of being exceeded in 50 years (50% in 50 years, 10% in 50 years and 2% in 50 years). Following this initial scaling procedure, the average value of the already

scaled seven SSRS compatible ground motions was rescaled to obtain an average value larger than or equal to 1.4 times the SSRS within a period range of 0.2T-1.5T (T=0.53 s for the school building and T=0.87 s for the office building). In the NLTH analyses, the scale factor of the earthquake ground motion is calculated by multiplying the initial scale factor by the latter one for each earthquake level. The scale factors used in NLTH analyses of the school buildings are given for each earthquake ground motion in Table 4.8. Figure 4.11 shows the response spectra of the selected earthquakes vs. the SSRS for the school building for the earthquake level associated with 10% probability of being exceeded in 50 years. Figure 4.12 shows the comparison of the average of the scaled earthquake ground motions with the design spectrum and 1.4 x the design spectrum. Response spectra for the other earthquake levels are similar. The shape of the SRSS of the office building is very similar to that of the school building. Therefore, the same earthquake accelerograms (but scaled using different factors) were used in the retrofitting design of the two buildings. The scale factors used in NLTH analyses of the office buildings are given for each earthquake ground motion in Table 4.9

**Table 4.7** Selected earthquakes and their properties

| Important Features of Earthquake Records Used in The Analyses | | | | | | |
|---|---|---|---|---|---|---|
| **Earthquake** | **Station/Component** | **Distance to Fault(km)** | **Soil Type** | **Ap(g)** | **Vp(cm/s)** | **Ap/Vp(1/s)** |
| IMPERIAL VALLEY 1979 | 6605 Delta/ 262 | 43.6 | D | 0.238 | 26 | 9.0 |
| COALINGA 1983 | 46314 Cantua Creek School/ 270 | 25.5 | D | 0.227 | 23.6 | 9.4 |
| NORTHRIDGE 1994 | 14403 LA - 116th St School/ 360 | 41.9 | D | 0.133 | 13.5 | 9.7 |
| LOMA PRIETA 1989 | 1656 Hollister Diff. Array/ 255 | 25.8 | D | 0.279 | 35.6 | 7.7 |
| WHITTIER NARROWS 1987 | 90079 Downey - Birchdale/ 180 | 56.8 | D | 0.299 | 37.8 | 7.8 |
| IMPERIAL VALLEY 1940 | 117 El Centro Array #9/ 270 | 12 | D | 0.215 | 30.2 | 7.0 |
| IMPERIAL VALLEY 1979 | 0439, EL CENTRO ARRAY#9,270 | 30.8 | D | 0.113 | 11.1 | 10.0 |

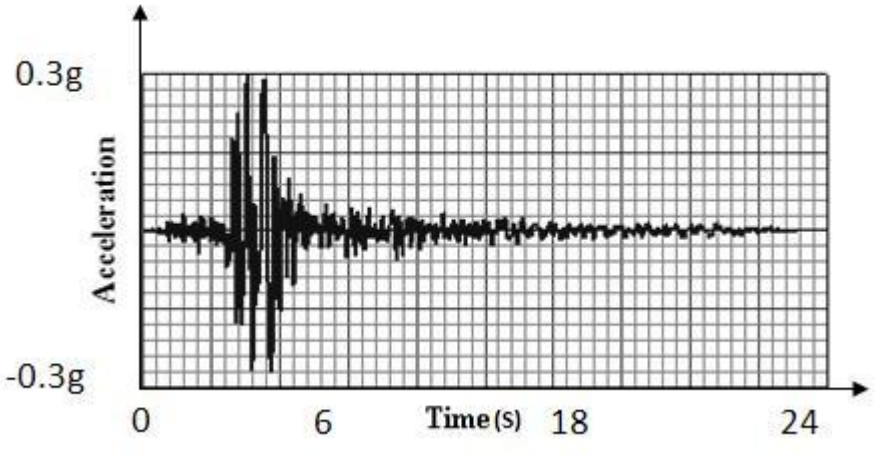


**Figure 4.4** Whittier Narrows-1987 acceleration vs. time graph

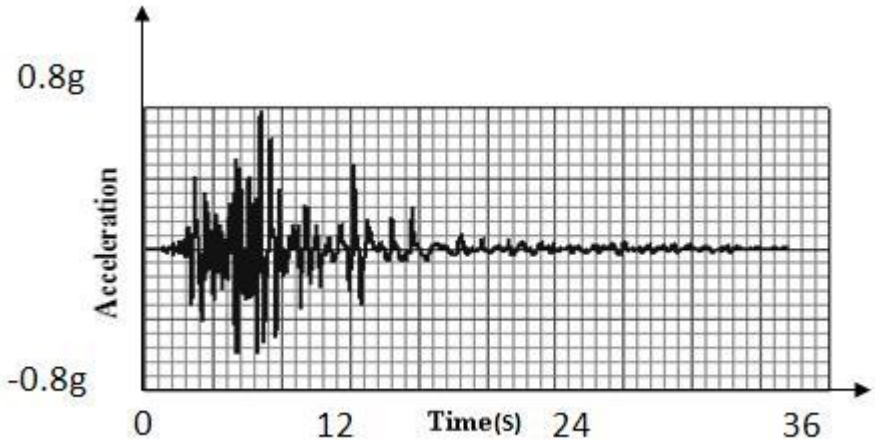


**Figure 4.5** Imperial Valley-1979 acceleration vs. time graph

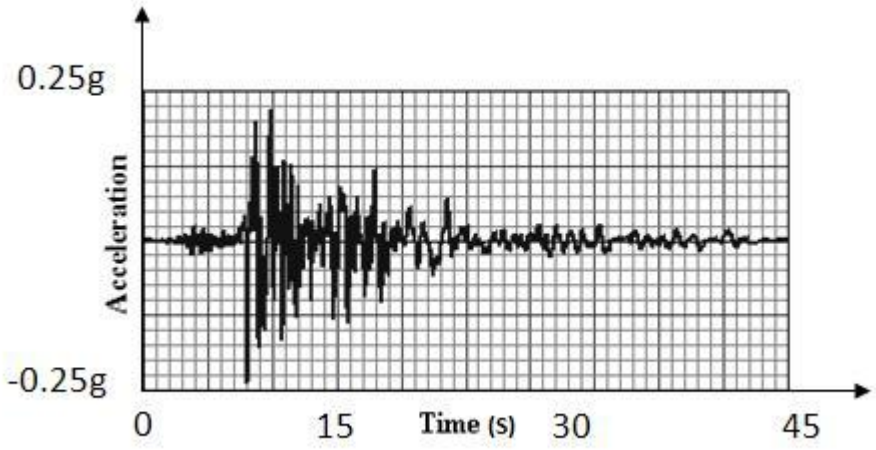


**Figure 4.6** Coalinga-1983 acceleration vs. time graph

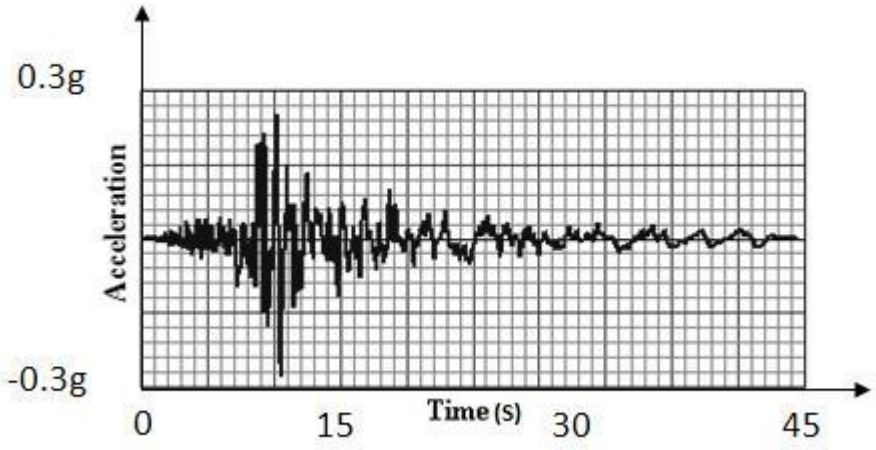


**Figure 4.7** Loma Prieta -1989 acceleration vs. time graph

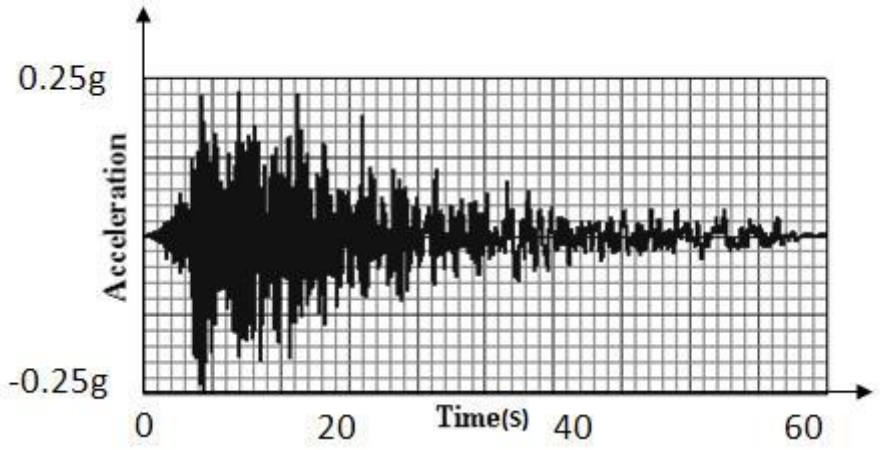


**Figure 4.8** Imperial Valley-1979 acceleration vs. time graph

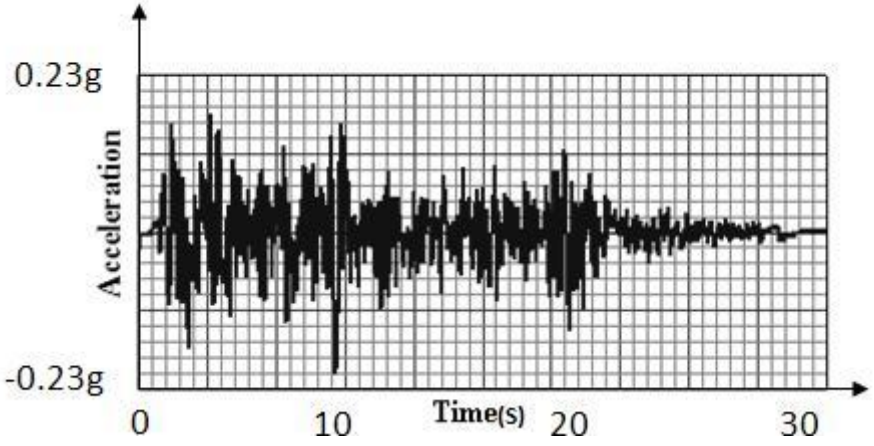


**Figure 4.9** Imperial Valley-1940 acceleration vs. time graph

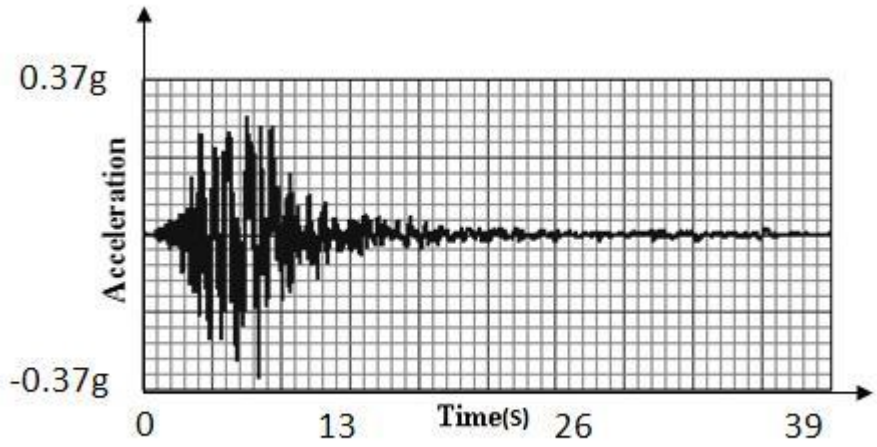


**Figure 4.10** Westmore Land-1981 acceleration vs. time graph

**Table 4.8** Scale factors of the earthquakes used in the analyses of the school building

| Earthquake | General Scale Factors(g) | | |
|---|---|---|---|
| | 2% | 10% | 50% |
| IMPERIAL VALLEY 1979 | 2.56 | 1.80 | 1.15 |
| COALINGA 1983 | 2.68 | 1.88 | 1.21 |
| WESTMORLAND 1981 | 1.65 | 1.16 | 0.74 |
| LOMA PRIETA 1989 | 2.18 | 1.53 | 0.98 |
| WHITTIER NARROWS 1987 | 2.04 | 1.43 | 0.92 |
| IMPERIAL VALLEY 1940 | 2.83 | 1.99 | 1.27 |
| IMPERIAL VALLEY 1979 | 0.79 | 0.55 | 0.35 |

**Table 4.9** Scale factors of the earthquakes used in the analyses of the office building

| Earthquake | General Scale Factors(g) | | |
|---|---|---|---|
| | 2% | 10% | 50% |
| IMPERIAL VALLEY 1979 | 1.61 | 1.21 | 0.72 |
| COALINGA 1983 | 1.69 | 1.27 | 0.75 |
| WESTMORLAND 1981 | 1.04 | 0.78 | 0.47 |
| LOMA PRIETA 1989 | 1.38 | 1.03 | 0.61 |
| WHITTIER NARROWS 1987 | 1.28 | 0.96 | 0.57 |
| IMPERIAL VALLEY 1940 | 1.79 | 1.34 | 0.80 |
| IMPERIAL VALLEY 1979 | 0.50 | 0.37 | 0.22 |

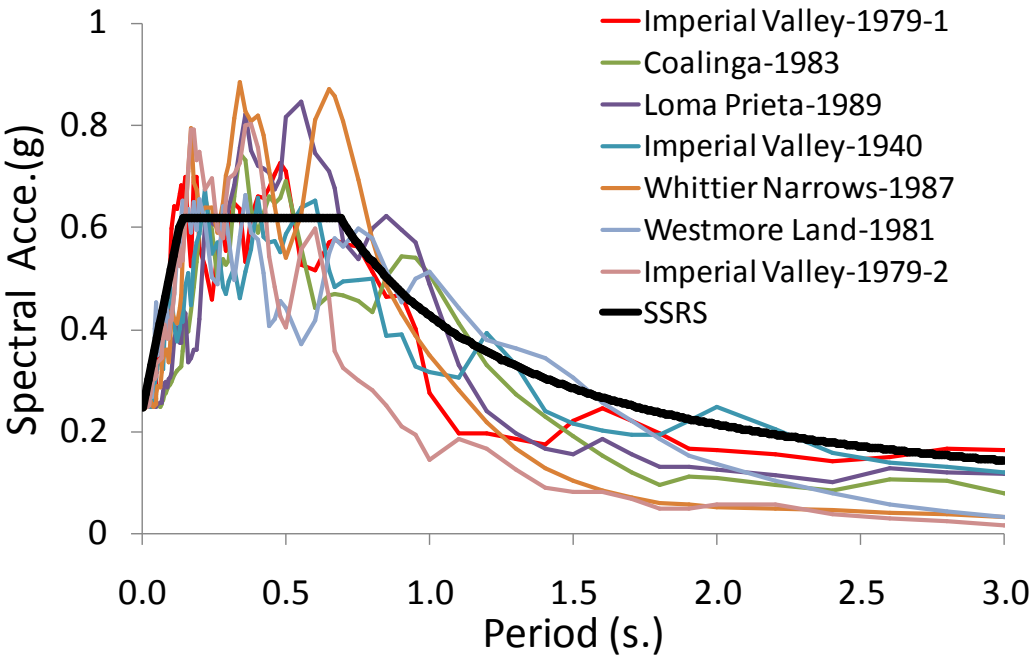


**Figure 4.11** Design spectrum and acceleration spectra of the ground motions scaled to the PGA of the design spectrum

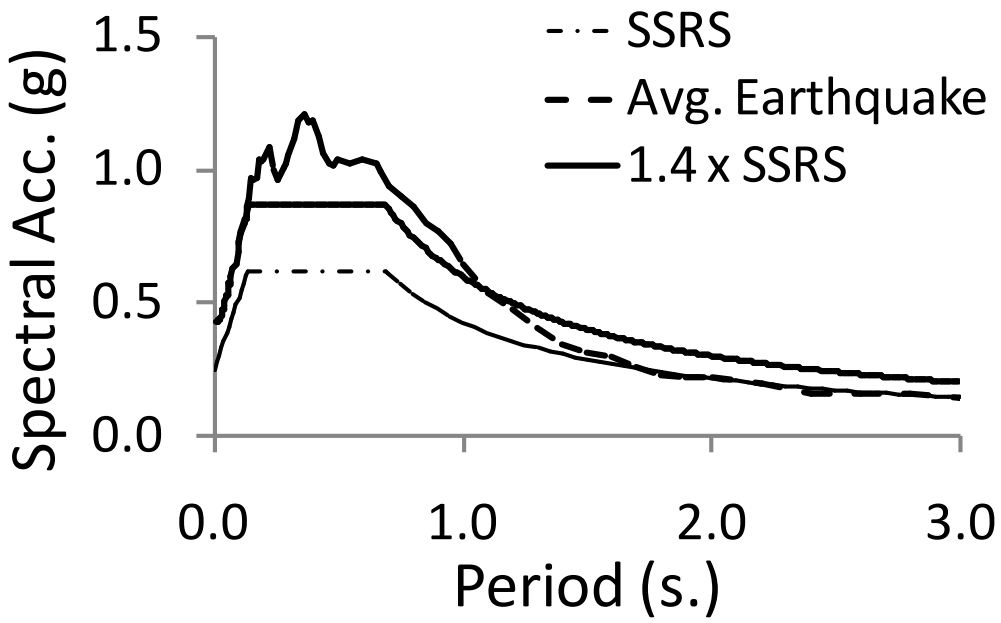


**Figure 4.12** Comparison of the average of the scaled earthquake ground motions with the design spectrum and 1.4 x the design spectrum.

# CHAPTER 5

# NONLINEAR MODELLING OF EXISTING BUILDINGS

## 5.1 Introduction

A number of nonlinear structural analyses were conducted to assess the seismic performance of the original and retrofitted example buildings used in this research study. For this purpose, nonlinear structural models of the original and retrofitted example buildings were built. The nonlinear structural models of the example buildings used in this study include reinforced concrete beams and columns, joints connecting these structural members as well as brick masonry infill walls. In addition, the structural model for the conventionally retrofitted example buildings contain squat infill shear walls while the structural model for the buildings retrofitted using the proposed method contain steel panels composed of steel frame elements, a shear link and chevron braces. In the subsequent sections the modeling procedure for the aforementioned structural elements and the structure as a whole will be given in detail.

Another important point to be considered is the capabilities of the software, which is used for the nonlinear modeling and analyses of the example buildings. In this study, the finite element based software SAP2000 v11.04 (Computers and Structures, Inc 2006) is used for the structural modeling of the example buildings. Several assumptions and simplifications were made in the structural modeling of the example buildings to facilitate the nonlinear analyses and to match the capabilities of the software. The effects of these modeling assumptions and simplifications are illustrated by comparative nonlinear analyses of small scale and full scale structural models. In all of the cases, the effects of these assumptions and simplifications were found to be negligible. Detailed

information about these modeling assumptions and simplifications will be given in the subsequent sections.

## 5.2. General Features of the Structural Models

A three dimensional structural model of the school building and two dimensional structural model of the office building are built and analyzed using the program SAP2000 (2006). For the office building, a two dimensional structural model is preferred due to the nearly symmetrical configuration of the building and convergency problems associated with large number of degrees of freedom in the nonlinear analyses of the three dimensional structural model. The structural models of the original buildings are shown in Figures 5.1 and 5.2 while the structural models of the retrofitted buildings using the proposed and conventional methods are shown respectively in Figures 5.3 and 5.4 for the school building and Figures 5.5 and 5.6 for the office building. These structural models are capable of simulating the nonlinear behavior of the structural components. The reinforced concrete beams and columns as well as the components of the steel panel used for seismic retrofitting of the buildings are modeled using three dimensional elastic beam elements. The masonry infill brick walls are modeled using diagonal beam elements with end moment releases while the infill squat shear walls are modeled using a combination of rigidly connected two horizontal and one vertical elastic beam elements. The nonlinear behavior of the structural members are simulated by using nonlinear link/hinge (link for NLTH and hinge for NLP analyses) elements connected at appropriate locations or at the ends of the elastic beam elements as shown in Figure 5.7(a) for reinforced concrete columns and beams, 5.7(b) for brick masonry infill walls, 5.7(c) for the proposed steel panel and 5.7(d) for squat infill shear panels.

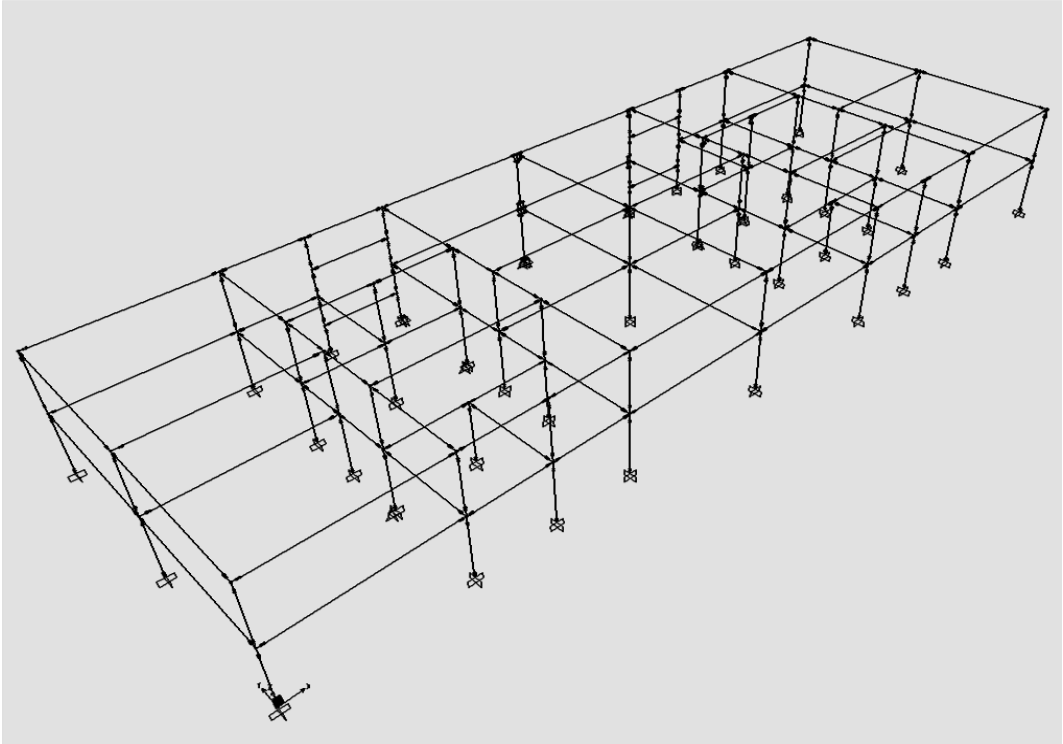

**Figure 5.1** Structural model of the original school building

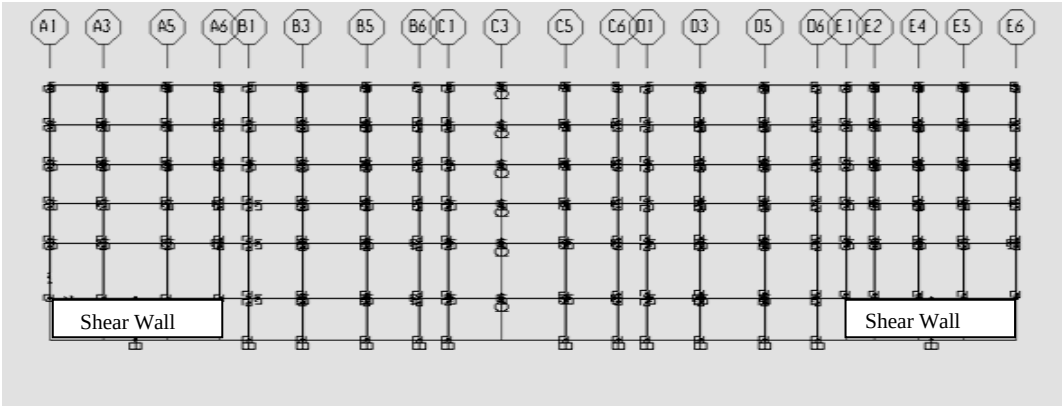


**Figure 5.2** Structural model of the original office building in x-direction

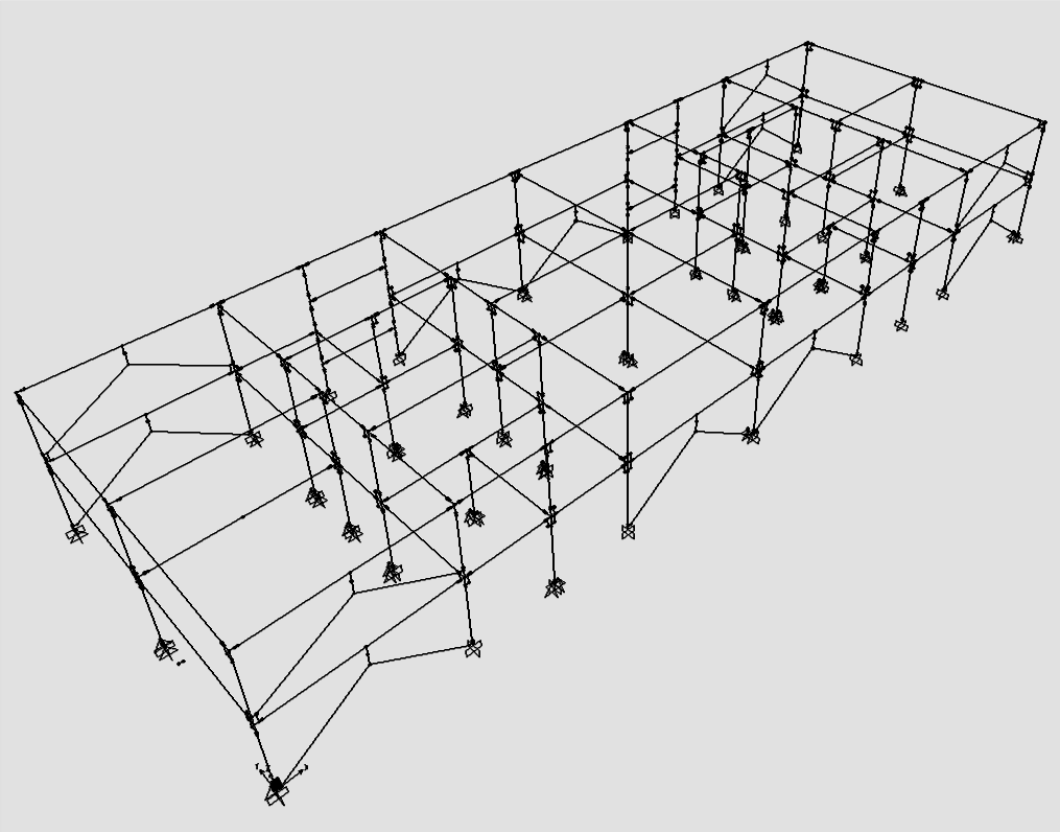

**Figure 5.3** Structural model of the school building retrofitted with the proposed method

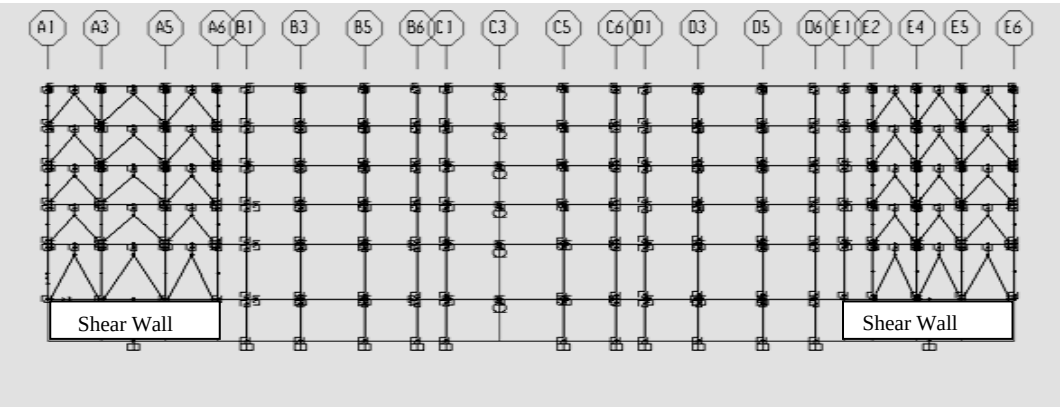


**Figure 5.4** Structural model of the office building retrofitted with the proposed method in x- direction

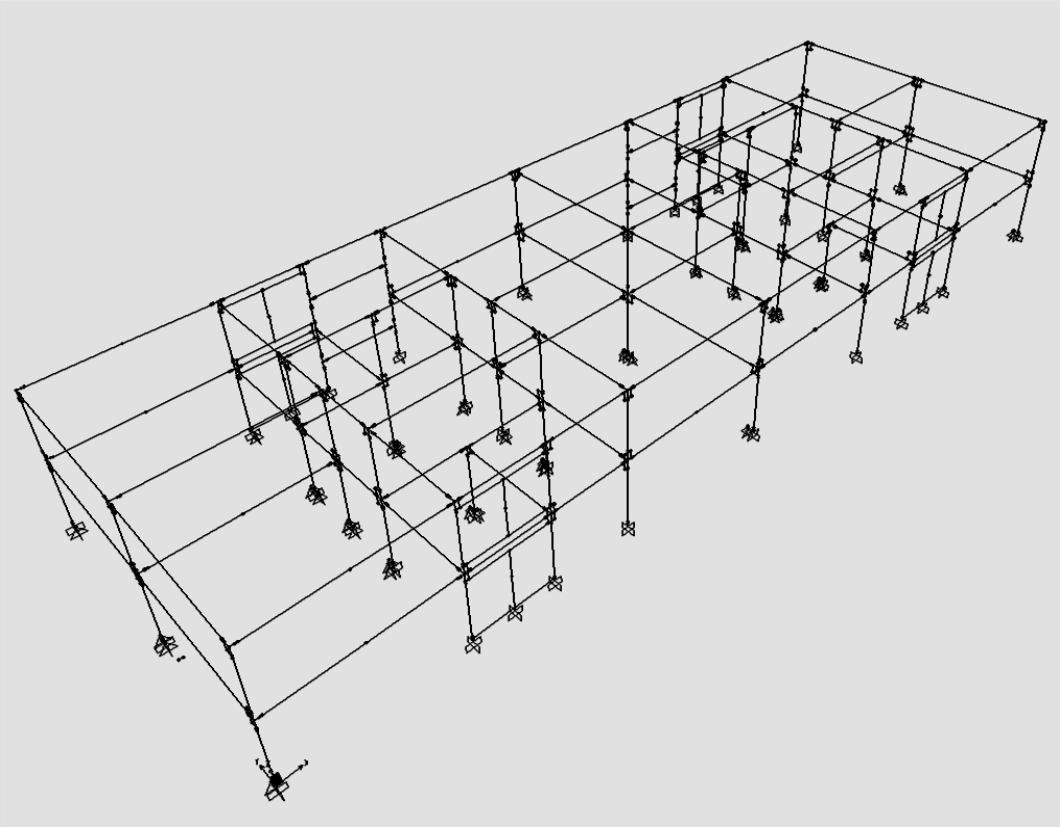

**Figure 5.5** Structural model of the school building retrofitted with the conventional method

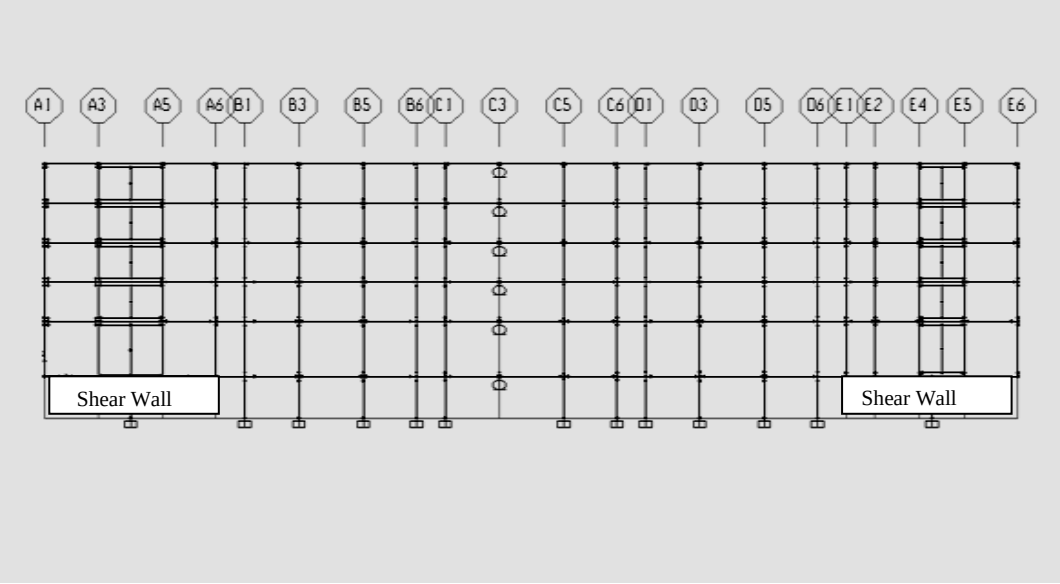


**Figure 5.6** Structural model of the office building retrofitted with the conventional method

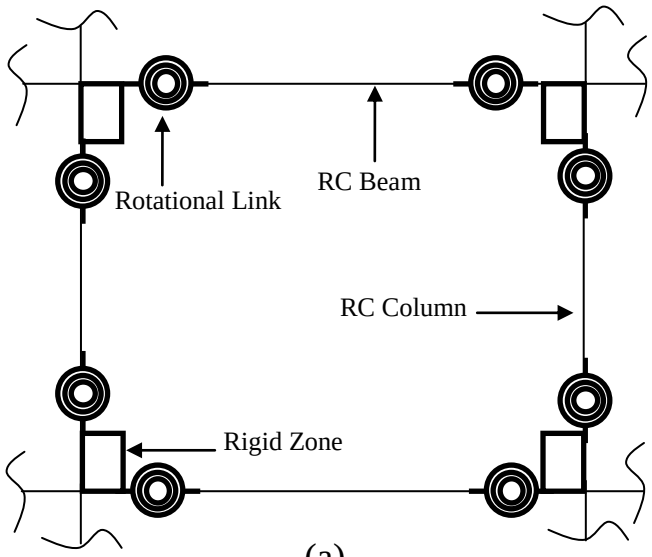
Rotational Link
RC Beam
RC Column
Rigid Zone

(a)

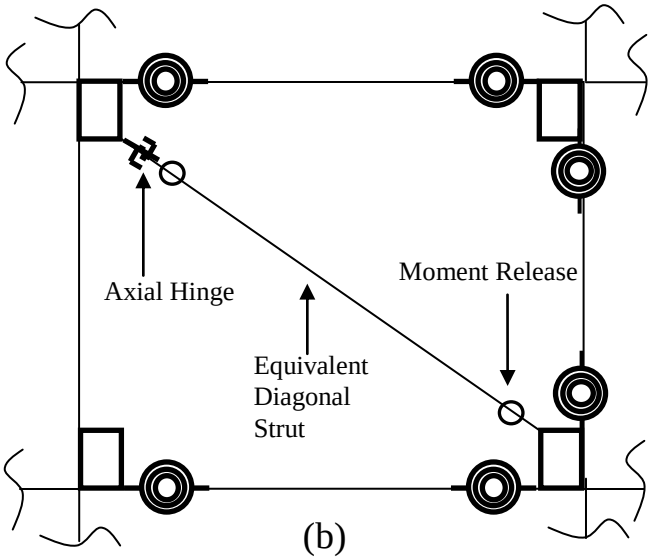
Axial Hinge
Moment Release
Equivalent
Diagonal
Strut

(b)

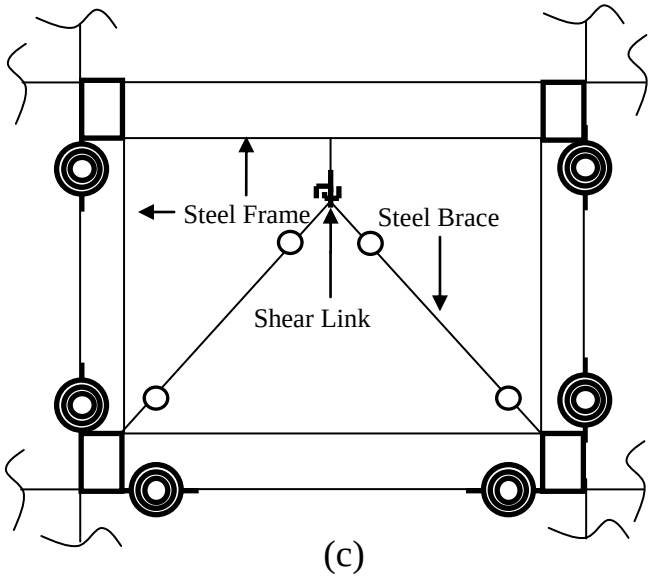
Steel Frame
Steel Brace
Shear Link

(c)

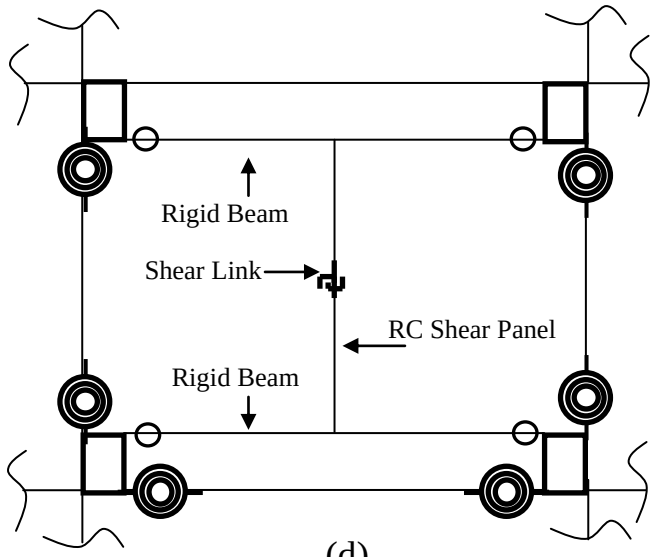


(d)

RC: reinforced concrete

**Figure 5.7** Nonlinear link elements and other structural elements used in the nonlinear modeling of example building: (a) reinforced concrete frame, (b) BMI wall, (c) proposed seismic retrofitting method, (d) squat infill shear panel

## 5.3. Modeling of the Reinforced Concrete Columns and Beams for NLTH Analyses

### 5.3.1 Selection of Hysteresis Model

Tests of reinforced concrete members under lateral load reveals indicate that their inelastic deformations are mainly composed of those due to flexure, shear and anchorage slip (Saatçioğlu and Özcebe, 1989). While deformations due to shear forces may be small in slender structural members such as beams and columns (due to their relatively long shear spans), the flexural deformations in such members are generally significant. Therefore, in this study the deformations of the beams and columns due to shear are neglected. Accordingly, the nonlinear behavior of the reinforced concrete columns and beams of the example buildings used in this study are defined in the structural model by using nonlinear flexural

link elements at the ends of the structural members. The nonlinear behavior of these link elements is defined by various hysteresis models. A variety of hysteresis models defining the nonlinear behavior of reinforced concrete members are available in the literature (Clough, 1966; Takeda et al. 1970; Jirsa et al.1999). Among these hysteresis models, Takeda et al.'s (1970) hysteresis model is the most commonly accepted one for defining the nonlinear flexural behavior of reinforced concrete members (İlki and Kumbasar, 2000). Moreover, Takeda et al.'s (1970) hysteresis model is a realistic theoretical model which recognizes the continually varying stiffness and energy absorbing characteristics of reinforced concrete members (Takeda et al. 1970) under moment reversal. Therefore, the hysteresis model proposed by Takeda et al. (1970) was used to model the nonlinear cyclic flexural behavior of the reinforced concrete beam and column elements of the example buildings used in this study. Figure 5.8 shows Takeda et al.'s (1970) hysteretic model. Figure 5.9 shows a sample hysteretic curve taken from NLTH analyses performed in this study. The Takeda et al.'s (1970) model uses the monotonic moment curvature (or rotation) relationship of the reinforced concrete section as a backbone curve. Therefore, an accurate estimation of the moment curvature relationship is important to correctly simulate the nonlinear cyclic behavior of a reinforced concrete member. In the following section the procedure followed to obtain the moment curvature relationship of the reinforced concrete members is explained in detail.

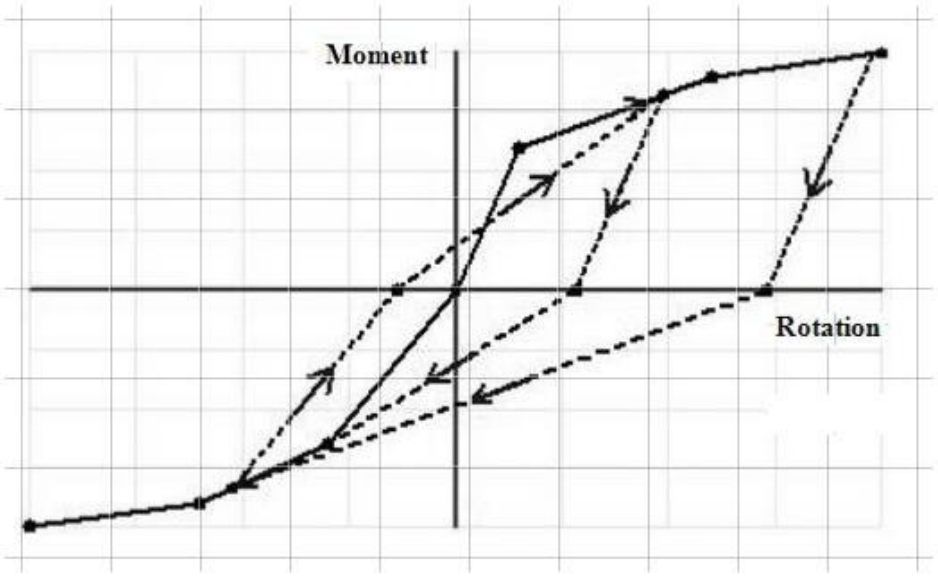


**Figure 5.8** Typical Takeda Hysteresis Loop

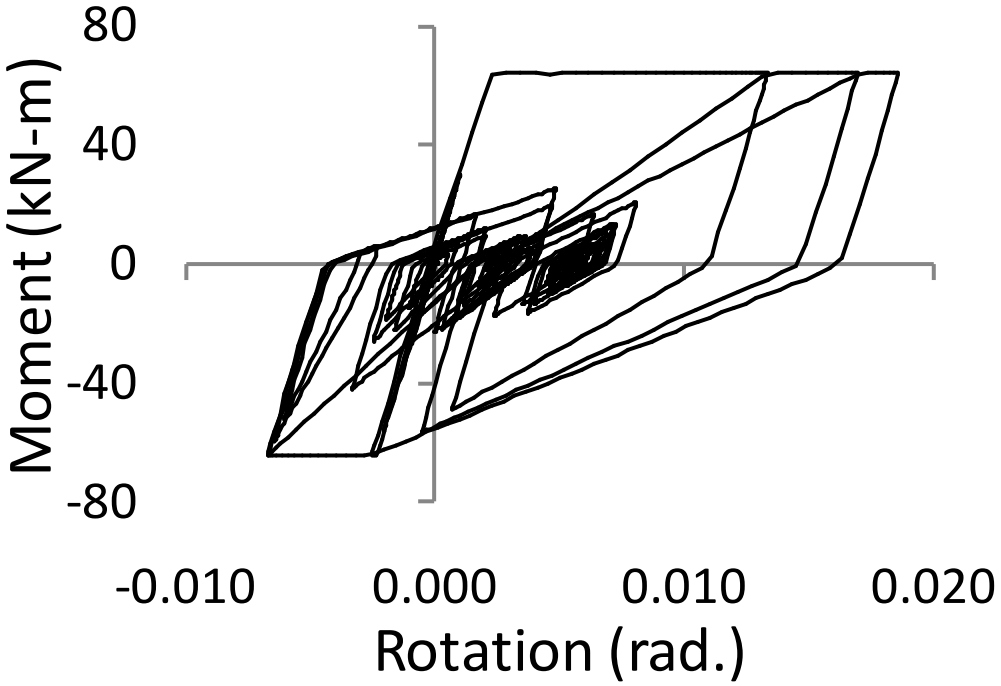


**Figure 5.9** A sample hysteresis loop taken from NLTH analyses

### 5.3.2 Moment Rotation Relationship for the Hysteresis Model

Takeda et al.'s (1970) hysteresis relationship requires the monotonic moment rotation relationship of the reinforced concrete member to define the envelope curve used in the hysteresis model. In this study, a computer software that was developed by Yalçın and Saatçioğlu (2000) was used to obtain the inelastic moment-rotation relationship of the reinforced concrete columns and beams of the example buildings used in this study. The software, referred to as COLumn Analysis (COLA), provides sectional moment-curvature analyses and member analyses, including the P-Δ effects, buckling and anchorage slip of the reinforcement bars. The material models used in this study, include a model for unconfined and confined concrete, and a model for reinforcing steel. The model used for concrete was developed by Saatcioglu and Razvi (1992). The model is shown in Figure 5.10. The concrete material model is valid for unconfined and confined concretes. For unconfined concrete, it reduces to Hognestad's (1951) concrete model with an ascending branch described by a second-degree parabola, and a descending branch linearly changing to a strain corresponding to 20% of the peak (Yalçın and Saatçioğlu, 2000). When the reinforced concrete element is well confined, the characteristics of stress-strain curve change. Confinement produces significant enhancements in strength and ductility of the reinforced concrete member (Yalçın and Saatçioğlu, 2000). The expressions that are developed for ascending and descending branches of the confined concrete model can be found in the related literature (Yalçın and Saatçioğlu, 2000; Saatcioglu and Razvi, 1992).

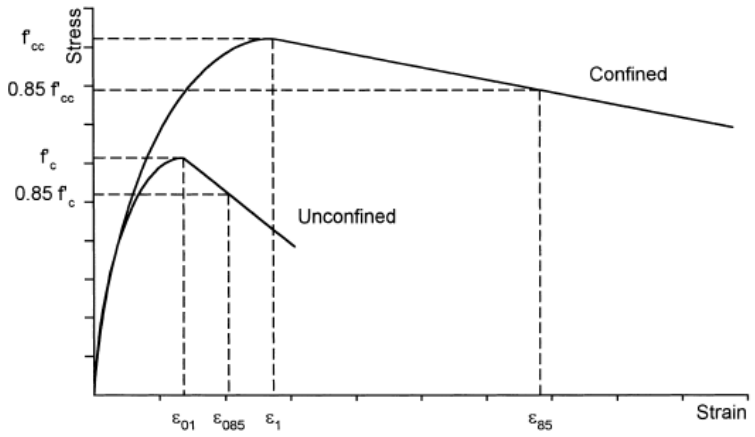


**Figure 5.10** Material models for unconfined and confined concrete (Saatçioğlu and Razvi, 1992)

While the stress-strain characteristics of steel are the same in tension and compression, the model for compression reinforcement in the program COLA also includes the buckling of the reinforcing bars in compression (Yalçın and Saatçioğlu, 2000). In this study, the stress-strain relationship for the reinforcing steel is conservatively assumed to be elasto-plastic both in compression and tension. However, depending on the size of the compression bars and the spacing of stirrups, the stress-strain relationship in compression can be quite different due to buckling effects. Under unfavorable lateral confinement conditions, the compression reinforcement can lose its stability prior to developing full strain-hardening (Yalçın and Saatçioğlu, 2000). Stress-strain relationship of reinforcing steel in compression is given in Figure 5.11 (Yalçın and Saatçioğlu, 2000). The stability of the curve depends on the aspect ratio of the reinforcing bar, which is defined as the ratio of the unsupported bar length between two ties to its diameter (Yalçın and Saatçioğlu, 2000). The aspect ratio of 8.0 is taken as the limit value for stability of steel bars, where the reinforcement can maintain its stability with zero slope upon yielding (Figure 5.11). For aspect ratios greater than 8.0, the slope becomes negative as shown in Figure 5.11 (Yalçın and Saatçioğlu, 2000; Mau et al. 1989; Mau, 1990)

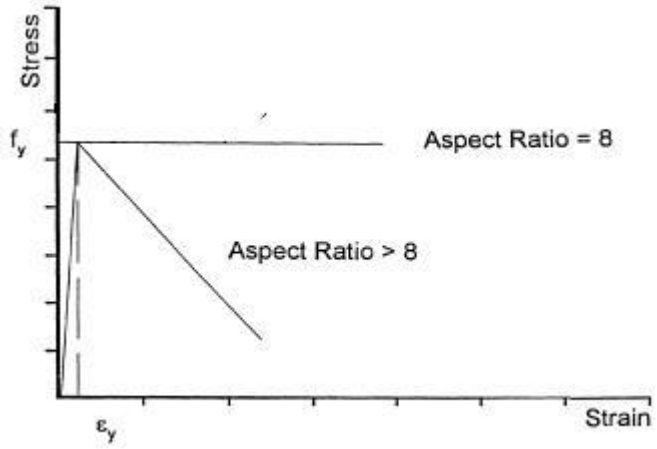


**Figure 5.11** Material models for unconfined and confined concrete (Saatçioğlu and Razvi, 1992)

Deformations originated from penetration of yielding into the adjacent member may be significant which reduces the stiffness of the reinforced concrete sections and members. These deformations consist of slippage and/or extension of reinforcement bars within the adjacent member (Yalçın and Saatçioğlu, 2000). Deformations originated from anchorage slip are considered in the program COLA by using the height ($H_L$) and spacing ($S_L$) of the lugs on the steel bars and the compressive strength of concrete ($f_c$ in Mpa) as input data. These variables define the bond stress, $U_f$, between the reinforcement bars and concrete that is given by Equation 5.1 (Yalçın and Saatçioğlu. 2000)

$$U_f = \left(5.5 - 0.07\frac{S_L}{H_L}\right)\sqrt{\frac{f_c}{27.6}} \qquad (5.1)$$

The reinforcement steel that is used in the construction of the selected buildings was composed of plain bars. These plain bars obviously do not have any lugs. Consequently, it was not possible to determine the parameters $S_L$ and $H_L$ required by the program to include the effect of anchorage slip in the moment curvature analyses. To overcome this difficulty, tabulated values of bond stress for plain bars were found in the literature (BS-8110, 1985). A nonlinear curve fitting

technique is then used on the tabulated bond stress values given in Table 5.1 to obtain a power function (Figure 5.12) defining the bond stress for plain bars as a function of the concrete strength. Next, for the concrete strength used in the example buildings, the corresponding bond stress is obtained and substituted in Equation 5.2 to calculate fictitious values of $S_L$ and $H_L$. These values are then used as input data in the program COLA to take into consideration the effect of anchorage slip on the moment curvature relationship of the reinforced concrete members of the example buildings used in this study.

**Table 5.1** Bond stress values vs. bar type and concrete grade (BS-8110 1985)

| Bar Type | Concrete grade | | | |
|---|---|---|---|---|
| | 20 ($N/mm^2$) | 25 ($N/mm^2$) | 30 ($N/mm^2$) | 40 or more ($N/mm^2$) |
| Plain bar in tension | 1.3 | 1.4 | 1.5 | 1.8 |
| Plain bar in compression | 1.6 | 1.8 | 1.9 | 2.2 |

Figure 5.12 shows the data used to obtain the bond stress value for poor grade concrete. Afterwards, The required lug height and lug spacing values were selected to satisfy the bond stress value obtained by curve fitting procedure.

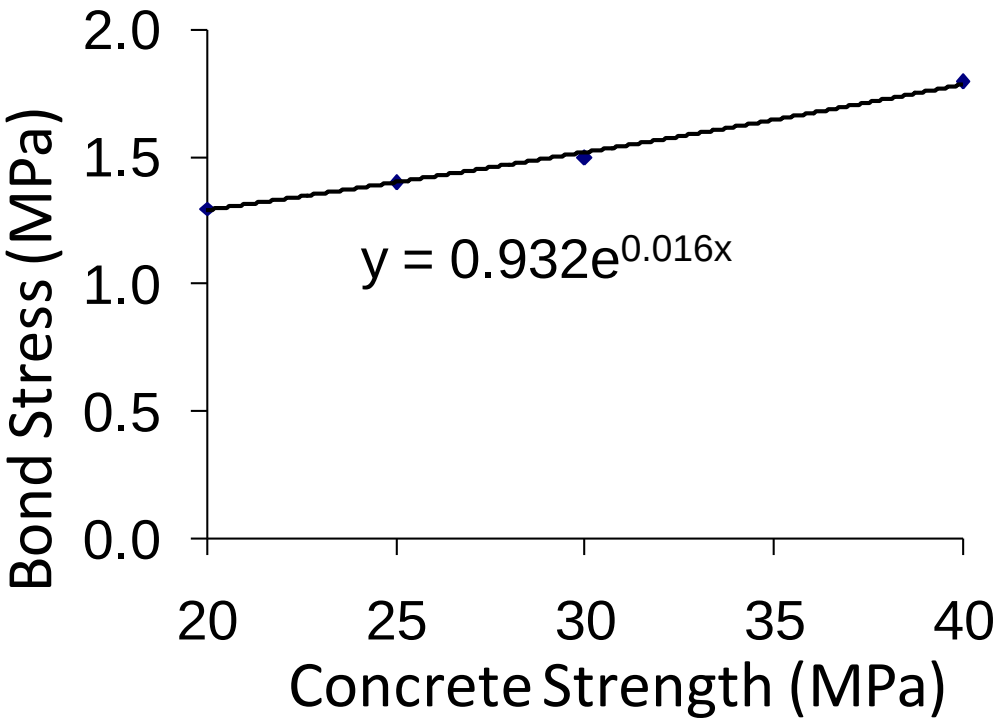


**Figure 5.12** Curve fitting data to obtain bond stress

### 5.3.3 Failure Criteria for Columns and Beams

A reinforced concrete section may fail either due to rupture of reinforcing steel in tension or crushing of concrete in compression. If the spacing of the transverse reinforcement is sufficient to confine the concrete, the crushing of the concrete compression fibers simultaneously occur with the rupture of the transverse reinforcement. If the concrete is not confined well enough, the crushing of the concrete in compression occurs before the rupture of the transverse reinforcement. The strain limit for the rupture of transverse reinforcements is defined by the following Equation (Priestley et al. 1996).

$$\varepsilon_{cu} = 0.004 + \frac{1.4\rho_s \varepsilon_{su}}{f_{cc}^{'}} \quad (5.2)$$

where $\rho_s$ is the sum of the volumetric ratios of the transverse reinforcement in both orthogonal directions ( $\rho_x + \rho_y$ ) for rectangular sections, $f_{yh}$ is the yield strength of transverse steel, $\varepsilon_{su}$ is the transverse reinforcing steel strain at maximum stress and $f_{cc}^{'}$ is the confined concrete strength.

Equation 5.2 is suitable for reinforced concrete sections under the effect of axial loading. For reinforced concrete sections under the combined effect of axial loads and bending moments (this is the case for reinforced concrete columns) the results given by Equation 5.2 must be factored by two (Priestley et al. 1996).

As previously stated, the buckling of the longitudinal reinforcement bars is also considered in the sectional moment-curvature analyses. If buckling of a longitudinal bar occurs, the program COLA (Yalçın and Saatçioğlu, 2000) continues the sectional moment-curvature analyses with zero resistance assigned to the buckled bar. Sample moment curvature relationships of reinforced concrete beam and column elements obtained from the program COLA are shown in Figure 5.13

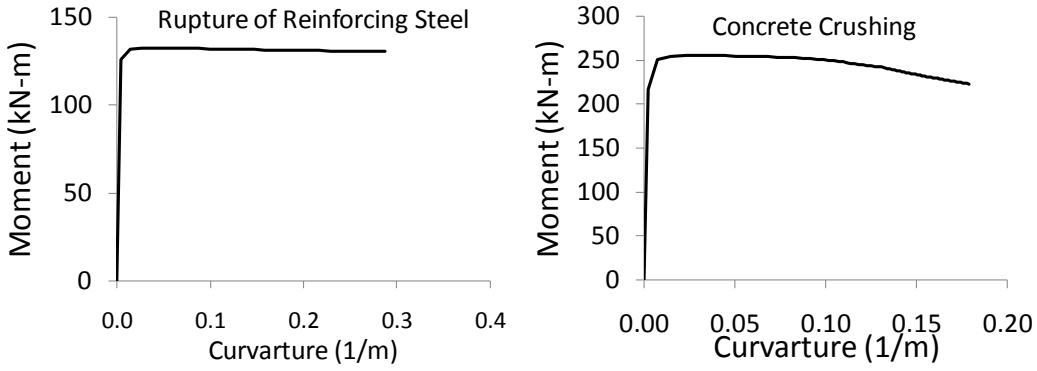


**Figure 5.13** Sample moment curvature relationships obtained from the program COLA

## 5.4 Modeling of the Reinforced Concrete Columns and Beams for NLP Analyses

The structural model used for NLP analyses is similar to that of NLTH analyses. The only difference is that hinge elements are used at member ends instead of link elements. The monotonic moment rotation relationships used to define the nonlinear behavior of the hinge elements is obtained from the results of the moment curvature relationships described in the above section.

.

## 5.5 Modeling of Reinforced Concrete Squat Infill Shear Panels for NLTH Analyses as Part of Conventional Seismic Retrofitting

### 5.5.1. Hysteretic Behavior of Squat Infill Shear Panels

Squat infill shear panels were used for the conventional seismic retrofitting of the example buildings employed in this research study. Squat infill shear panels are structural elements where shear behavior is more dominant. Pinching, which is a common phenomenon in the hysteretic behavior of reinforced concrete members, is more pronounced in the hysteretic shear force-deformation relationships of squat infill shear panels (Saatçioğlu and Humar, 2003). Hysteresis loops of reinforced concrete squat infill shear panels generally show a distinct alteration in slope during reloading (Saatçioğlu and Humar, 2003). The alteration in slope in concrete elements is related with opening and closing of cracks under cyclic shear loading (Saatçioğlu and Humar, 2003). Following a crack caused by a load in one direction, reversed loading in the opposite direction meets with little initial resistance as the crack closes. Afterward, the cracked surfaces come in full contact, increasing the load resistance. This phenomenon is reflected in the force–deformation relationship as a change in slope during reloading and is known as pinching of hysteresis loops (Saatçioğlu and Humar, 2003). If the cracks are inclined diagonal tension cracks, as in the case of the shear response of squat infill shear panels, some sliding occurs between the cracked surfaces before they come

in full contact (Saatçioğlu and Humar, 2003). Also, the slippage of reinforcing bar in the vicinity of a crack results in increased deformations with very low resistance in the opposite direction as the reinforcement slips back to its previous position before the crack is completely closed and full resistance is attained. Effect of pinching on the hysteretic behavior of reinforced concrete elements is shown in Figure 5.14. Pinching effect reduces the area under the hysteresis loop and hence, the energy dissipated by squat infill shear panels. Consequently, this behavior should be considered in the hysteretic models used for the analysis of squat infill shear panels.

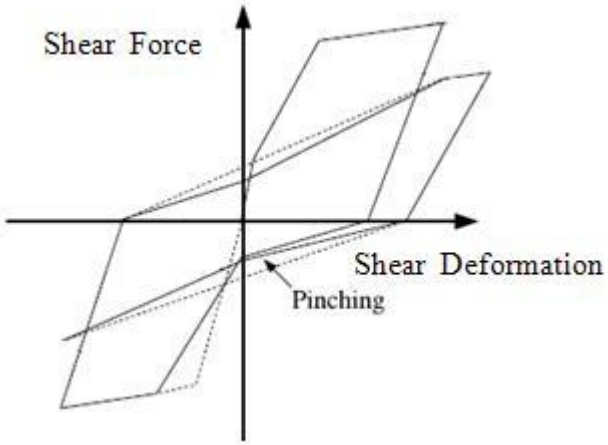


**Figure 5.14** Effect of pinching

In this study, the hysteretic shear behavior of squat infill shear panels was simulated with the pivot hysteresis model (Dowell et al. 1998) available in SAP2000 (2006). This hysteresis model can capture the pinching and stiffness degradation effects in shear dominant elements under cyclic loading. Figure 5.15 shows the Pivot hysteresis model.

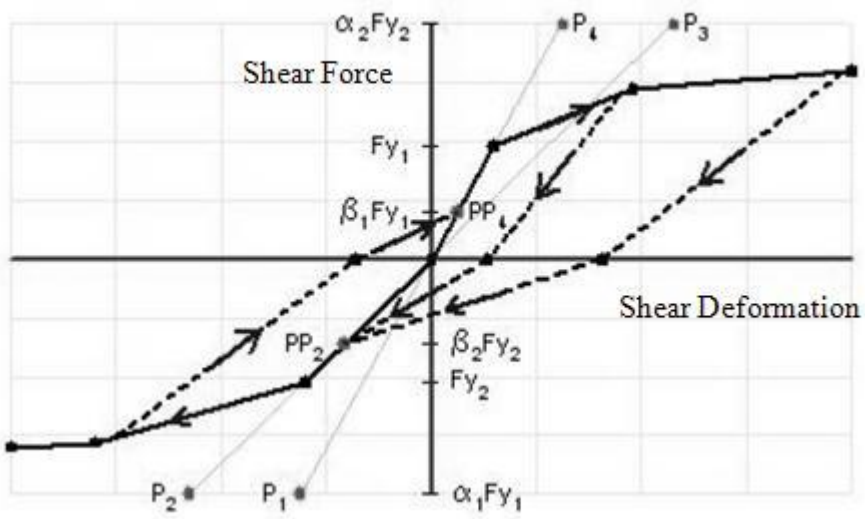


**Figure 5.15** Pivot hysteresis model (CSI Analyses Reference Manual, 2007)

The pivot hysteresis model (Dowell et al. 1998) requires the shear force-deformation envelope as well as two additional parameters for capturing the pinching and stiffness degradation properties of reinforced concrete members. In Figure 5.14, the term "**α**" refers to the stiffness degradation parameter and the term "**β**" corresponds to pinching parameter. In the literature, there are limited reliable data defining these parameters. Lack of analytical tools for defining these parameters forced several researchers to conduct many experimental studies (Aoyama et al.1984; Khan 1976; Hayashi et al. 1980; Sugano et al. 1980; Higashi et al. 1980; Corley et al. 1981; Ogata et al. 1984; Gaynor, 1988; Shah, 1989). Some other researchers have tried to get empirical formulae to define pinching and stiffness degradation for squat infill shear panels (Phan et al. 1993). Nevertheless, these empirical formulae are related to a great extend to the geometric and material properties of the reinforced concrete elements used to derive these empirical equations. This makes these equations impractical to use in nonlinear structural modeling. Hence, a set of test specimens with properties similar to those of the squat infill shear panels used in this study were investigated. Then, the necessary parameters for the shear panels employed in this study are obtained by using the average of the experimental test results from these

research studies(Aoyama et al.1984; Khan, 1976; Hayashi et al. 1980; Sugano et al. 1980; Higashi et al. 1980) Table 5.2 shows the details of the experimental test data used in the analyses.

A typical nonlinear structural model of the squat infill shear panel used in SAP2000 (2006) is given in figure 5.16. The pivot hysteresis relationship (Dowell et al. 1998) is assigned to the nonlinear link element shown in the model.

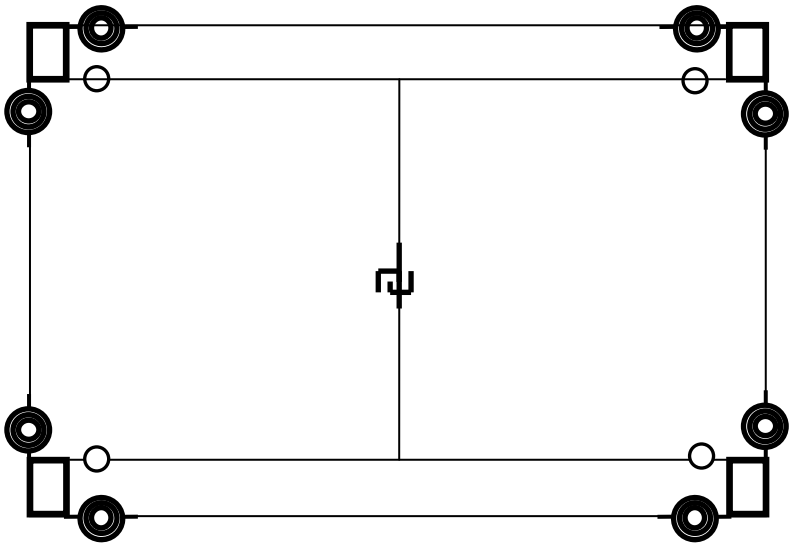

**Figure 5.16** model of the squat infill shear panel

**Table 5.2** Investigated test specimens for pinching and stiffness degradation parameters of squat infill shear panels (Phan et al. 1993).

| Name | Type | Concrete $F_c$ (Mpa) | | Aspect Ratio | Pinching Parameter | Stiffness Deg. | Description |
|---|---|---|---|---|---|---|---|
| | | Frame | Wall | | | | |
| AOYAMA C2005-1 | C.I.P | 23 | 20 | 1.86 | 0.25 | 11.00 | Non Ductile Columns-1950-1960 construction |
| AOYAMA C2005-2 | C.I.P | 23 | 20 | 1.86 | 0.31 | 9.00 | Non Ductile Columns-1950-1960 construction |
| AOYAMA C2005-3 | C.I.P | 22 | 22 | 1.86 | 0.40 | 11.50 | Non Ductile Columns-1950-1960 construction |
| AOYAMA C2015-A | C.I.P | 22 | 15 | 1.86 | 0.50 | 9.00 | Non Ductile Columns-1950-1960 construction |
| AOYAMA C2015-B | C.I.P | 19 | 15 | 1.86 | 0.30 | 7.25 | Non Ductile Columns-1950-1960 construction |
| AOYAMA C2015-C | C.I.P | 40 | 39 | 1.86 | 0.20 | 2.50 | Non Ductile Columns-1950-1960 construction |
| AOYAMA M2005 | C.I.P | 30 | 29 | 1.86 | 0.94 | 12.50 | Non Ductile Columns-1950-1960 construction |
| AOYAMA C4015 | C.I.P | 23 | 29 | 1.65 | 0.32 | 4.00 | Non Ductile Columns-1950-1960 construction |
| KAHN SP3 | C.I.P | 25 | 19 | 1.63 | 0.15 | 7.50 | No transverse reinforcement at joints |
| HAYASHI W4 | C.I.P | 18 | 27 | 1.78 | 0.75 | 11.50 | 1950-1960 Japanese building code provisions |
| HAYASHI W5 | C.I.P | 18 | 30 | 1.78 | 0.35 | 12.50 | 1950-1960 Japanese building code provisions |
| HAYASHI W6 | C.I.P | 18 | 30 | 1.78 | 0.50 | 12.50 | 1950-1960 Japanese building code provisions |
| SUGANO-WHA | C.I.P | 24 | 38 | 1.88 | 0.16 | 4.50 | |
| SUGANO-WCO | C.I.P | 24 | 38 | 1.88 | 0.50 | 12.50 | |
| HIGASHI 2-PW | C.I.P | 17 | 21 | 1.78 | 0.47 | 17.50 | Low column shear reinforcement ratio |
| **Average** | | | | | **0.41** | **9.68** | |

### 5.5.2. Modeling Procedure to Obtain Shear Force Deformation Envelope

The pivot hysteresis model (Dowell et al. 1998) requires the monotonic shear force-deformation relationship of the reinforced concrete squat shear panel to define the envelope curve used in the hysteresis model. For squat infill shear panels, the equilibrium equations and solution for primary curves can be obtained from the softened truss model theory of Hsu and Mo (1985) through an iterative analysis procedure. The stress strain curve for the softened diagonal concrete struts used in the analysis is given in Figure 5.17 (Vechio and Collins, 1993) and the program algorithm for the iterative calculation of envelope curves for squat infill shear panels is given in Figure 5.18 (Mansour et al. 2004) . In the figures $\varepsilon_d$ and $\varepsilon_l$ are the average strains of the element in the corresponding direction, $\alpha$ is the is the angle of the diagonal concrete struts from the vertical axis, $\lambda$ is the coefficient for softening effect, $\sigma_d$ is the stress on the cross section of the diagonal concrete struts, $\tau$ is the average shear stress on the horizontal cross section of the wall, $\gamma$ is the shear distortion in the wall, $\delta$ is the deflection at the top of a shear wall and $\mu$ is the ductility factor. A sample monotonic shear force deformation relationship of a squat infill shear wall is given in Figure 5.19.

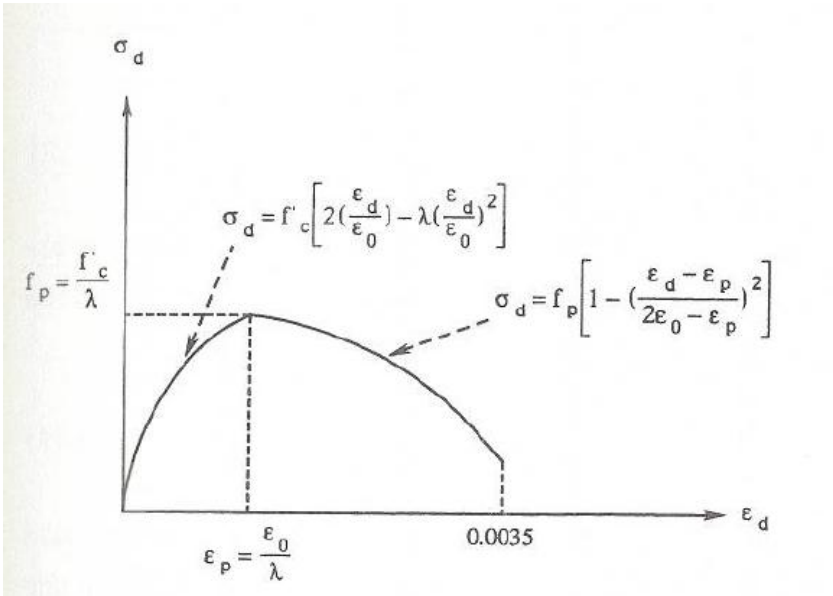


**Figure 5.17** Stress strain curve for the softened diagonal concrete struts

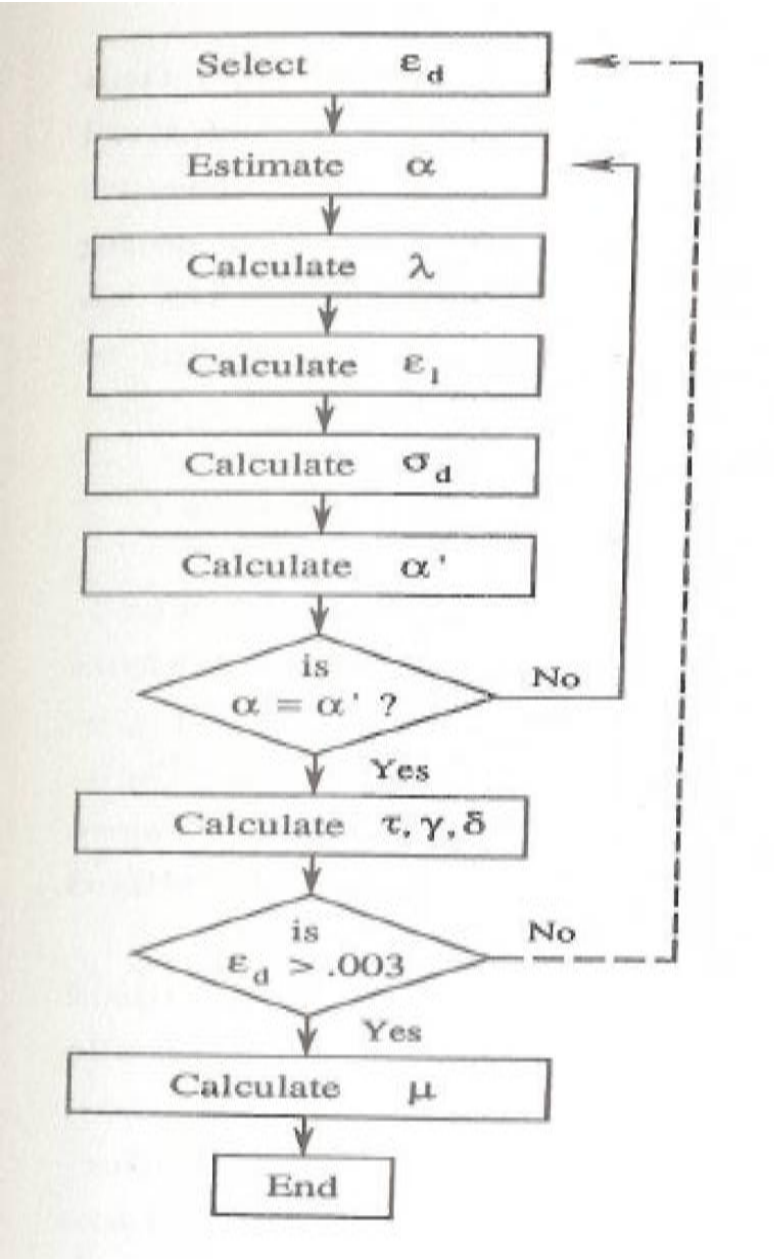


**Figure 5.18** Algorithm for determination of primary curve (Mansour et al. 2004)

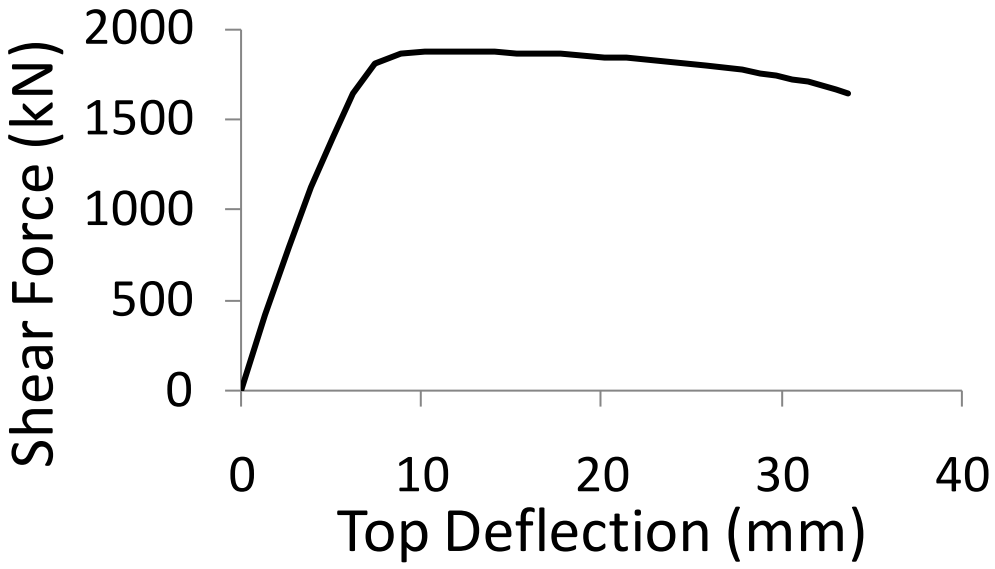


**Figure 5.19** Sample monotonic shear force deformation relationship of a squat infill shear wall

### 5.6 Modeling of Reinforced Concrete Squat Infill Shear Panels for NLP Analyses as Part of Conventional Seismic Retrofitting

The structural model used for NLP analyses is similar to that of NLTH analyses. the only difference is that hinge elements are used instead of link elements. The monotonic shear force-deformation relationships used to define the nonlinear behavior of the hinge elements is obtained from the results of Subsection 5.5.2

.

### 5.7. Modeling of Reinforced Concrete Joints for NLP and NLTH Analyses

Reinforced concrete beam-column joints are rigid zones in the structural systems. This rigidity must be modeled by a realistic modeling approach. For this purpose, the beam-column joints in the structural models in this study were modeled with rigid elements which have higher modulus of elasticity than other reinforced concrete elements. Figure 5.20 shows a typical beam column joint.

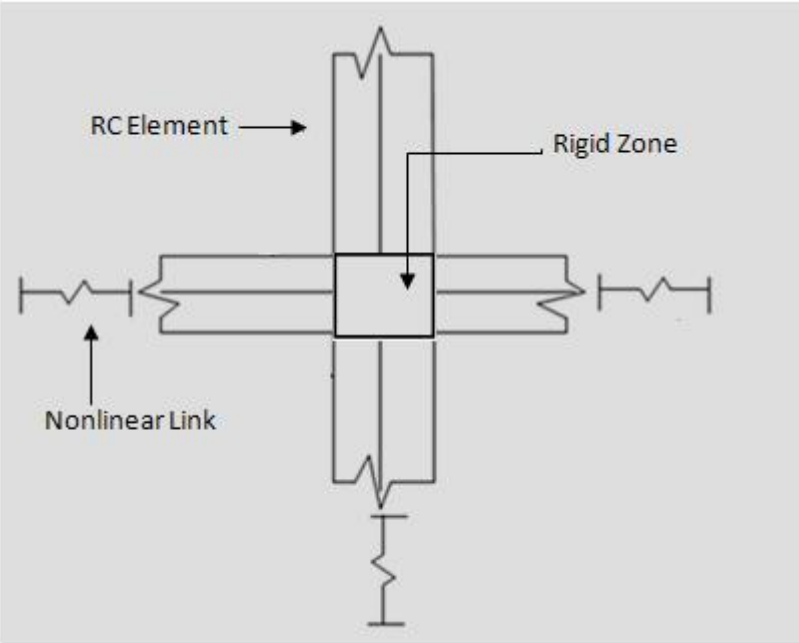


**Figure 5.20** A typical beam-column joint model

## 5.8. Modeling of Brick Masonry Infill Walls for NLP Analyses

### 5.8.1 Importance of Brick Masonry Infills in Structural Analysis and Design

A large number of buildings are constructed with brick masonry infills (BMIs) for serviceability or architectural needs or aesthetics reasons (Madan et al. 1997). Since they are usually considered as non structural elements, their interaction with the supporting frame is often ignored. However, when subjected to a strong lateral load, infill panels tend to interact with the supporting frame and may induce a load resistance mechanism that is not accounted for in the design (Mehrabi et al. 1997). Clearly, such an assumption may lead to substantial inaccuracy in predicting the lateral stiffness, strength and ductility of the structure. If the BMI fails partially or totally, the large earthquake forces previously attracted and carried by the stiff infilled frame will be suddenly transferred to the more flexible reinforced concrete frame (El-Dakhakhni et al. 2003) resulting in damage. In addition to that, change in stiffness distribution can result in larger seismic forces

in some structural components due to torsional effects (El-Dakhakhni et al. 2003). Another detrimental effect of neglecting the presence of the brick masonry infills is the soft story effect. In many areas, the lower stories of buildings have been used as shops. For commercial and aesthetics concerns the BMIs at these lower stories were replaced by shop windows. This type of construction causes the soft story effect in structures where BMIs present at upper stories. Figure 5.21 shows a structure damaged at Loma Prieta Earthquake by soft story mechanism occurred due to the constructed garage at the lowest story.

**Figure 5.21** Soft story effect on a building (De Anza College Faculty Web Sites)

### 5.8.2 Current State of Modeling Techniques for Masonry Infills

Knowledge from the recent earthquakes guided the researchers to focus on the appropriate modeling of BMIs. Modeling the behavior of BMIs is quite complex and the presence of window or door holes makes this task even more difficult.

There are some modeling techniques in the literature. The common ground of these techniques is using diagonal struts to model BMIs. The model proposed by El-Dakhakhni et al. (2003) uses three equivalent diagonal struts to model the BMI. Figure 5.22 shows the three strut model of El-Dakhakhni et al. (2003). Smith and Coull (1991) offered a design method for infilled frames based on diagonal compression struts. In their research study, they assumed that the effective width of the diagonal compression strut is equal to one-tenth of the diagonal length of the infill panel.

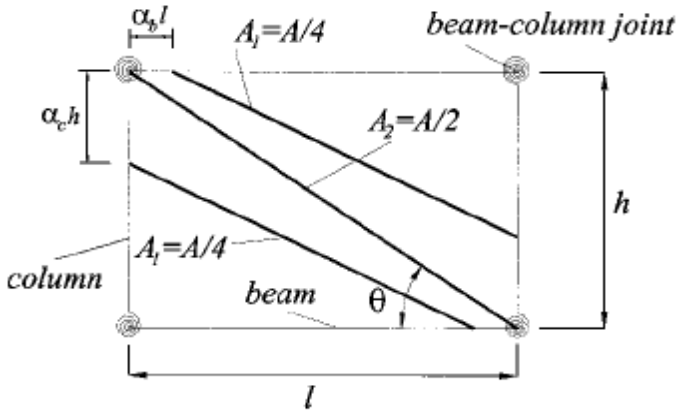


**Figure 5.22** Three struts model (El-Dakhakhni et al. 2003)

FEMA-356 (2000) also recommends an equivalent strut modeling procedure for BMIs. The recommendations of FEMA-356 (2000) for modeling of BMIs vary for the perforated and imperforated cases. Figures 5.23 and 5.24 show the recommendations of FEMA-356 (2000) for modeling of BMIs.

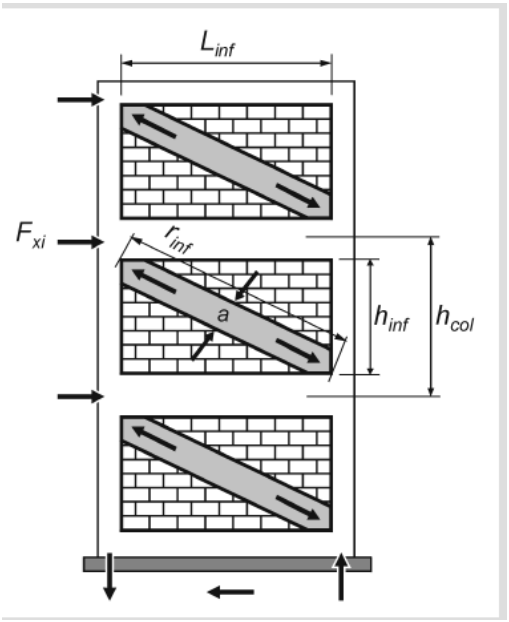


**Figure 5.23** Compression strut analogy for concentric struts (FEMA-356, 2000)

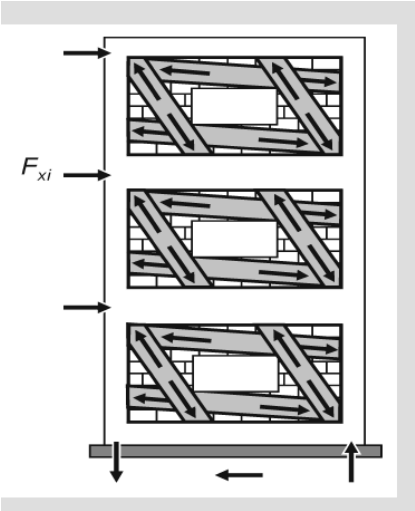


**Figure 5.24** Compression strut analogy for perforated infills (FEMA-356, 2000)

### 5.8.3 Modeling Procedure for Brick Masonry Infills

The method proposed by FEMA 356 (2000) is widely accepted and used by the structural engineering community at large. Therefore, the method proposed by FEMA-356 (2000) is used in this study. The recommended model by FEMA-356

(2000) for perforated infills is not practical to apply. Hence, the stiffness reduction factor proposed by Mosalam (1996) is used to introduce the effect of window/door holes, instead of using FEMA-356 (2000) recommendations. BMI walls in the school building were modeled as equivalent diagonal compression struts for NLP analyses only. In NLTH analyses, including the BMIs in the structural model resulted in convergency problems. However, from the NLP analyses, the BMIs are observed to fail at the initial stages of the building lateral deformation. Therefore, it is expected that neglecting the BMIs in NLTH analyses will not result in significant differences in the nonlinear performance of the structure.

In the NLP analyses, the stiffness, ultimate strength and the lateral deformation capacity of the BMI is required. The lateral stiffness of the BMI is defined as the axial stiffness of an equivalent compression strut. The stiffness of the equivalent compression strut is represented by the following geometric properties; (i) the actual infill thickness that is in contact with the frame ($t_{inf}$), (ii) the diagonal length ($r_{inf}$) of the BMI wall and (iii) an equivalent width, a, given by FEMA-306 (1998):

$$a = 0.175(\lambda_1 h_{col})^{-0.4} r_{inf} \tag{5.3}$$

$$\lambda_1 = \left[\frac{E_{me} t_{inf} \sin 2\theta}{4 E_{fe} I_{col} h_{inf}}\right]^{\frac{1}{4}} \tag{5.4}$$

$h_{col}$ is the column height between centerlines of beams, in.
$h_{inf}$ is the height of infill panel, in.
$E_{fe}$ is the expected modulus of elasticity of frame material, ksi
$E_{me}$ is the expected modulus of elasticity of infill material, ksi
$I_{col}$ is the moment of inertia of column, in 4.
$L_{inf}$ is the length of infill panel, in.
$r_{inf}$ is the diagonal length of infill panel, in.
$t_{inf}$ is the thickness of infill panel and equivalent strut, in.
$\theta$ is the angle whose tangent is the infill height to length aspect ratio in radians

Perforations in the infills such as windows are also taken into account by reducing the stiffness of the diagonal compression strut with a stiffness reduction factor related to the opening ratios (ratio of opening area to total infill area) in the infills (Mosalam, 1996). The stiffness reduction factors for introducing the effect of opening on the modeling of BMIs are obtained from Figure 5.25 (Mosalam, 1996). The BMIs, which have opening areas greater than 20% of the total infill area, are neglected in the modeling of the school building.

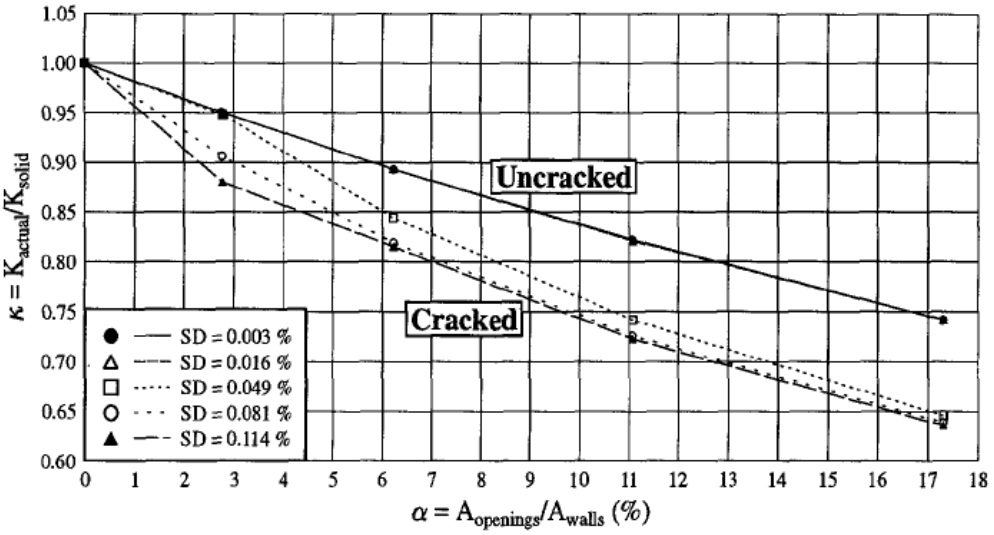


**Figure 5.25** Graph of stiffness reduction factor for BMIs (Mosalam, 1996)

According to FEMA-306 (1998) there are four main failure modes for BMIs. These are; (i) sliding shear failure (may occur from the weakest section in horizontal by sliding), (ii) compression failure (may occur by compression failure of the equivalent diagonal strut), (iii) diagonal tension failure and (iv) general shear failure. The stated four failure modes for BMIs are considered and the one that gives the minimum shear force capacity is taken as the ultimate capacity, $V_{inf}$, of the BMI. The analytical formulation of ultimate capacity at each failure mode is given below.

1. For the sliding shear failure:

$$V_{slide}^{i} = \mu L_{inf} t_{inf} E_m \theta^2 \quad (5.5)$$

where θ is the interstory drift angle, μ is the coefficient of sliding friction along the bed joint.

2. For the compression failure, using the method suggested by Stafford-Smith and Carter. (1969), the horizontal (shear) component of diagonal strut under compression is obtained as:

$$V_c = a t_{inf} f_{m90} \cos\theta \quad (5.6)$$

where $f_{me90}$ is the expected strength of masonry in the horizontal direction, which may be set at 50% of the expected stacked prism strength $f_{me.}$

3. For the diagonal tension failure, using the recommendation of Saneinejad and Hobbs. (1995), the cracking shear in the infill is given by

$$V_{cr} = \frac{2\sqrt{2} t_{inf} \sigma_{cr}}{\left(\frac{L_{inf}}{h_{inf}} + \frac{h_{inf}}{L_{inf}}\right)} \quad (5.7)$$

$$\sigma_{cr} = 20\sqrt{f_{me}} \quad (5.8)$$

where $\sigma_{cr}$ is the cracking capacity of masonry.

4. For the general shear failure, based on the recommendations of FEMA-273 (1997), as well as Paulay and Priestley (1992), the initial and final contributions of shear carried by the infill panel may be defined by;

$$V_{mi} = A_{vh} 2\sqrt{f_{me}} \quad (5.9)$$

where, $V_{mi}$ is the available initial shear capacity that is consumed during the first half-cyclic (monotonic) loading and $A_{vh}$ is the net horizontal shear area of the infill panel.

Rotation capacities of the infill panels are determined according to the recommendations of FEMA-356 (2000). Table 5.3 which is obtained from FEMA-356 (2000) shows the nonlinear rotation capacity limits for BMIs. Using Table 5.3 to obtain the rotation capacities of BMIs requires two shear force parameters for reinforced concrete columns and for BMIs respectively. These parameters are; $V_{fre}$, which is the expected story shear strength of the frame, taken as the shear capacity of the column and $V_{ine}$, which is the shear force capacity of the BMI that is described earlier. $V_{fre}$ is defined as follows (ACI 318M-05, 2005);

$$V_{fre} = V_c + V_s \tag{5.10}$$

Where $V_c$ is the shear force capacity provided by concrete and Vs is the shear force capacity provided by transverse reinforcement of the reinforced concrete column. They are defined as follows (ACI 318M-05, 2005);

$$V_c = 0.17\left(1 + \frac{N_u}{14A_g}\right)\sqrt{f_c}\,b_w d \tag{5.11}$$

$$V_s = \frac{A_v f_{yt} d,,}{s} \tag{5.12}$$

where, $N_u$ is the factored axial force normal to cross section. Load Factor is taken as 0.9 (0.9xDead Load), $A_g$ is the gross area of concrete section, $mm^2$, $f'_c$ is the specified compressive strength of concrete (Mpa), $A_v$ is the area of shear reinforcement within spacing, s and $f_{yt}$ is the yield strength of transverse reinforcement.

**Table 5.3** Rotation capacities of BMIs (FEMA-356, 2000)

*Table 7-9* ***Nonlinear Static Procedure—Simplified Force-Deflection Relations for Masonry Infill Panels***

| $\beta = \frac{V_{fre}}{V_{ine}}$ | $\frac{L_{inf}}{h_{inf}}$ | c | d % | e % | Acceptance Criteria | |
|---|---|---|---|---|---|---|
| | | | | | LS % | CP % |
| $\beta < 0.7$ | 0.5 | n.a. | 0.5 | n.a. | 0.4 | n.a. |
| | 1.0 | n.a. | 0.4 | n.a. | 0.3 | n.a. |
| | 2.0 | n.a. | 0.3 | n.a. | 0.2 | n.a. |
| $0.7 \le \beta < 1.3$ | 0.5 | n.a. | 1.0 | n.a. | 0.8 | n.a. |
| | 1.0 | n.a. | 0.8 | n.a. | 0.6 | n.a. |
| | 2.0 | n.a. | 0.6 | n.a. | 0.4 | n.a. |
| $\beta \ge 1.3$ | 0.5 | n.a. | 1.5 | n.a. | 1.1 | n.a. |
| | 1.0 | n.a. | 1.2 | n.a. | 0.9 | n.a. |
| | 2.0 | n.a. | 0.9 | n.a. | 0.7 | n.a. |

Note: Interpolation shall be used between table values.

A diagonal compression strut is used for modeling the BMIs within the reinforced concrete frames. A structural BMI model for a typical one bay two story reinforced concrete frame is shown in Figure 5.26. In the model, the diagonal compression strut is not directly connected to the beam column joint, it is rather connected to the ends of the rigid elements defining the beam-column joint. The calculated ultimate shear and lateral displacement capacity of the BMI is modified and assigned to an axial plastic hinge located at the end of the diagonal strut to simulate the post-elastic behavior of the BMI.

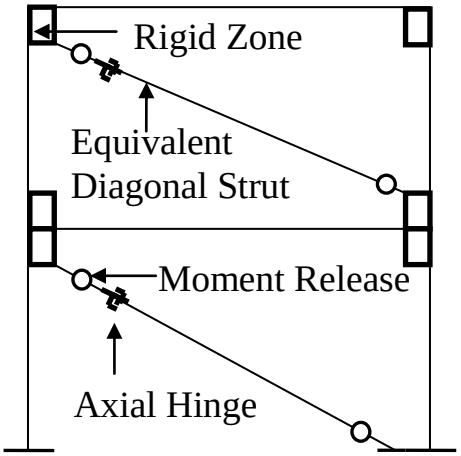


**Figure 5.26** compression strut model

SAP2000 (2006) requires the axial force-deformation values for modeling of plastic hinges. The calculated ultimate capacities and rotation values taken from Table 5.3 are converted to axial force and displacement values by the short procedure given below with reference to Figure 5.27 which describes the relationship between the wall rotation, wall displacement and axial displacement of the diagonal strut on a diagram.

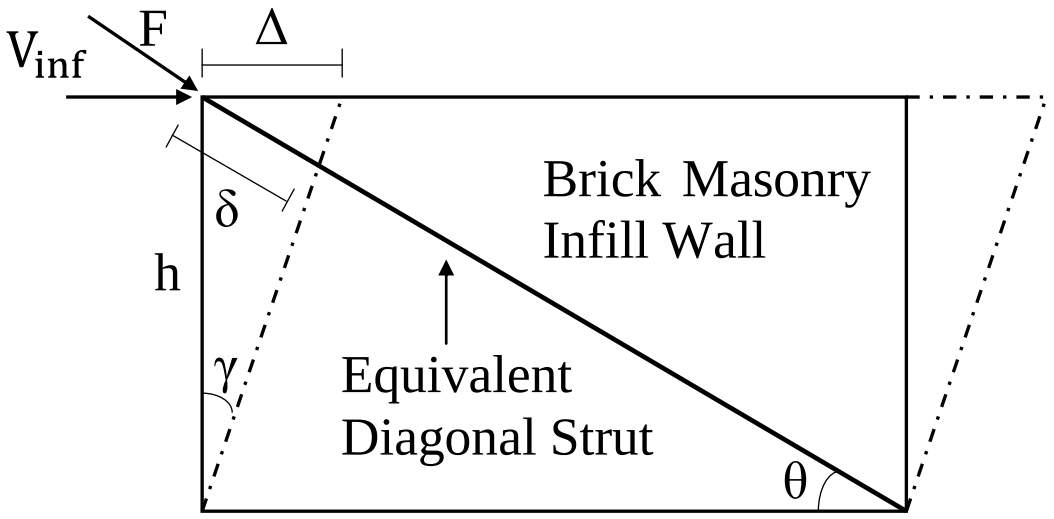


**Figure 5.27** Rotation-displacement relations for BMIs

$$\Delta = \gamma h \tag{5.13}$$

$$\delta = \Delta \cos\theta \tag{5.14}$$

$$\delta = \gamma h \cos\theta \tag{5.15}$$

$$F = \frac{V_{inf}}{\cos\theta} \tag{5.16}$$

### 5.9. Modeling of Proposed Steel Retrofitting System for NLTH Analyses

The nonlinear modeling of the proposed retrofitting system with the finite element based software SAP2000 (2006) is shown in Figure 5.28 for a typical reinforced

concrete bay. The proposed retrofitting system is composed of a steel frame chevron braces and a nonlinear shear link connected between the braces and steel frame beam. The hysteretic behavior of the shear link for NLTH analyses is modeled by the plastic Wen element in SAP2000 (2006), which has an elasto-plastic shear force displacement hysteresis. The steel frame members and the braces are modeled using elastic beam elements. Moment releases are introduced at the end of the brace elements. The steel beam elements are connected to the nodes at the ends of the rigid elements defining the reinforced concrete joints.

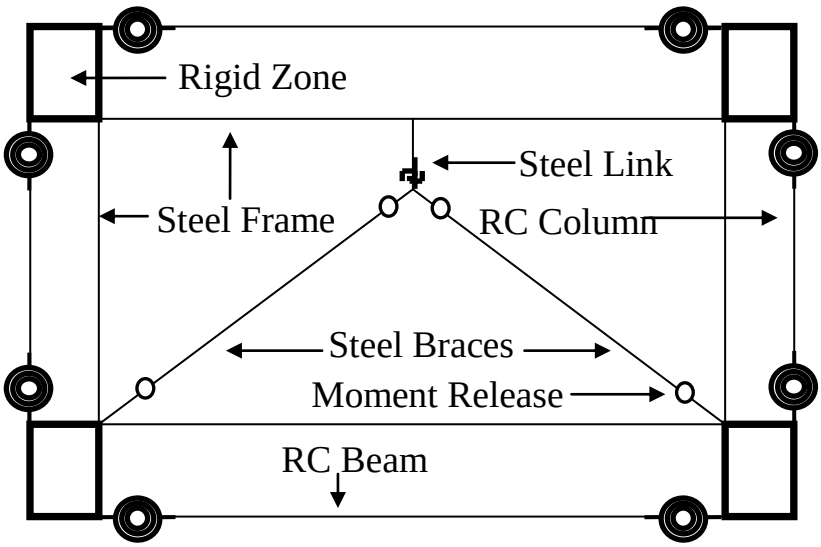


**Figure 5.28** A Side view of the proposed retrofitting system

### 5.10. Modeling of Proposed Steel Retrofitting System for NLP Analyses

The structural model used for NLP analyses is similar to that of NLTH analyses. The only difference is that hinge elements are used at member ends instead of link elements. The monotonic shear force-deformation relationships used to define the nonlinear behavior of the hinge element for the steel shear link is defined as elastoplastic in SAP2000 (2006).

## 5.11. Procedure, Simplifications and Modeling Assumptions for NLP Analyses

### 5.11.1. General

A number of nonlinear structural analyses were conducted to assess the seismic performance of the original and retrofitted example buildings used in this research study. NLP analyses were conducted to obtain the sequence of the nonlinear hinging on the example buildings in the original and retrofitted conditions. Also, NLP analyses were used to obtain the lateral top displacement vs. base shear force relationships of the example buildings in the original and retrofitted conditions. In addition to that, the lateral top displacement of the buildings corresponding to the rotation limits of the reinforced concrete beams and columns are obtained from NLP analyses. Another important issue was including the effect of the gravitational loads on the lateral force deformation behavior of the example buildings. For this purpose, vertical pushover analyses were conducted to introduce the effect of gravitational loads in lateral NLP and NLTH analyses.

### 5.11.2 Force Controlled Vertical Pushover Analyses

Vertical pushover analyses were conducted to simulate the effect of gravity loads on the structural models of the selected buildings. These force controlled pushover analyses were conducted by considering the gravity loads that are distributed to the beams of the selected buildings. The vertical loads on the slabs are distributed to the beams by the tributary areas formed by yield lines. Figure 5.29 shows the distribution of the gravity loads to the beams for a typical slab.

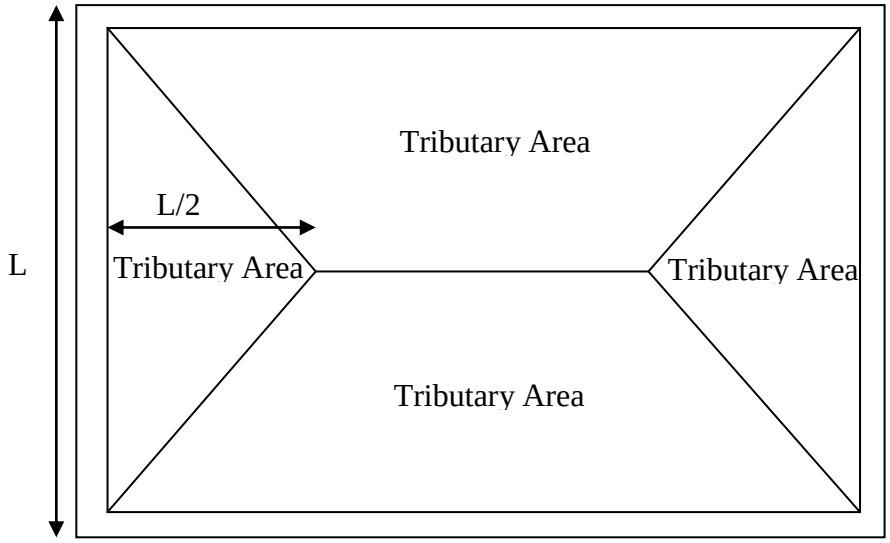


**Figure 5.29** Tributary area method

### 5.11.3 Displacement Controlled Nonlinear Pushover Analyses

The NLP analysis method used in SAP2000 (2006) adopts a lumped-plasticity approach that model the inelastic behavior through the formation of nonlinear plastic hinges at the frame element's ends during the static loading process. Hence, in this study, plastic hinges are used at the ends of the beam and column elements to simulate their nonlinear behavior. Figure 5.30 shows a typical envelope curve for a plastic hinge used in SAP2000 (2006) where the parameter Q is the force or moment value of the plastic hinge and the parameters θ and Δ represent the rotation and deformation of the hinge. The other parameters are used for defining the envelope curve of the force-deformation or moment-rotation relationship of the associated hinge.

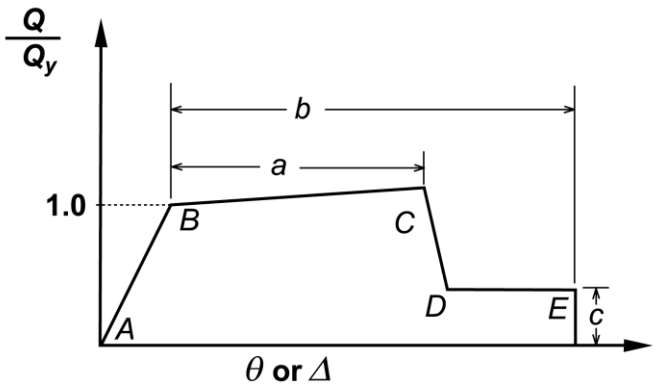


**Figure 5.30** A typical envelope curve for plastic hinges (FEMA356)

### 5.11.3.1. Discussion of Lateral Load Patterns for NLP Analyses

The lateral load pattern used in NLP analyses should be able to simulate the actual load distribution during an earthquake. Therefore, an accurate determination of the lateral load pattern along the height of the building is important in NLP analyses. In the literature, several methods are available to obtain a suitable lateral load pattern for NLP analyses. Some of these methods are as follows. FEMA-356 (2000) recommends a variety of methods that include the use of story forces proportional to the deflected shape of the structure, the use of load patterns based on mode shapes derived from secant stiffnesses at each load step and the use of load patterns proportional to the story shear resistance at each step. FEMA-368 (2001) recommends an adaptive method for obtaining the lateral load pattern. Other methods proposed by various researchers include simple methods such as using an inverted triangular lateral load pattern (İnel et al. 2003) or a rectangular lateral load pattern (İnel et al. 2003) along the height of the building and more complicated methods such as those proposed by (Kalkan and Kunnath, 2006; Yi and Jiang, 2007).

In this study, a SSRS based method is used to obtain the lateral load patterns along the height of the example reinforced concrete buildings. In order to provide a realistic story shear force that are expected to occur during a probable

earthquake, the SSRS with 5% damping are used in RS analyses of the example buildings. The distribution of the story shear forces obtained from RS analyses are used as shape vectors for lateral load patterns along the height of the example buildings in NLP analyses. The NLP analyses results using load pattern used in this study is compared with more complicated adaptive pushover analyses results for simple frames. The differences from both analyses results were found to be negligible. More details are given in the following subsection.

#### 5.11.3.2. Simplifications of NLP and NLTH Analyses.

In NLP analyses, complicated modeling of the actual nonlinear structural behavior, including negative post elastic slopes due to loss of strength, increases the degree of nonlinearity. This, in turn, may result in convergency problems in NLP analyses. In this study, the complicated nonlinear behavior of reinforced concrete members is carefully simplified without losing the desired accuracy to defeat convergency problems in NLP analyses. The effects of these simplifications and assumptions on the accuracy of the NLP analyses were investigated.

Preliminary NLP analyses of the school building showed that a soft story condition at the first story occurs at small values of roof displacement due to the premature failure of the BMIs at the first story. Consequently, the overall stiffness characteristics of the building abruptly changes upon failure of the first story BMIs. To capture this abrupt change in the lateral stiffness of the building an adaptive NLP analysis technique seems to be more appropriate. Initially this method was adopted for the NLP analysis of the school building. However, since this method requires a new NLP analysis with a modified lateral load pattern each time the stiffness of the structure changes due to the formation of plastic hinges, convergency problems were encountered throughout the successive NLP analyses. To avoid these convergency problems the adaptive pushover method was abandoned. Instead, a lateral load pattern based on RS analyses (SSRS was used in the analyses) of the building without the BMIs is used in a single NLP analysis

to obtain the lateral force-deformation relationship of the building. This simplification was based on the fact that failure of the BMIs would take place at very early stages of a probable earthquake and hence, may not significantly affect the seismic response of the building. To assess the effect of this simplification on the accuracy of the NLP analyses results a small 3D one bay frame is extracted from the school building and analyzed using both the adaptive and proposed lateral load pattern. The NLP analysis results are displayed in Figure 5.31. As observed from the figure both methods give nearly identical lateral force deformation relationships. To further assess the effect of the load pattern on the NLP analyses results, the school building is analyzed using a rectangular and triangular load pattern. The analyses results are displayed in Figure 5.32. As observed from the figure both load patterns produce nearly identical lateral force deformation relationship for the building. Thus, the more realistic load pattern obtained from RS analyses is used in this study.

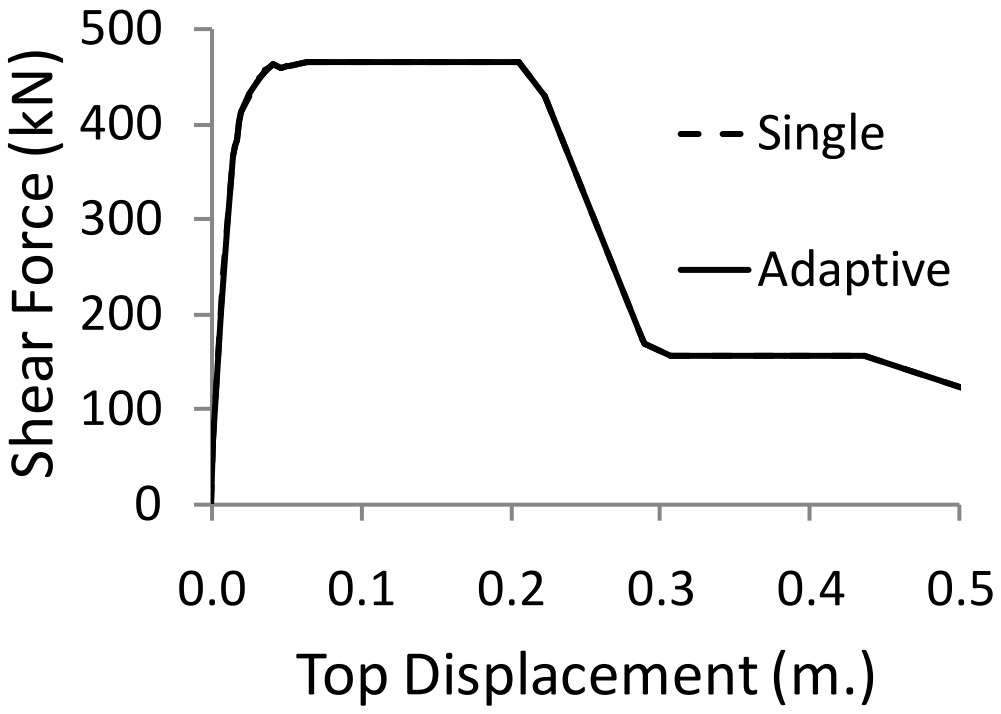


**Figure 5.31** Adaptive lateral load patterns vs. RS lateral load pattern

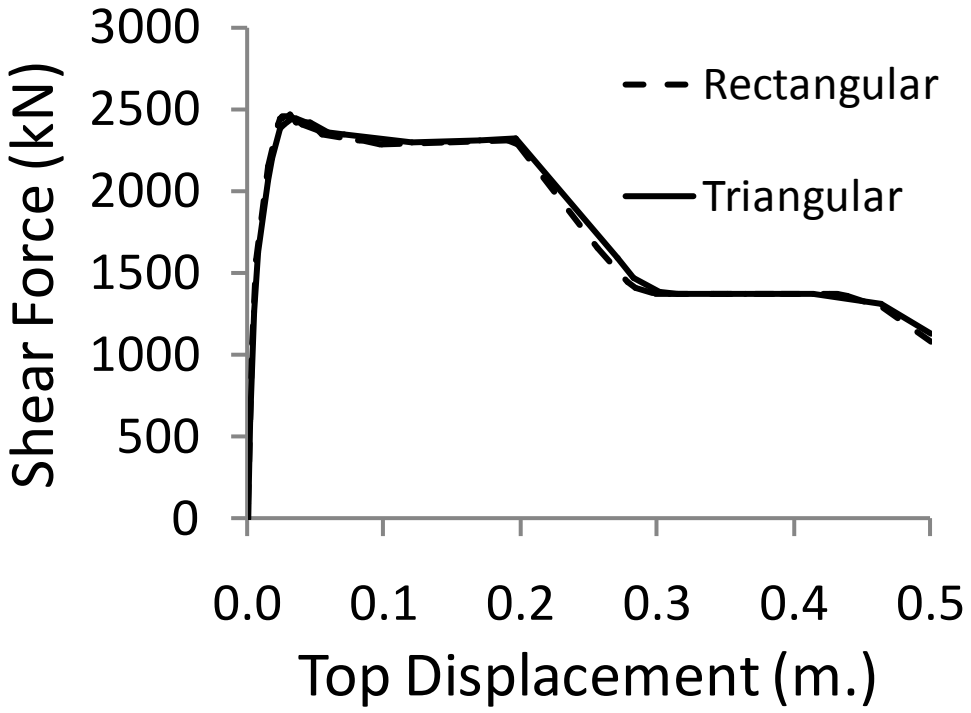


**Figure 5.32** Rectangular vs. inverted triangular lateral load pattern

Furthermore, the negative slopes in moment curvature relationships (e.g. due to buckling of compression reinforcement) of the reinforced concrete members were not modeled due to convergency problems. Instead an elasto-plastic moment curvature relationship was obtained based on equal energy principle and used in both NLP and NLTH analyses.

It is noteworthy that the alterations of the axial loads due to seismic effects were observed to be nearly 10%-15% of the column axial force due to dead load and 25% of live load (FEMA-356, 2000). This small alteration of the axial loads on the columns is considered as negligible. Thus, axial load-moment (P-M) interaction was neglected in both NLP and NLTH analyses. The columns were analyzed under a constant axial load calculated using the full dead load and 25% of the live load (FEMA-356, 2000).

# CHAPTER 6

# PERFORMANCE BASED RETROFITTING DESIGN PROCEDURE

## 6.1 General

This chapter includes a detailed description of the performance based seismic retrofitting design procedure developed as part of this research study. First, general information about the performance based seismic design procedure including the drift and member rotation limits at various performance levels is given. This is followed by a step-by-step description of the performance based seismic retrofitting procedure used in this study.

## 6.2 Performance Based Design Approach

Since the early development of seismic design codes, global response modification factors (or R-factors) are used in the seismic design of structures to reduce the elastic seismic forces. The R-factors are intended to account for the benefits of over-strength, redundancy, yielding and associated energy dissipation by simple elastic analyses. Although R-factors greatly simplify the analysis process in seismic design, they are global response measures that do not provide an assessment of structural performance at the component level. Thus, using R-factors for seismic design have serious shortcomings. For instance, these factors are independent of the building period and ground motion characteristics (Kunnath, 2006). Additionally the same R-factor is used for moment resisting reinforced concrete, steel and braced frames. It is clear that a single global response modifier cannot capture the progressive distribution of nonlinearities between various structural elements, the resulting redistribution of seismic demands inside the structure and changes that occur during the course of seismic motion (Kunnath, 2006).

Because of the stated shortcomings of the existing code provisions, the performance based design approach is used in the retrofitting design of the buildings considered in this study. Performance based design approach is based on some structural and nonstructural criteria which are defined in detail in FEMA-356 (2000). These criteria are a combination of structural and nonstructural damage level to the structures and life saving objectives, which are mainly defined by plastic rotation limits of the reinforced concrete members. The performance based design approach is based on matching various probable earthquakes with target performance levels. The terminology used for the target performance levels represent the design goals at various performance levels. Target performance levels can be summarized in a very simple manner as follows: (i) no damage for minor levels of earthquake excitations, (ii) low or repairable structural and non-structural damage for moderate earthquake excitations, (iii) structural and non structural damage but no collapse for major earthquake excitations. Ground motion levels, which represent the minor, moderate and major earthquakes used in the performance based design approach are listed in Table 6.1.

**Table 6.1** Earthquake levels for performance based design approach

| **Earthquake, Having Probability of Exceedance** | **Mean Return Period (years)** |
|---|---|
| 50%/50 year | 72 |
| 10%/50 year | 475 |
| 2%/50 year | 2475 |

The earthquake levels given in Table 6.1 represent; (i) the frequent earthquakes, which may occur many times during the economical life of a structure (50%/50 year, weak earthquake), (ii) moderate earthquakes that have a moderate probability of occurrence during the economical life of a structure (10%/50year, moderate earthquake) and (iii) strong earthquakes (2%/50year, strong earthquake) which have a low probability of occurrence during the economical life of a

structure. Under the stated earthquake levels, the structures should achieve the performance criteria described in terms of the safety afforded by the building occupants during and after the event, the cost and feasibility of restoring the building to pre-earthquake condition, the length of time the building is removed from service during repairs and economical, architectural or historic impacts on the larger community. These performance characteristics are directly related to the extent of damage that would be sustained by the building FEMA-356 (2000). The general performance criteria expected from structures is described in FEMA-356 (2000) as follows;

- **Immediate Occupancy Structural Performance Level (I.O.)**: Immediate Occupancy, means the post-earthquake damage state in which only very limited structural damage has occurred. The basic vertical- and lateral-force-resisting systems of the building retain nearly all of their preearthquake strength and stiffness. The risk of life threatening injury as a result of structural damage is very low, and although some minor structural repairs may be appropriate, these would generally not be required prior to reoccupancy.

- **Life Safety Structural Performance Level (L.S.)** : Life Safety means the post-earthquake damage state in which significant damage to the structure has occurred, but some margin against either partial or total structural collapse remains. Some structural elements and components are severely damaged, but this has not resulted in large falling debris hazards, either within or outside the building. Injuries may occur during the earthquake; however, the overall risk of life-threatening injury as a result of structural damage is expected to be low. It should be possible to repair the structure; nevertheless, for economic reasons this may not be practical. While the damaged structure is not an imminent collapse risk, it would be prudent to implement structural repairs or install temporary bracing prior to reoccupancy.

- **Collapse Prevention Structural Performance Level (C.P.)**: Collapse Prevention, means the post-earthquake damage state is such that the building is on the verge of partial or total collapse. Substantial damage to the structure has occurred, potentially including significant degradation in the stiffness and strength of the lateral-force resisting system, large permanent lateral deformation of the structure, and, to a more limited extent, degradation in vertical-load-carrying capacity. However, all significant components of the gravity load- resisting system must continue to carry their gravity load demands. Significant risk of injury due to falling hazards from structural debris may exist. The structure may not be technically practical to repair and is not safe for reoccupancy, as aftershock activity could induce collapse.

### 6.3. Drift Limits (Capacities) for Structures

As stated earlier, two existing reinforced concrete buildings are retrofitted as part of this research study. In the retrofitting procedure of the buildings, the nonlinear drift limits (capacities) of the buildings for each performance level are obtained from NLP analyses in compliance with the recommendations given in FEMA-356 (2000). FEMA-356 (2000) defines the related plastic rotation limits of reinforced concrete members for the expected performance levels. In NLP analyses, the program SAP2000 (2006) can show the rotation value of the each plastic hinge at each incremental roof displacement step. Accordingly, the nonlinear drift limit (interstory and roof) for each performance level is obtained from NLP analyses results as the value corresponding to the maximum plastic rotation of a member within the structure matching that defined by FEMA-356 (2000) for the performance level under consideration. Table 6.2 shows the FEMA-356 (2000) rotation limits for reinforced concrete beams at different performance levels while Table 6.3 shows similar information for reinforced concrete columns. Figure 6.1 shows a typical force displacement curve with various performance levels.

**Table 6.2** Plastic rotation limits of RC beams (FEMA-356, 2000)

| | | | Modeling Parameters[3] | | | Acceptance Criteria[3] | | | | |
|---|---|---|---|---|---|---|---|---|---|---|
| | | | Plastic Rotation Angle, radians | | Residual Strength Ratio | Plastic Rotation Angle, radians | | | | |
| | | | | | | Performance Level | | | | |
| | | | | | | | Component Type | | | |
| | | | | | | | Primary | | Secondary | |
| Conditions | | | a | b | c | IO | LS | CP | LS | CP |
| i. Beams controlled by flexure[1] | | | | | | | | | | |
| $\frac{\rho - \rho'}{\rho_{bal}}$ | Trans. Reinf.[2] | $\frac{V}{b_w d \sqrt{f'_c}}$ | | | | | | | | |
| ≤ 0.0 | C | ≤ 3 | 0.025 | 0.05 | 0.2 | 0.010 | 0.02 | 0.025 | 0.02 | 0.05 |
| ≤ 0.0 | C | ≥ 6 | 0.02 | 0.04 | 0.2 | 0.005 | 0.01 | 0.02 | 0.02 | 0.04 |
| ≥ 0.5 | C | ≤ 3 | 0.02 | 0.03 | 0.2 | 0.005 | 0.01 | 0.02 | 0.02 | 0.03 |
| ≥ 0.5 | C | ≥ 6 | 0.015 | 0.02 | 0.2 | 0.005 | 0.005 | 0.015 | 0.015 | 0.02 |
| ≤ 0.0 | NC | ≤ 3 | 0.02 | 0.03 | 0.2 | 0.005 | 0.01 | 0.02 | 0.02 | 0.03 |
| ≤ 0.0 | NC | ≥ 6 | 0.01 | 0.015 | 0.2 | 0.0015 | 0.005 | 0.01 | 0.01 | 0.015 |
| ≥ 0.5 | NC | ≤ 3 | 0.01 | 0.015 | 0.2 | 0.005 | 0.01 | 0.01 | 0.01 | 0.015 |
| ≥ 0.5 | NC | ≥ 6 | 0.005 | 0.01 | 0.2 | 0.0015 | 0.005 | 0.005 | 0.005 | 0.01 |

**Table 6.3** Plastic rotation limits of RC columns (FEMA-356, 2000)

| | | | Modeling Parameters[4] | | | Acceptance Criteria[4] | | | | |
|---|---|---|---|---|---|---|---|---|---|---|
| | | | Plastic Rotation Angle, radians | | Residual Strength Ratio | Plastic Rotation Angle, radians | | | | |
| | | | | | | Performance Level | | | | |
| | | | | | | | Component Type | | | |
| | | | | | | | Primary | | Secondary | |
| Conditions | | | a | b | c | IO | LS | CP | LS | CP |
| i. Columns controlled by flexure[1] | | | | | | | | | | |
| $\frac{P}{A_g f'_c}$ | Trans. Reinf.[2] | $\frac{V}{b_w d \sqrt{f'_c}}$ | | | | | | | | |
| ≤ 0.1 | C | ≤ 3 | 0.02 | 0.03 | 0.2 | 0.005 | 0.015 | 0.02 | 0.02 | 0.03 |
| ≤ 0.1 | C | ≥ 6 | 0.016 | 0.024 | 0.2 | 0.005 | 0.012 | 0.016 | 0.016 | 0.024 |
| ≥ 0.4 | C | ≤ 3 | 0.015 | 0.025 | 0.2 | 0.003 | 0.012 | 0.015 | 0.018 | 0.025 |
| ≥ 0.4 | C | ≥ 6 | 0.012 | 0.02 | 0.2 | 0.003 | 0.01 | 0.012 | 0.013 | 0.02 |
| ≤ 0.1 | NC | ≤ 3 | 0.006 | 0.015 | 0.2 | 0.005 | 0.005 | 0.006 | 0.01 | 0.015 |
| ≤ 0.1 | NC | ≥ 6 | 0.005 | 0.012 | 0.2 | 0.005 | 0.004 | 0.005 | 0.008 | 0.012 |
| ≥ 0.4 | NC | ≤ 3 | 0.003 | 0.01 | 0.2 | 0.002 | 0.002 | 0.003 | 0.006 | 0.01 |
| ≥ 0.4 | NC | ≥ 6 | 0.002 | 0.008 | 0.2 | 0.002 | 0.002 | 0.002 | 0.005 | 0.008 |

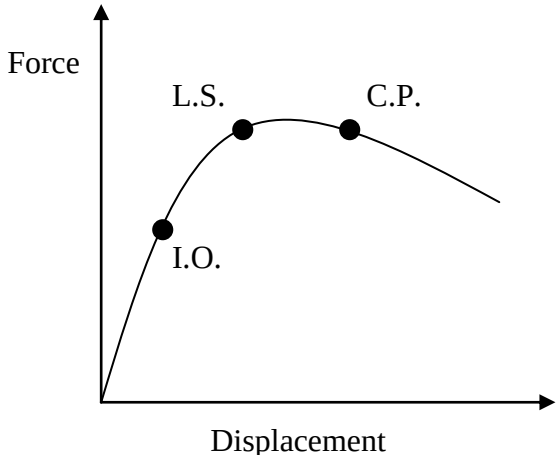


**Figure 6.1** Force displacement curve of a structure matched with expected performance levels.

### 6.4 Proposed Retrofitting Methodology

Most of the existing ordinary buildings (e.g. school, residential and low to mid-rise office buildings) have fundamental vibration periods that fall in the intermediate period range. In this period range, the energy dissipated by an elastic system can be assumed to be equal to an identical (nonlinear) system that yields at a certain lateral force level. The seismic retrofitting design methodology used for the example reinforced concrete buildings employed in this study is mainly based on this equal energy dissipation principle. In the proposed methodology, monotonic energy dissipation capacities of the example buildings in the linear elastic and nonlinear inelastic cases were calculated and compared. The difference between the monotonic linear elastic and nonlinear inelastic energy dissipation capacities (the difference between the areas under the base shear force vs. roof displacement curves) is defined as the required additional energy that needs to be absorbed by the retrofitted building. The necessary amount of additional energy is provided by adding lateral load resisting members (e.g. steel shear link with braces or infill squat shear panels) to the building to increase its lateral strength while keeping nearly the same lateral drift capacity. A typical graph of linear

elastic and nonlinear inelastic base shear force vs. roof displacement relationships is shown in Figure 6.2. The force-displacement relationships given in Figure 6.2 can be obtained by NLP analyses for the nonlinear inelastic case and by RS analyses for the linear elastic case.

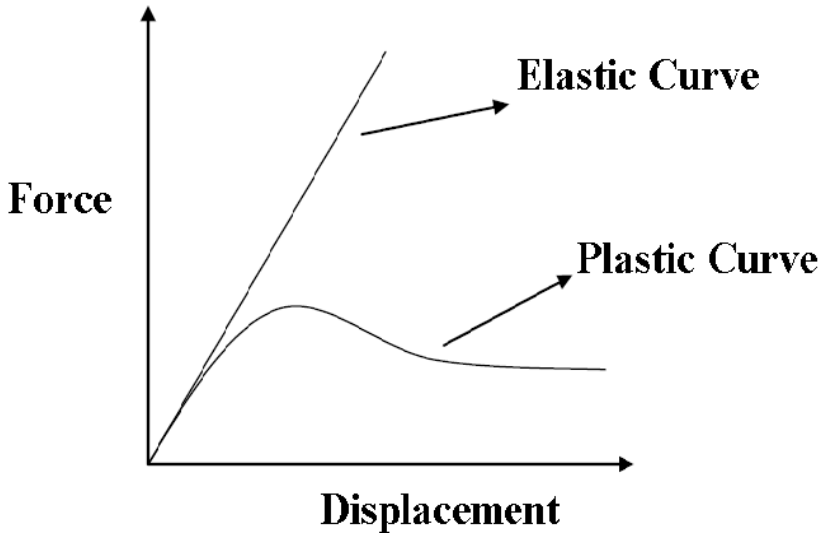


**Figure 6.2** Linear elastic and nonlinear force displacement curves

### 6.4.1 Step by Step Definition of the Proposed Retrofitting Procedure

In this section, a step by step definition of the proposed seismic retrofitting procedure is given.

1. In the first step of the retrofitting design procedure, RS analyses of the building in the retrofitted stage is conducted to obtain the linear elastic base shear force vs. roof displacement relationship as shown in Figure 6.3. Since the retrofitting scheme is not known at the initial stage of the design procedure, the original unretrofitted building is used in the analyses. However, it is a known fact that seismic retrofitting (e.g. using steel shear link with braces or infill squat shear

panels) results in an increase in the stiffness of the building. Accordingly, the stiffness of the original building needs to be increased by a certain amount (e.g. initially by 20%) in the RS analyses. In the structural model, the desired increase in the lateral stiffness of the building is achieved by adjusting the modulus of elasticity of the reinforced concrete members of the structure.

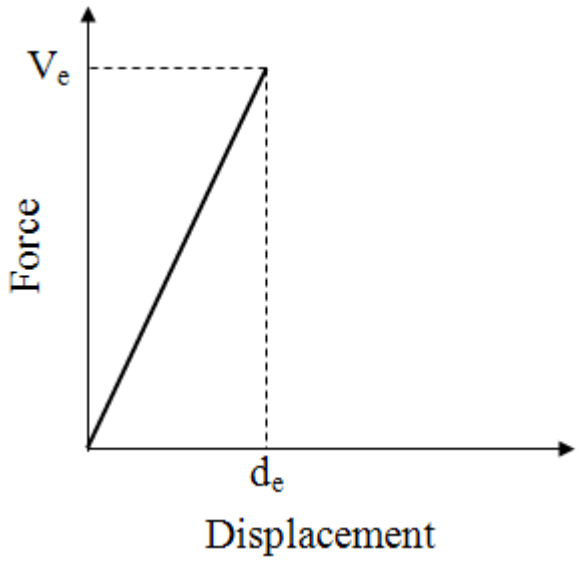


**Figure 6.3** Linear elastic base shear force vs. roof displacement relationship

2. In the second step of the retrofitting design procedure the NLP analyses of the original building is conducted to obtain the base shear force vs. roof displacement relationship. This relationship is plotted up to the displacement level corresponding to the displacement capacity of the building for the performance level under consideration. The plotted curve is then idealized to have an elasto-plastic shape as described in FEMA-356 (2000) (Figure 6.4). The area under the elasto-plastic curve and the actual curve are identical. The yield base shear force, $V_y$, obtained from the elasto-plastic curve is used together with the elastic stiffness of the structure in the retrofitted stage (slope of the curve in Figure 6.3) to obtain a new elasto-plastic base shear force vs. roof displacement relationship (Figure 6.5). This new relationship will be used in the subsequent calculations.

This is done to have an accurate estimation of the required strength level for retrofitting purposes (due to equal energy concept for a linear elastic and an identical (same period) yielding system).

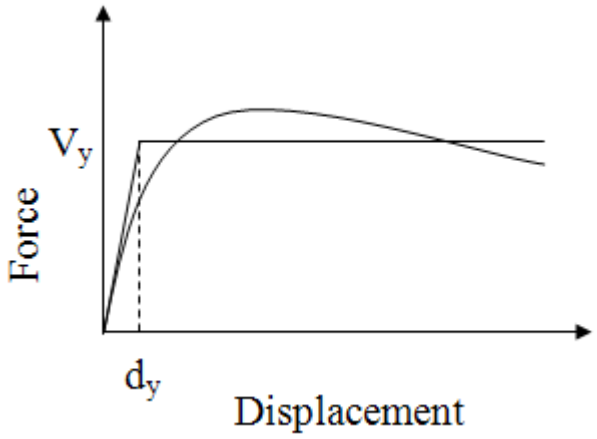


**Figure 6.4** Elasto-plastic base shear force vs. roof displacement relationship

3. In the third step of the procedure, first, the area, $A_e$, under the linear elastic base shear force vs. roof displacement curve will be calculated. Then the area, $A_p$, under the elasto plastic base shear force vs. roof displacement curve shown in Figure 6.5 will be calculated. The monotonic energy, $A_d$, that needs to be dissipated by the retrofitting system is then calculated as; $A_d = A_e - A_p$.

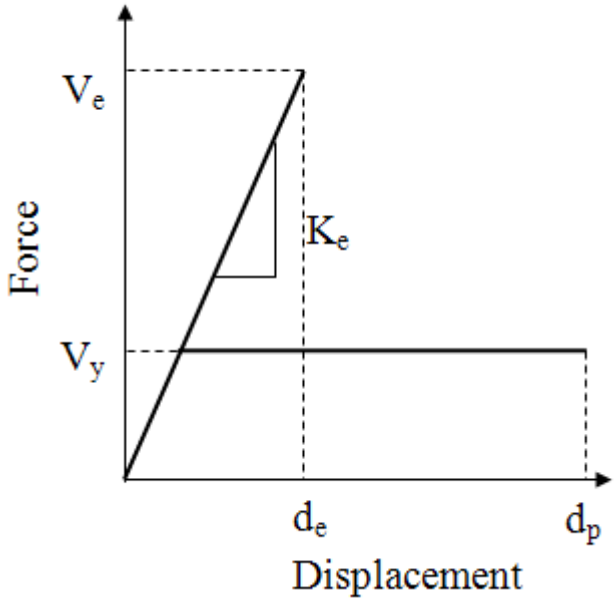


**Figure 6.5** Elasto-plastic base shear force vs. roof displacement relationship

4. In this step, the required strength, $Q_1$, of the retrofitting system at the base of the building is obtained with reference to Figure 6.6 as follows.

$$Q_{1\ 1,2} = K_e d_p - V_y \mp \sqrt{(V_y - K_e d_p)^2 - 2K_e A_d} \qquad (6.1)$$

One of the roots from the above equation will give the required strength ,$Q_1$, of the retrofitting system at the base of the building.

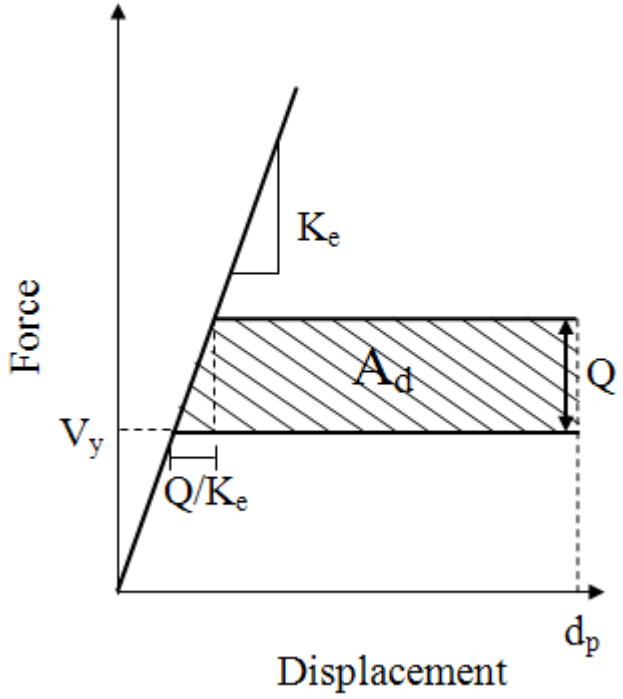


**Figure 6.6** Calculation of required strength, Q.

5. In this step of the design procedure, first, the shear force capacity, $R_{Fi}$, of each story of the original unretrofitted building is obtained. To obtain the shear force capacity of a story i, the lateral displacement of the stories below are restrained as shown in Figure 6.9. Then, NLP analyses of the building is conducted until the displacement capacity of the story level under consideration is reached (the displacement capacity is based on FEMA 356 member rotation limits). In the NLP analyses, nonlinear behavior is considered only for the story under consideration while the yielding of the other stories are prohibited (modeled as elastic).

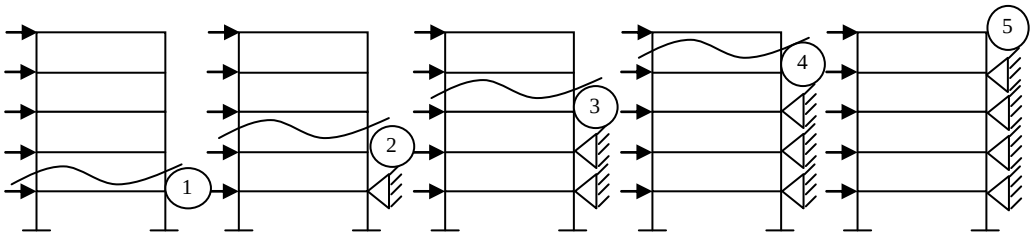


**Figure 6.7** Illustration of obtaining the plastic shear force capacity of each story.

6- In this step of the design procedure, the retrofitting system is designed. The design is based on uniform energy dissipation throughout the height of the building. For this purpose, the elastic shear, $V_{i,}$ at each story level, i is obtained from the RS analyses results in Step 1. Then, the total strength, $R_{1,}$ at the base of the retrofitted building is obtained by summing up its base shear capacity, $R_{F1,}$ and the required strength for retrofitting. That is; $R_1=R_{F1}+Q_1$. To ensure uniform energy dissipation along the building height, the ratios of the total strength of the retrofitted building at each story level i ($R_i=R_{Fi}+Q_i$) to the elastic shear, $V_i$, at the corresponding story level must be equal. That is;

$$\frac{R_1}{V_1} = \frac{R_2}{V_2} = \cdots = \frac{R_i}{V_i} = \cdots = \frac{R_n}{V_n} \tag{6.2}$$

where, the subscript, n, in the above equation denotes the number of stories. This will ensure that yielding will occur at all the story levels. The ratio of the total strength, $R_1$, of the retrofitted building to the elastic shear $V_1$ at the base of the building is already known. To calculate the required retrofitting system strength at any story level, i, the following relationship could be used;

$$\frac{R_1}{V_1} = \frac{R_{Fi}+R_i}{V_i} \tag{6.3}$$

Then solving for $Q_i$, the following equation is obtained;

$$Q_i = \frac{R_1}{V_1} V_i - R_{Fi} \quad (6.4)$$

Based on the calculated retrofitting system strengths, $Q_i$, at each story level, the retrofitting design is completed, for instance, by choosing the link shear capacities in the proposed retrofitting system.

7. The elastic stiffness of the designed building is recalculated and compared with the stiffness assumed in Step 1 of the retrofitting design procedure. If the difference is negligible the design is complete. Otherwise, the stiffness is updated and Steps 1, 3, 4, and 6 are repeated.

# CHAPTER 7

# SEISMIC RETROFIT EVALUATION OF THE SCHOOL BUILDING

## 7.1 General

In this chapter, the seismic performance of the school building is assessed in the original and the retrofitted conditions. The retrofitted conditions include the proposed seismic retrofitting technique using steel shear link and braces encased in a steel frame and a conventional seismic retrofitting technique using squat infill shear panels. Both NLP and NLTH analyses of the school building in the original and retrofitted conditions are conducted to assess its seismic performance. The seismic performance assessment of the building is performed in terms of seismic displacement demands and capacities as well as damage indices calculated for the original and retrofitted conditions of the building.

## 7.2 Details of the Proposed Seismic Retrofitting Method

The sizes of the steel shear links and braces for the proposed seismic retrofitting method are given in Tables 7.1 and 7.2 for the x and y directions of the building respectively. Figures 7.1 and 7.2 show the locations of the steel retrofitting panels used in the x direction respectively for the first and second stories while Figures 7.3 and 7.4 show the locations of the steel retrofitting panels used in the y direction respectively for the first and second stories. In the figures the locations of the retrofitting system are shown using thick black lines on the building plan.

**Table 7.1** Details of the steel retrofitting members in the x direction

| Steel sections used in X-direction | | | |
|---|---|---|---|
| **Story #** | **Shear Link** | **Braces** | **Frame Members** |
| **1** | HE300M | HE200M | HE300M |
| **2** | HE260M | HE260M | HE260M |

**Table 7.2** Details of the steel retrofitting members in the y direction

| Steel sections used in Y-direction | | | |
|---|---|---|---|
| **Story #** | **Shear Link** | **Braces** | **Frame Members** |
| **1** | HE260M | HE140M | HE260M |
| **2** | HE240M | HE120M | HE240M |

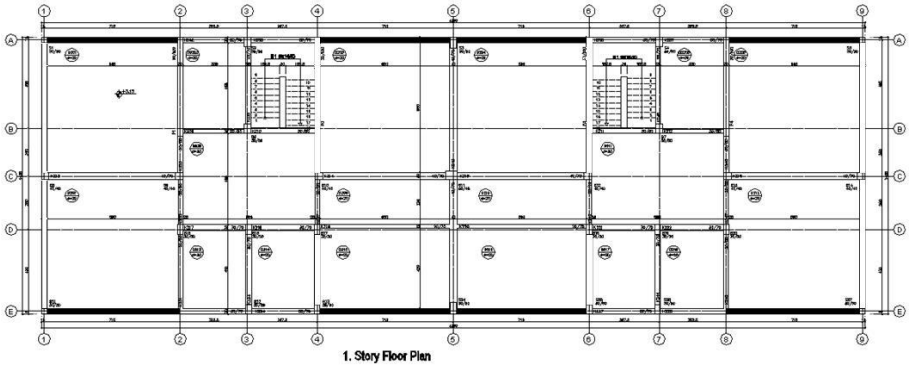


**Figure 7.1** Locations of the steel retrofitting panels within the first story in the x direction

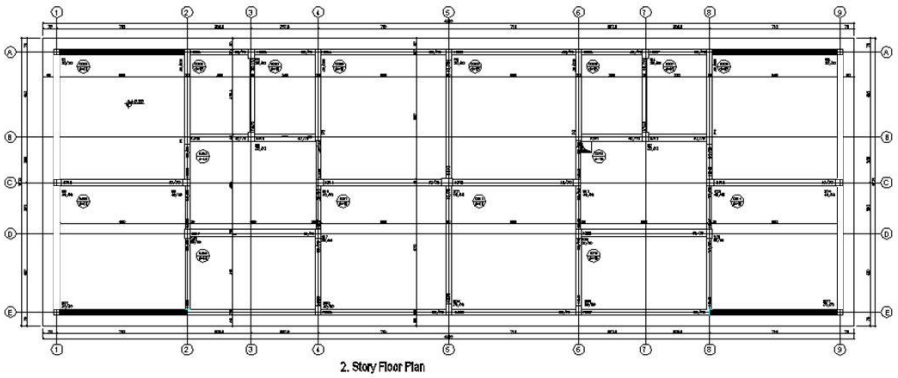


**Figure 7.2** Locations of the steel retrofitting panels within the second story in the x direction

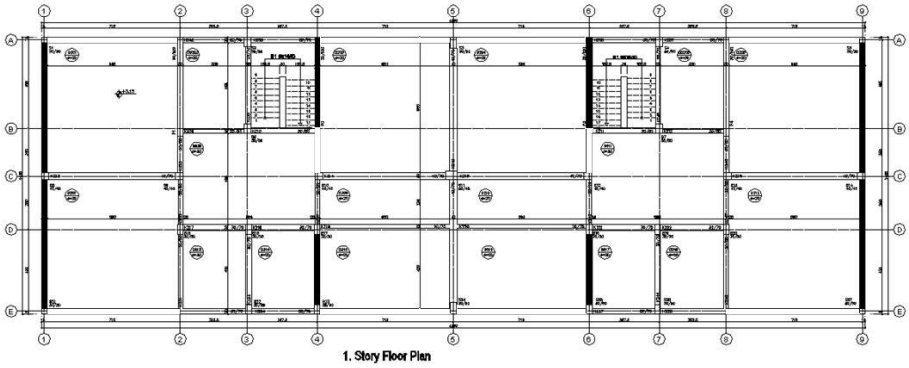


**Figure 7.3** Locations of the steel retrofitting panels within the first story in the y direction

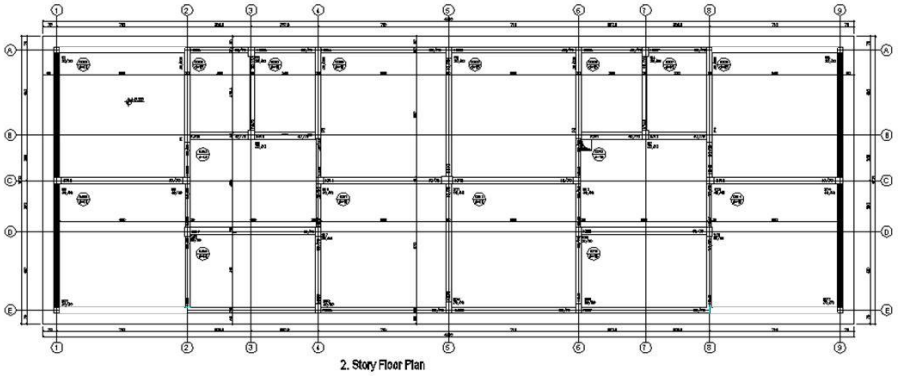


**Figure 7.4** Locations of the steel retrofitting panels within the second story in the y direction

### 7.3 Details of the Conventional Seismic Retrofitting Method

The details of the squat infill shear panels, used in the conventional seismic retrofitting of the building are given in Tables 7.3 and 7.4 for the x and y directions of the building respectively. Figures 7.5 and 7.6 show the locations of the squat infill shear panels used in the x direction respectively for the first and second stories while Figures 7.7 and 7.8 show the locations of the squat infill shear panels used in the y direction respectively for the first and second stories. In the figures the locations of the retrofitting system are shown using thick black lines on the building plan.

**Table 7.3** Details of the squat infill shear panels in the x direction

| **Squat infill shear panels used in X-direction** | | | | **$f_c'$ (Mpa)** | **$f_y$ (Mpa)** | **Reinforcement %** |
|---|---|---|---|---|---|---|
| **Story** | **Width (m)** | **Height (m)** | **Thickness (m)** | | | |
| **1** | 3.30 | 2.85 | 0.15 | 20 | 420 | 0.40 |
| **2** | 3.30 | 2.50 | 0.15 | 20 | 420 | 0.25 |

**Table 7.4** Details of the squat infill shear panels in the y direction

| **Squat infill shear panels used in Y-direction** | | | | **$f_c'$ (Mpa)** | **$f_y$ (Mpa)** | **Reinforcement %** |
|---|---|---|---|---|---|---|
| **Story** | **Width (m)** | **Height (m)** | **Thickness (m)** | | | |
| **1** | 4.25 & 4.00 | 2.85 | 0.15 | 20 | 420 | 0.25 |
| **2** | 4.25 & 4.00 | 2.70 | 0.15 | 20 | 420 | 0.25 |

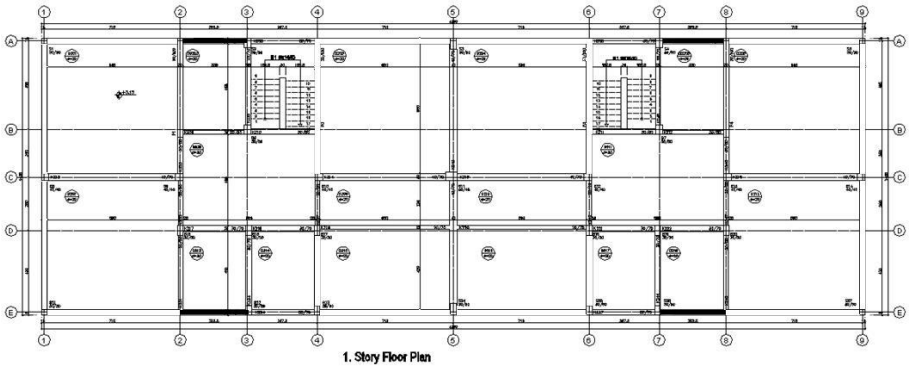


**Figure 7.5** Locations of the squat infill shear panels within the first story in the x direction

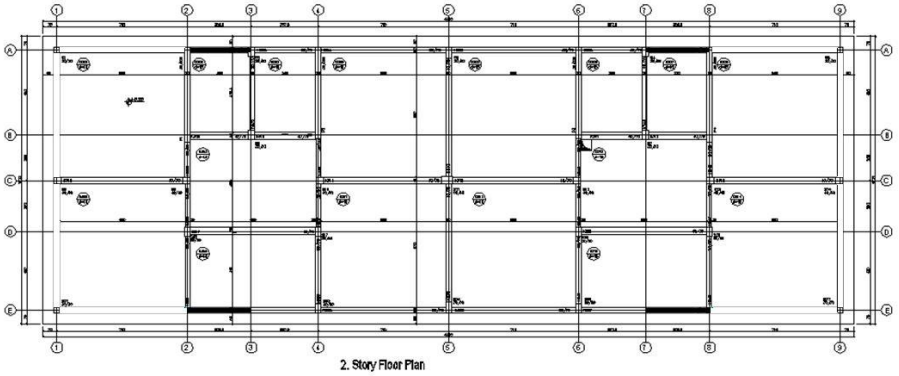


**Figure 7.6** Locations of the squat infill shear panels within the second story in the x direction

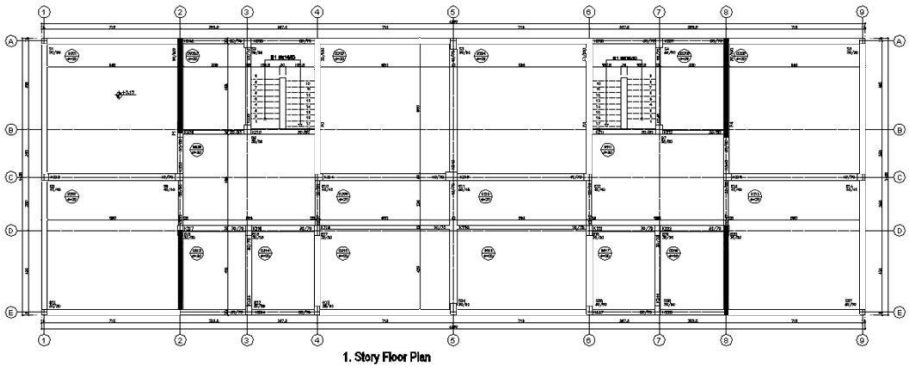


**Figure 7.7** Locations of the squat infill shear panels within the first story in the y direction

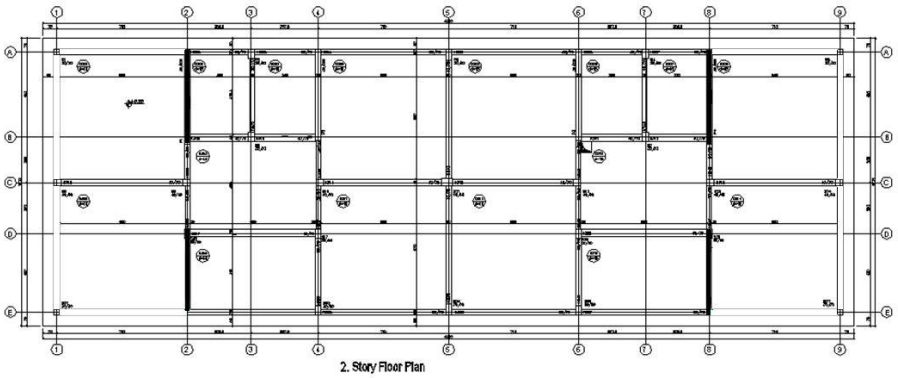


**Figure 7.8** Locations of the squat infill shear panels within the second story in the y direction

## 7.4. Seismic Performance Evaluation of the School Building Using the NLP Analyses Results

In this section, comparative performance evaluation of the original and seismically retrofitted buildings is performed using the NLP analyses results. More detailed information is given in the subsequent sections.

### 7.4.1 Comparative Assessment of the School Building's Performance in the X Direction

The NLP analyses results of the school building in the x direction for the original and retrofitted conditions is shown in Figure 7.9 in terms of a base shear vs. roof displacement plot. From the figure, it is observed that the elastic lateral stiffness of the conventionally retrofitted structure is smaller than the structure retrofitted with the proposed method. This difference is attributed to the larger number of steel panels required to achieve the same yield strength level as that of the squat infill shear panel. This, in turn resulted in a higher elastic stiffness for the building retrofitted using the proposed method. Thus, it is expected that the structure

retrofitted with the proposed technique will have a smaller drift, and hence a more desirable performance (e.g. less non structural damage) under the effect of small intensity earthquakes associated with the IO performance level. Figure 7.9 also demonstrates that the proposed retrofitting technique has a more stable lateral force-displacement relationship as compared to the conventional seismic retrofitting technique. The failure of the squat infill shear panels, which have limited drift capacities (approximately 25 mm-40 mm) causes a loss of lateral strength of the conventionally retrofitted school building as observed from Figure 7.9. This clearly shows that the proposed retrofitting technique have a larger monotonic energy dissipating capacity compared to that of the building retrofitted with squat infill shear panels. Compared to the original case, the retrofitted building for both the proposed and conventional cases exhibited a considerable increase in lateral stiffness and strength. This is indicative of a better seismic performance during a potential earthquake.

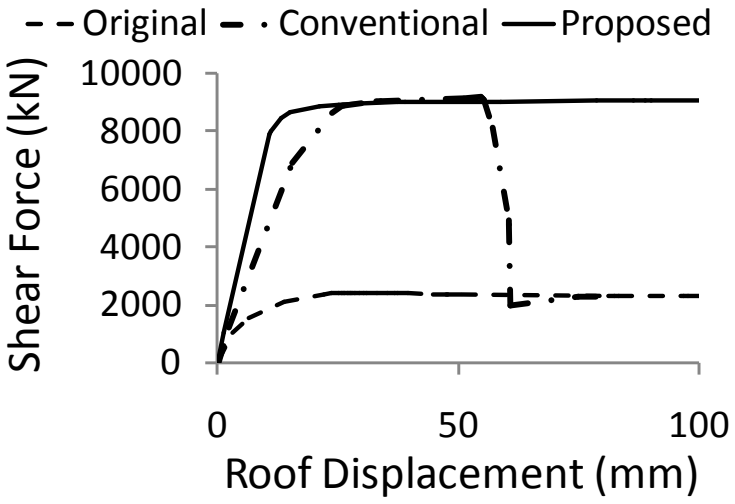


**Figure 7.9** The base shear force as a function of the drift at the top story level for the school building in x direction

### 7.4.2 Comparative Assessment of the School Building's Performance in the Y Direction

The NLP analyses results of the school building in the y direction for the original and retrofitted conditions is shown in Figure 7.10 in terms of a base shear vs. roof displacement plot. As observed from the figure, the performance of the building in the y direction is nearly identical to that in the x direction.

.

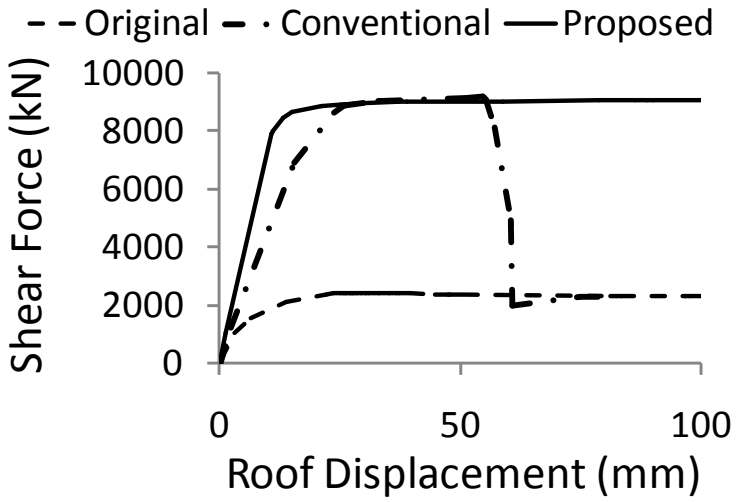


**Figure 7.10** The base shear force as a function of the drift at the top story level for the school building in y direction

## 7.5 Comparative Performance Assessment of the Original and Retrofitted Buildings by NLTH Analyses

In this section, comparative performance evaluation of the original and seismically retrofitted buildings is performed using the NLTH analyses results. The analyses results in terms of the maximum interstory drift, roof displacement and damage indices are presented for each earthquake as well as, using the average of the analyses results from the seven earthquakes. Each earthquake is assigned a number (Table 7.5) to facilitate the presentation of the analyses results

for each earthquake. More detailed information is given in the subsequent sections.

**Table 7.5** Earthquakes and their numbers

| Earthquake Name | ID No |
|---|---|
| Whittier-1987 | 1 |
| Imperial Valley-1979 (1) | 2 |
| Coalinga-1983 | 3 |
| Loma Prieta-1989 | 4 |
| Imperial Valley-1979 (2) | 5 |
| Imperial Valley-1940 | 6 |
| Westmoreland-1981 | 7 |

### 7.5.1 NLTH Analyses Results in the X Direction of the School Building

Tables 7.6, 7.7 and 7.8 compare the average of the interstory drift demands from the seven earthquakes with the interstory drift capacities respectively for the original building as well as the building retrofitted with the proposed and conventional methods. In the tables, the analyses results are presented for the three performance levels (IO, LS, CP) considered in the retrofitting design of the building. As observed from the tables, for the original building, the interstory drift demands severely exceed the interstory drift capacities for all the performance levels considered in the analyses. For the building retrofitted with the proposed method however, the interstory drift demands are smaller than the corresponding capacities for all the performance levels considered in the retrofitting design. Nevertheless, this is not the case for the building retrofitted with the conventional method. For this case, while the IO performance level is completely satisfied, the interstory drift demands at the LS and CP performance levels for the first story are larger than the corresponding capacities. It is worth noting that for the case of the building retrofitted with the conventional method, the interstory drift demands are even larger than those of the original building at the CP performance level. The

main reason for this type of a behavior is the low ductility, the heavy weight and pinching in the hysteresis loops of the squat infill shear panels used in conventional retrofitting of the building. At the CP performance level, the large intensity of the ground motions results in large seismic forces acting on the structure. The added weight of the squat infill shear panels further amplifies the magnitude of these forces. Moreover, due to the low ductility of the squat infill shear panels, these components fail at small interstory drift levels rendering the stiffness and strength contribution of the wall ineffective during the earthquake. This sudden failure results in an amplified interstory drift demands.

Figure 7.11 displays the maximum interstory drifts and maximum roof displacements of the original and seismically retrofitted buildings as a function of the earthquakes used in the analyses for each one of the seismic performance levels (IO, LS, CP) considered in the retrofitting design. Figure 7.12 displays the same information for the average of the maximum interstory drifts and maximum roof displacements from the seven earthquakes used in the analyses. For the IO performance level, Figure 7.11 shows that the lateral drift responses of the building retrofitted with the proposed and conventional techniques are comparable. For the LS and CP performance levels however, there is a considerable increase in the value of the lateral drifts of the original and conventionally retrofitted cases of the school building. The story drift demands in the case of the building retrofitted with the proposed method are quite low and uniform regardless of the earthquake ground motion used in the analyses. However, for the case of the building retrofitted with the conventional method, the drift demands fluctuate with respect to the ground motion used in the analyses and reach levels greater that those of the original building.

In summary, both seismic retrofitting techniques display a more desirable response than that of unretrofitted building for the IO performance level. However, for the LS and CP performance levels, the response of the building retrofitted with the conventional technique becomes unsatisfactory due to the effect of the heavy weight and premature failure of the squat infill shear panels. In

addition, the proposed seismic retrofitting technique displays a highly stable response regardless of the characteristics (e.g. frequency content) of the earthquake used in the analyses.

**Table 7.6** Comparison of the average of the maximum interstory drifts from the seven earthquakes with the interstory drift capacity for the original building in the x direction

| Story | Performance Level | | | | | |
|---|---|---|---|---|---|---|
| | IO | | LS | | CP | |
| | Demand (mm) | Capacity (mm) | Demand (mm) | Capacity (mm) | Demand (mm) | Capacity (mm) |
| 1 | 60 | 19 | 105 | 44 | 172 | 59 |
| 2 | 19 | 19 | 14 | 44 | 22 | 59 |

**Table 7.7** Comparison of the average of the maximum interstory drifts from the seven earthquakes with the interstory drift capacity for the building retrofitted with the proposed method in the x direction

| Story | Performance Level | | | | | |
|---|---|---|---|---|---|---|
| | IO | | LS | | CP | |
| | Demand (mm) | Capacity (mm) | Demand (mm) | Capacity (mm) | Demand (mm) | Capacity (mm) |
| 1 | 7 | 19 | 12 | 50 | 31 | 66 |
| 2 | 15 | 19 | 25 | 50 | 43 | 66 |

**Table 7.8** Comparison of the average of the maximum interstory drifts from the seven earthquakes with the interstory drift capacity for the building retrofitted with the conventional method in the x direction

| Story | Performance Level | | | | | |
|---|---|---|---|---|---|---|
| | IO | | LS | | CP | |
| | Demand (mm) | Capacity (mm) | Demand (mm) | Capacity (mm) | Demand (mm) | Capacity (mm) |
| 1 | 21 | 19 | 54 | 45 | 233 | 69 |
| 2 | 14 | 19 | 16 | 45 | 17 | 69 |

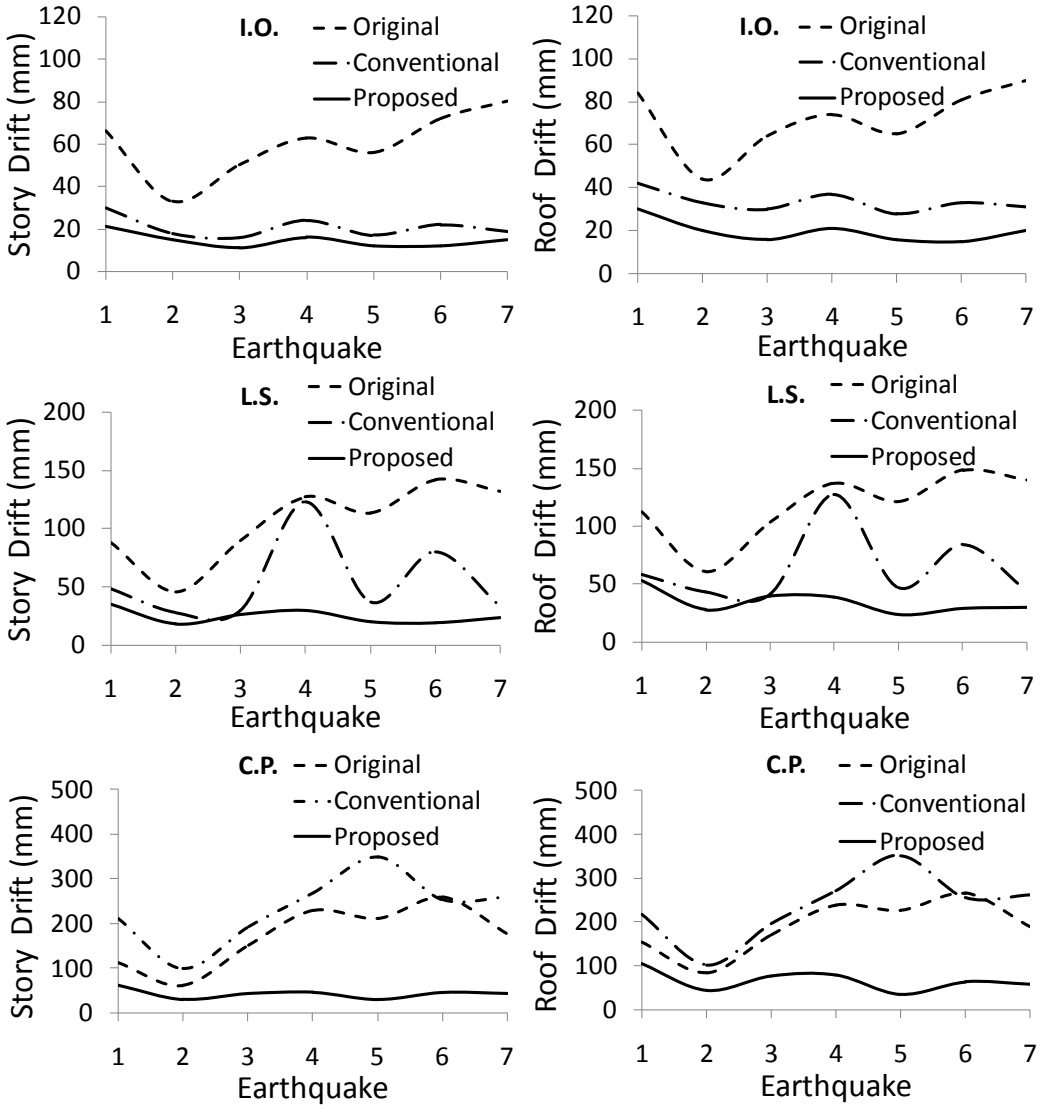


**Figure 7.11** Maximum interstory and roof drifts for the school building in x direction

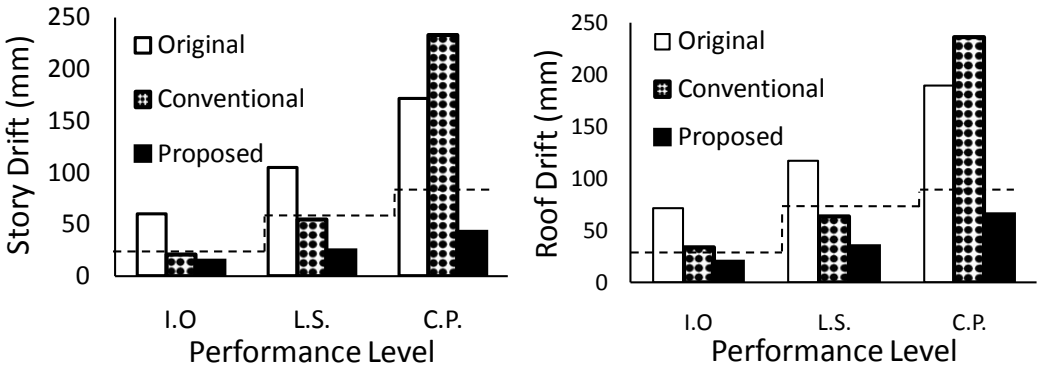


**Figure 7.12** Average interstory and roof drifts for the school building in x direction

### 7.5.2 NLTH Analyses Results in the Y Direction of the School Building

The NLTH analyses results of the school building in the y direction for the original and retrofitted conditions are tabulated in Tables 7.9, 7.10 and 7.11 and shown in Figures 7.13 and 7.14. As observed from the tables and figures, the performance of the building in the y direction is nearly identical to that in the y direction.

**Table 7.9** Comparison of the average of the maximum interstory drifts from the seven earthquakes with the interstory drift capacity for the original building in the y direction

| Story | Performance Level | | | | | |
|---|---|---|---|---|---|---|
| | IO | | LS | | CP | |
| | Demand (mm) | Capacity (mm) | Demand (mm) | Capacity (mm) | Demand (mm) | Capacity (mm) |
| 1 | 48 | 18 | 74 | 48 | 131 | 60 |
| 2 | 34 | 18 | 47 | 48 | 66 | 60 |

**Table 7.10** Comparison of the average of the maximum interstory drifts from the seven earthquakes with the interstory drift capacity for the building retrofitted with the proposed method in the y direction

| Story | Performance Level | | | | | |
|---|---|---|---|---|---|---|
| | IO | | LS | | CP | |
| | Demand (mm) | Capacity (mm) | Demand (mm) | Capacity (mm) | Demand (mm) | Capacity (mm) |
| 1 | 13 | 19 | 25 | 49 | 61 | 62 |
| 2 | 12 | 24 | 18 | 58 | 25 | 73 |

**Table 7.11** Comparison of the average of the maximum interstory drifts from the seven earthquakes with the interstory drift capacity for the building retrofitted with the conventional method in the y direction

| Story | Performance Level | | | | | |
|---|---|---|---|---|---|---|
| | IO | | LS | | CP | |
| | Demand (mm) | Capacity (mm) | Demand (mm) | Capacity (mm) | Demand (mm) | Capacity (mm) |
| 1 | 20 | 18 | 55 | 45 | 211 | 58 |
| 2 | 11 | 18 | 13 | 45 | 14 | 58 |

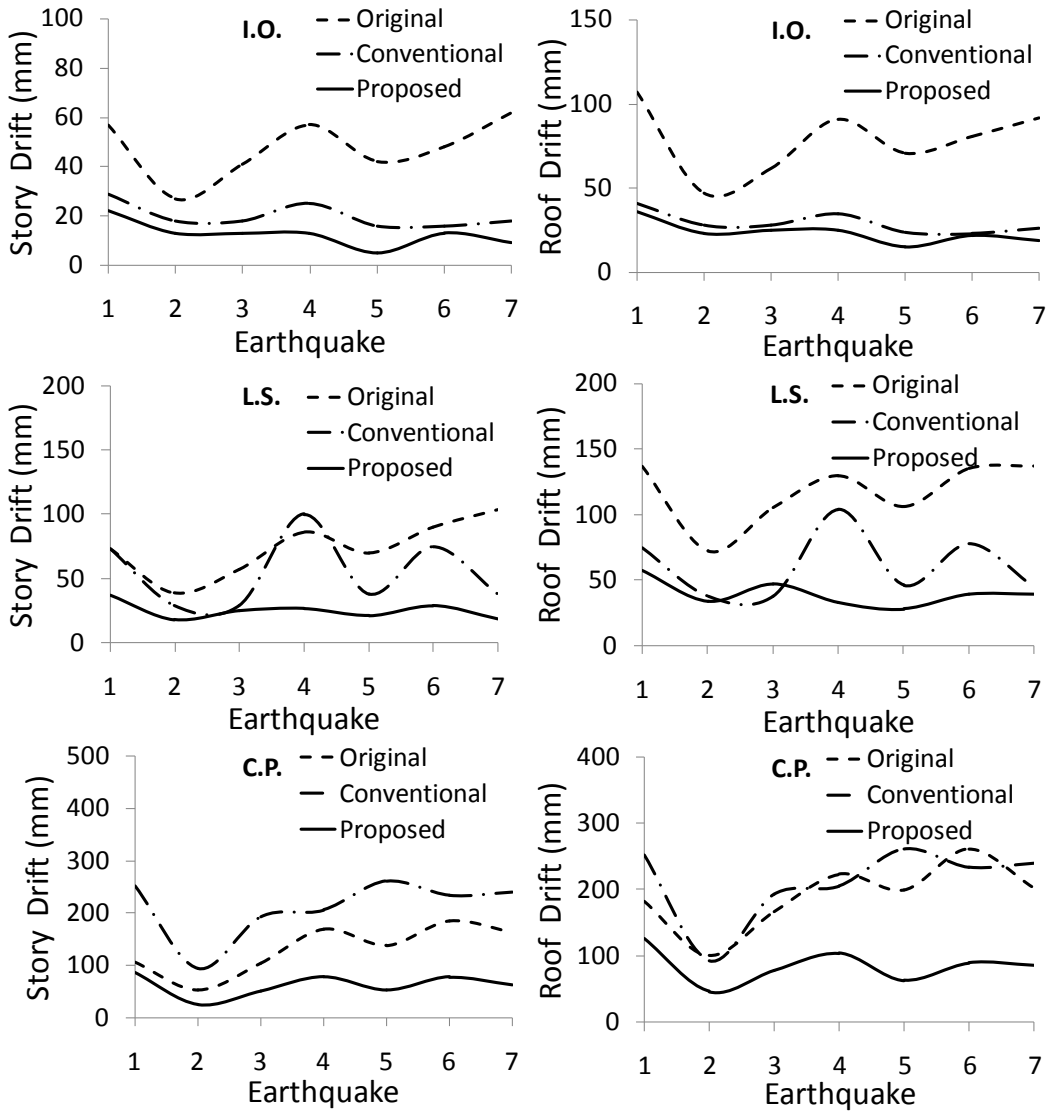


**Figure 7.13** Maximum roof and story drifts for the school building in y direction

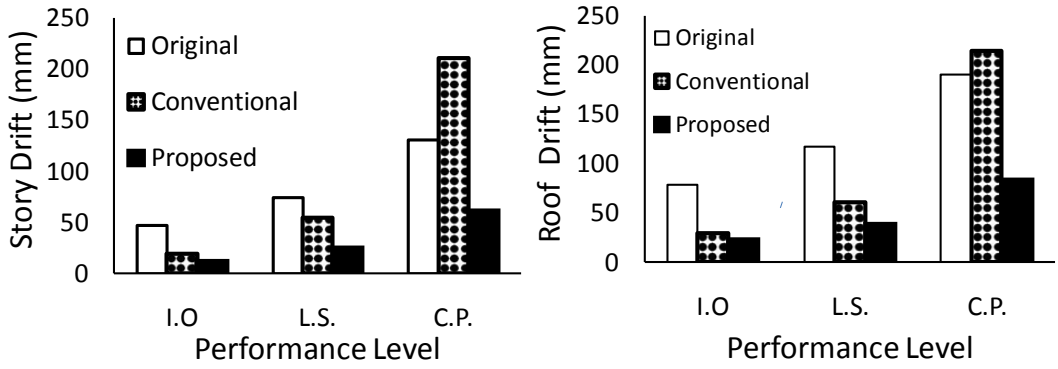


**Figure 7.14** Average roof and story drifts for the school building in y direction

## 7.6 Shear Link Rotations for the Proposed Retrofitting System of the School building

As mentioned earlier (Chapter 2), Kasai and Popov (1986a, 1986b) conducted experimental tests on shear links made of stiffened W-sections. The test results indicated a maximum rotation capacity of 0.1 radian for these sections. However, the HP sections used in this study as links are stockier (made of much thicker web plates) than the W-sections tested by Kasai and Popov (1986a, 1986b). Therefore, it is expected that the HP sections used in this study as links may have rotation capacities larger than 0.1 radian. This needs to be verified experimentally. The rotation values of the most critical shear links in the most critical performance level (CP) are presented for x and y directions of the school building in Figure 7.15. Table 7.12 gives the locations and ID numbers of the links used in the NLTH analyses. In the table, the link locations are labeled as s-x(a1-a2) where s is the story number, x is the axis label along the retrofitted bay and a1 and a2 are the axis labels at the left and right ends of the retrofitted bay of the frame. As observed from Figure 7.15 the link rotations are smaller than or equal to 0.1 radian. Thus, the shear links used as part of the proposed retrofitting system are expected to function as intended.

**Table 7.12** Shear link locations and ID numbers

| X Direction | | Y Direction | |
|---|---|---|---|
| **Location** | **Link ID** | **Location** | **Link ID** |
| 2-1(A-C) | 1 | 2-A(1-2) | 1 |
| 2-1(C-E) | 2 | 2-A(8-9) | 2 |
| 2-9(A-C) | 3 | 2-E(1-2) | 3 |
| 2-9(C-E) | 4 | 2-E(8-9) | 4 |
| 1-1(A-C) | 5 | 1-A(1-2) | 5 |
| 1-1(C-E) | 6 | 1-A(4-5) | 6 |
| 1-4(A-B) | 7 | 1-A(5-6) | 7 |
| 1-4(D-E) | 8 | 1-A(8-9) | 8 |
| 1-6(A-B) | 9 | 1-E(1-2) | 9 |
| 1-6(D-E) | 10 | 1-E(4-5) | 10 |
| 1-9(A-C) | 11 | 1-E(5-6) | 11 |
| 1-9(C-E) | 12 | 1-E(8-9) | 12 |

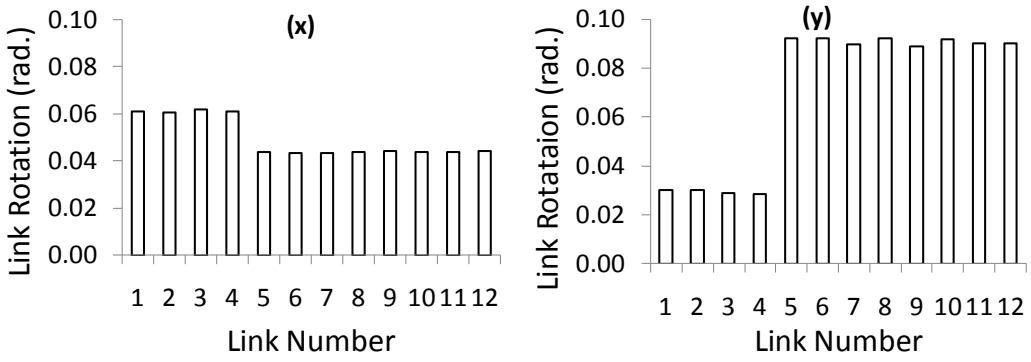


**Figure 7.15** Shear link rotations for the proposed retrofitting system of the school building in the x and y directions

### 7.7. Evaluation of the Story Drifts Along the Height of the School Building

Maximum story drift levels along the height of the school building is shown to further assess the performance of the proposed seismic retrofitting system in relation to original and conventional seismically retrofitted cases of the school building.

#### 7.7.1. Evaluation of the Story Drifts in X Direction

Maximum story drift levels along the height of the school building in the x-direction are given in this section. The deformed shapes of the buildings are obtained at the instant when the maximum interstory drift occurs. Figure 7.16 compares the deformed shapes of the original building as well as the building retrofitted with the proposed and conventional methods for the average of the seven ground motions for IO, LS and CP performance levels.

For the IO performance level, the figure shows that both the building retrofitted with the proposed and conventional method display similar deformed shapes. For LS and CP performance level however, both the original and the conventionally retrofitted building display similar deformed shapes. The deformation of both buildings is mostly concentrated at the first-story level with the deformation at the upper story level being relatively modest. This clearly indicates the formation of a soft story and the concentration of the energy dissipation at the first story level. For the CP performance level, the collapse of the squat infill shear panels in the case of the conventional method dominates the behavior of the retrofitted building, where interstory drifts larger than those of the original building are observed. In the case of the building retrofitted with the proposed method the deformations at the first and second story levels are uniform indicating a uniform distribution of energy along the building height.

In summary, the building retrofitted with the proposed method has a smaller interstory drifts compared to the other buildings for all performance levels

considered. This is indicative of less damage in the case of a potential earthquake. Furthermore, compared to the original and the conventionally retrofitted building, the building retrofitted with the proposed technique exhibit a more uniform lateral deformation pattern, and hence a more even distribution of energy dissipation along the height of the building.

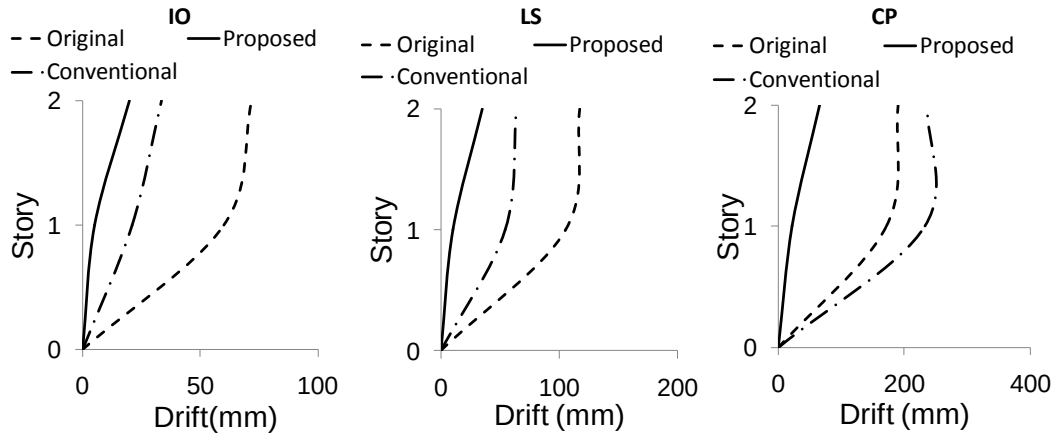


**Figure 7.16** Maximum story drifts along the height of the building for x direction

### 7.7.2. Evaluation of the Story Drifts in Y Direction

Maximum story drift levels along the height of the school building in the y-direction are shown in Figure 7.17. As observed from the figure, the performance of the buildings in the y direction is nearly identical to that in the x direction.

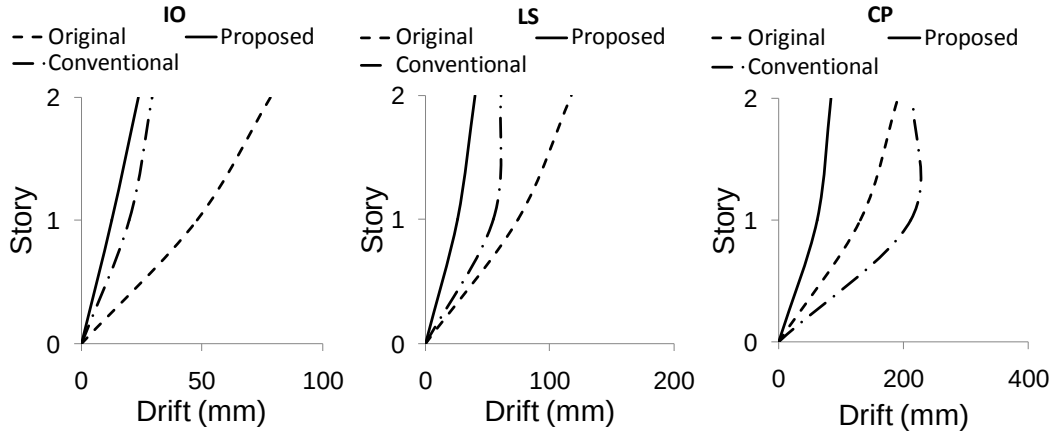


**Figure 7.17** Maximum story drifts along the height of the building for y direction

## 7.8 Comparative Damage Analyses of the Original and Retrofitted Buildings

### 7.8.1 General

In this section, damage analyses of the school building are performed to further assess the performance of the proposed seismic retrofitting system in relation to the original and conventional seismically retrofitted cases of the school building. Seismic damage quantification is generally represented by damage indices that range between 0 (no damage) and 1 (complete collapse). Many researchers have proposed a number of damage models that calculate damage indices (Banon et al. 1981; Park and Ang, 1985; Kunnath et al. 1997; Chai, 1999; Perera et al. 2000; Mehanny and Deierlein, 2001; Khashaee, 2005). However, most of these damage models have concentrated almost exclusively on flexural modes of failure. Thus, they may not be applicable to the proposed and conventional retrofitting systems used in this study, due to the presence of shear yielding of shear links and shear dominant behavior and failure of squat infill shear panels. Nevertheless, the damage model proposed by Hindi and Sexsmith (2001) is primarily based on the monotonic energy dissipating capacity of structural elements before and after the application of reversed cyclic loading. Therefore, it may be universally applicable to structural members exhibiting failure modes other than flexure, including steel members failing in the shear mode. The validity of the model proposed by Hindi

and Sexsmith (2001) to predict shear induced damage in squat infill shear panels has already been proven by Hindi et al (2004). Furthermore, the damage model proposed by Hindi and Sexsmith (2001) is different than most existing damage models in that it does not require any tuning of damage equation coefficients for a particular type of failure. Consequently, it is used for the damage assessment of the retrofitted buildings employed in this study.

### 7.8.2 Damage Model of Hindi and Sexsmith (2001)

The damage model takes as a reference the monotonic energy dissipation capacity of a structure in the undamaged virgin state, which is defined as the area, $A_o$, under the static pushover curve up to the point of failure (Figure 7.18 (a)). With the actual "n" cycles of load-displacement history applied on the structure due to a potential earthquake, the remaining monotonic energy dissipation capacity of the structure, compared to that in its virgin state, defines the extent of damage. The remaining monotonic energy dissipation capacity of the structure is defined as the area, $A_n$, under the static pushover curve obtained from the end of the last cycle, n, to the failure point (Figure 7.18 (b)). Accordingly, the damage index is the ratio

$$D_n = \frac{A_o - A_n}{A_0} \tag{7.1}$$

A damage index of 0 ($A_n=A_o$) is indicative of no damage, whereas a damage index of 1 ($A_n=0$) is indicative of complete damage or collapse.

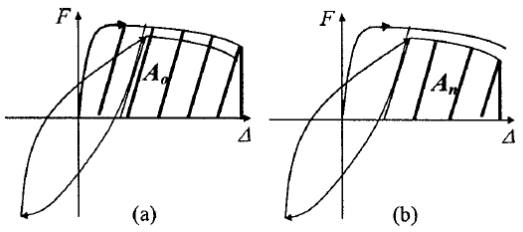


**Figure 7.18** Damage model of Hindi and Sexsmith (2001)

### 7.9.3 Damage Analyses of the School Building

The damage analyses of the original and seismically retrofitted cases (with conventional and proposed techniques) of the school building are performed as part of this study. NLP analyses results of (Figures 7.9 and 7.10) are used to obtain the monotonic energy dissipation capacity**,** Ao**,** in the virgin state. The failure point is calculated, based on the recommendations of FEMA-356 (2000) story drift limits for CP performance level. The school building is then subjected to seven SSRS compatible ground motions with different scale factors for the three performance levels considered in the retrofitting design. At the end of the seismic event, the properties of the school building are different from the original state, as the building undergoes permanent plastic deformation and suffer a reduction in the lateral stiffness and strength values. Displacement controlled NLP analyses are then performed on the frames starting from the end of the last cycle of the hysteretic load-displacement curve due to the applied earthquake ground motion. The area (energy) under the static pushover curve, $A_n$, is then calculated for the damaged state and substituted in Equation 7.1 to obtain the damage indices for the school building.

### 7.8.4 Discussion of Damage Analyses Results

The results of the damage analyses of the school building for the x and y directions are presented in Figure 7.19. In the figure, the averages of the damage indices from the seven earthquakes used in the analyses are plotted as a function of the performance level. It is observed from the figure that for the IO performance level a complete collapse ($D_n$=1) of the original building is observed while the damage indices for the buildings retrofitted with the proposed and conventional methods are quite low and comparable. For the LS and CP performance levels the building retrofitted with the proposed method experiences significantly less damage than the one retrofitted with the conventional method. This indicates a greater reserve energy dissipation capacity, less damage, and smaller rehabilitation cost after a major seismic activity in the case of the building

retrofitted with the proposed method. Thus, the damage analyses further reinforce the more desirable behavior of the building retrofitted with the proposed technique, as compared to that retrofitted with the conventional technique.

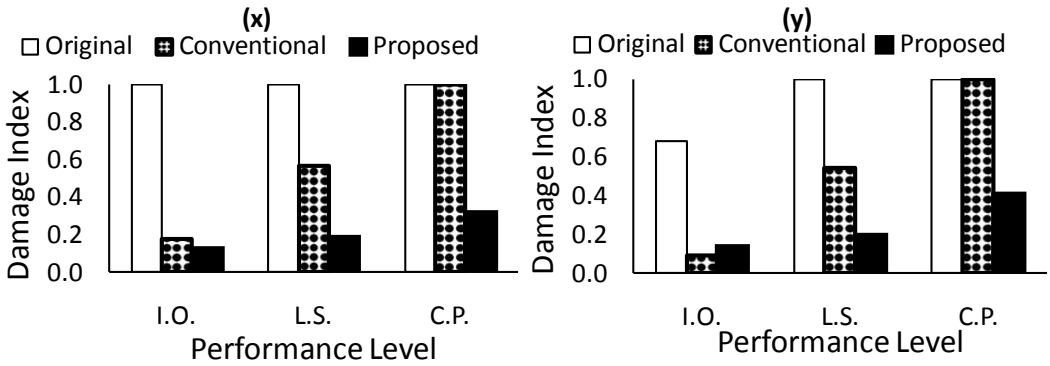


**Figure 7.19** Damage analyses results of the school building in the x and y directions

# CHAPTER 8

# SEISMIC RETROFIT EVALUATION OF THE OFFICE BUILDING

## 8.1 General

In this chapter, the seismic performance of the office building is assessed in the original and the retrofitted conditions. The retrofitted conditions include the proposed seismic retrofitting technique using steel shear link and braces encased in a steel frame and a conventional seismic retrofitting technique using squat infill shear panels. Both NLP and NLTH analyses of the office building in the original and retrofitted conditions are conducted to assess its seismic performance. The seismic performance assessment of the building is performed in terms of seismic displacement demands and capacities as well as damage indices calculated for the original and retrofitted conditions of the building.

## 8.2 Details of the Proposed Seismic Retrofitting Method

The sizes of the steel shear links and braces for the proposed seismic retrofitting method are given in Tables 8.1 and 8.2 for the x and y directions of the building respectively. Figure 8.1 shows the locations of the steel retrofitting panels used in the x direction while Figure 8.2 shows the locations of the steel retrofitting panels used in the y direction. In the figures the locations of the retrofitting system are shown using thick black lines on the building plan.

**Table 8.1** Details of the steel retrofitting members in the x direction

| Steel sections used in X-direction | | | |
|---|---|---|---|
| **Story #** | **Shear Link** | **Braces** | **Frame Members** |
| 2 | HE200M | HE120M | HE220B |
| 3 | HE180M | HE100M | HE220B |
| 4 | HE180M | HE100M | HE220B |
| 5 | HE140M | HE100B | HE180B |
| 6 | HE140B | HE100B | HE180B |

**Table 8.2** Details of the steel retrofitting members in the y direction

| Steel sections used in Y-direction | | | |
|---|---|---|---|
| **Story #** | **Shear Link** | **Braces** | **Frame Members** |
| 1 | HE200M | HE120M | HE220B |
| 2 | HE200M | HE120M | HE220B |
| 3 | HE200M | HE100M | HE220B |
| 4 | HE200M | HE100M | HE220B |
| 5 | HE160M | HE100B | HE180B |
| 6 | HE140B | HE100B | HE180B |

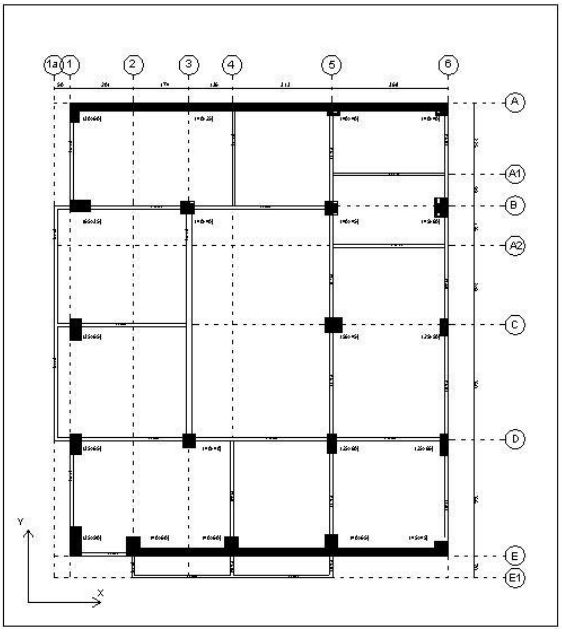


**Figure 8.1** Locations of the steel retrofitting panels within a story in the x direction

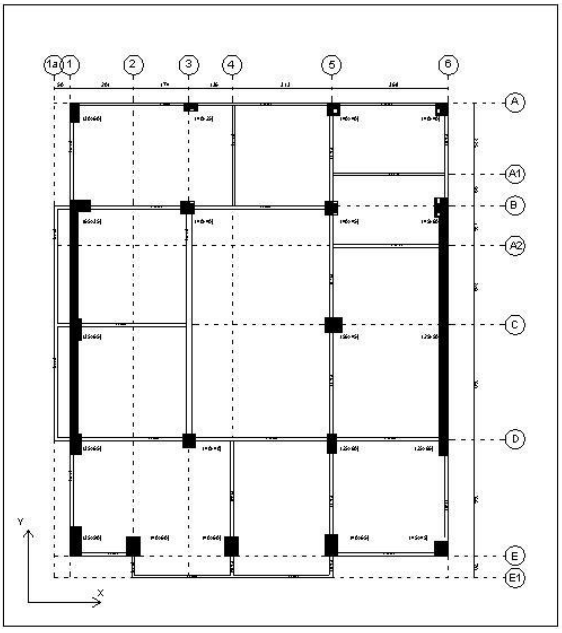


**Figure 8.2** Locations of the steel retrofitting panels within a story in the y direction

### 8.3 Details of the Conventional Seismic Retrofitting Method

The details of the squat infill shear panels, used in the conventional seismic retrofitting of the building are given in Tables 8.3 and 8.4 for the x and y directions of the building respectively. Figure 8.3 shows the locations of the squat infill shear panels used in the x direction while Figure 8.4 shows the locations of the squat infill shear panels used in the y direction. In the figures the locations of the retrofitting system are shown using thick black lines on the building plan.

**Table 8.3** Details of the squat infill shear panels in the x direction

| **Squat infill shear panels used in X-direction** | | | | **$f_c'$ (Mpa)** | **$f_y$ (Mpa)** | **Reinforcement %** |
|---|---|---|---|---|---|---|
| **Story** | **Width (m)** | **Height (m)** | **Thickness (m)** | | | |
| **2** | 3.30 & 2.93 | 3.35 & 3.55 | 0.10 & 0.12 | 20 | 420 | 0.30 & 0.25 |
| **3** | 3.30 & 2.93 | 2.25 & 2.55 | 0.10 & 0.12 | 20 | 420 | 0.21 & 0.20 |
| **4** | 3.30 & 2.93 | 2.25 & 2.55 | 0.10 & 0.12 | 20 | 420 | 0.21 & 0.20 |
| **5** | 3.30 & 2.93 | 2.25 & 2.55 | 0.10 & 0.12 | 20 | 420 | 0.13 & 0.13 |
| **6** | 3.30 & 2.93 | 2.25 & 2.55 | 0.10 & 0.10 | 20 | 420 | 0.13 & 0.13 |

**Table 8.4** Details of the squat infill shear panels in the y direction

| **Squat infill shear panels used in Y-direction** | | | | **$f_c'$ (Mpa)** | **$f_y$ (Mpa)** | **Reinforcement %** |
|---|---|---|---|---|---|---|
| **Story** | **Width (m)** | **Height (m)** | **Thickness (m)** | | | |
| **1** | 3.40 | 2.70 | 0.10 | 20 | 420 | 0.13 |
| **2** | 3.40 | 3.40 | 0.10 | 20 | 420 | 0.13 |
| **3** | 3.40 | 2.55 | 0.10 | 20 | 420 | 0.13 |
| **4** | 3.40 | 2.55 | 0.10 | 20 | 420 | 0.13 |
| **5** | 3.40 | 2.55 | 0.10 | 20 | 420 | 0.11 |
| **6** | 3.40 | 2.55 | 0.10 | 20 | 420 | 0.11 |

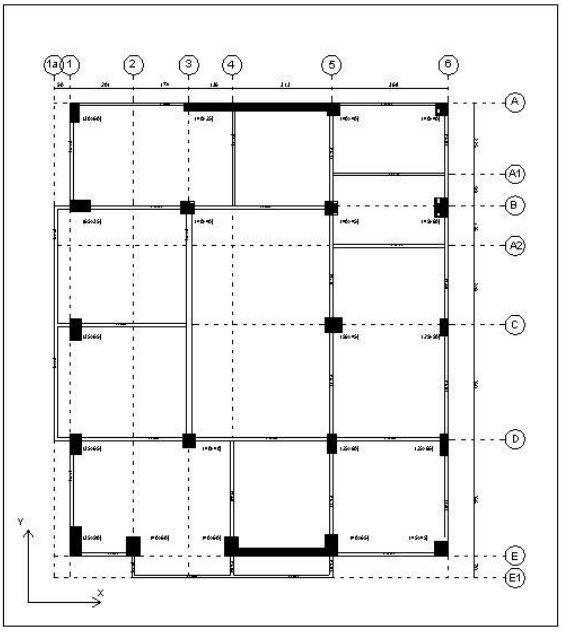


**Figure 8.3** Locations of the squat infill shear panels within a story in the x direction

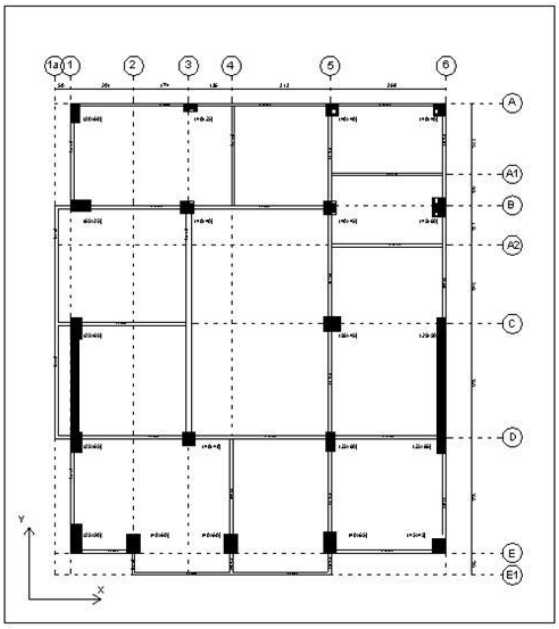


**Figure 8.4** Locations of the squat infill shear panels within a story in the y direction

## 8.4. Seismic Performance Evaluation of the Office Building Using the NLP Analyses Results

In this section, comparative performance evaluation of the original and seismically retrofitted buildings is performed using the NLP analyses results. More detailed information is given in the subsequent sections.

### 8.4.1 Comparative Assessment of the Office Building's Performance in the X Direction

The NLP analyses results of the office building in the x direction for the original and retrofitted conditions is shown in Figure 8.5 in terms of a base shear vs. roof displacement plot. Figure 8.5 shows that the proposed retrofitting technique has a larger monotonic energy dissipating capacity compared to that of the building retrofitted with squat infill shear panels. Compared to the original case, the retrofitted building for both the proposed and conventional cases exhibited a considerable increase in lateral stiffness and strength. This is indicative of a better seismic performance during a potential earthquake.

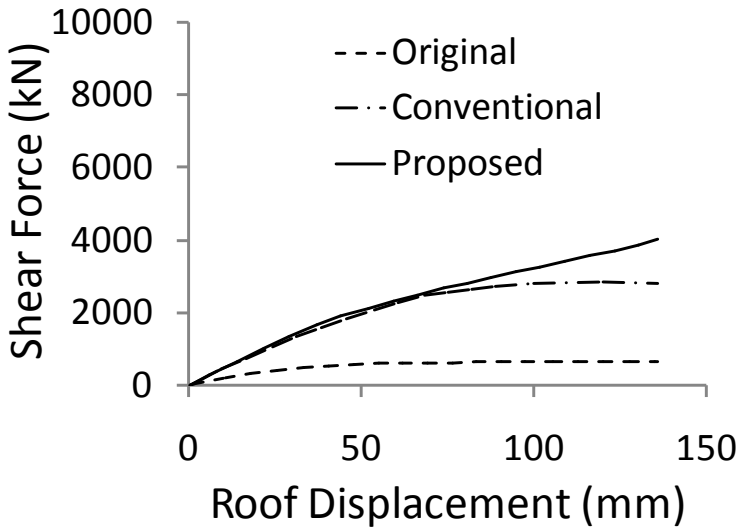


**Figure 8.5** The base shear force as a function of the drift at the top story level for the office building in x direction

### 8.4.2 Comparative Assessment of the Office Building's Performance in the Y Direction

The NLP analyses results of the office building in the y direction for the original and retrofitted conditions is shown in Figure 8.6 in terms of a base shear vs. roof displacement plot. From the figure, it is observed that the elastic lateral stiffness of the conventionally retrofitted structure is smaller than the structure retrofitted with the proposed method. As in the case of the school building, this difference is attributed to the larger number of steel panels required to achieve the same yield strength level as that of the squat infill shear panels. This, in turn resulted in a higher elastic stiffness for the building retrofitted using the proposed method. Thus, it is expected that the structure retrofitted with the proposed technique will have a smaller drift, and hence a more desirable performance (e.g. less non structural damage) under the effect of small intensity earthquakes associated with the IO performance level. Figure 8.6 clearly shows that the proposed retrofitting technique have a larger monotonic energy dissipating capacity compared to that of the building retrofitted with squat infill shear panels. Compared to the original case, the retrofitted building for both the proposed and conventional cases exhibited a considerable increase in lateral stiffness and strength. This is indicative of a better seismic performance during a potential earthquake.

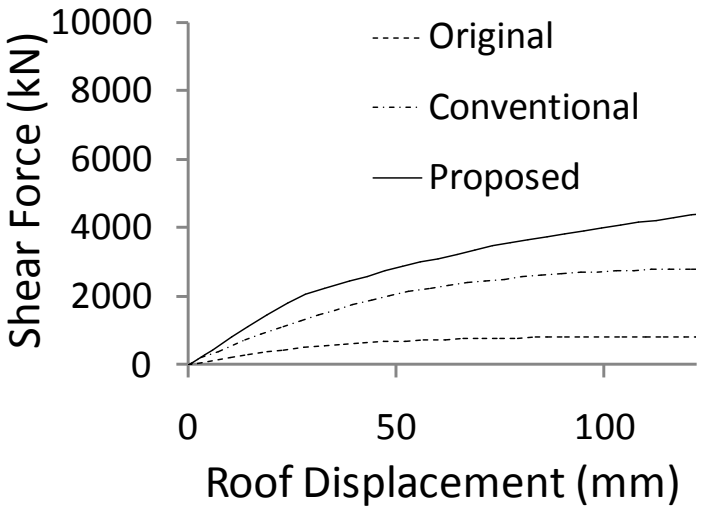


**Figure 8.6** The base shear force as a function of the drift at the top story level for the office building in y direction

## 8.5 Comparative Performance Assessment of the Original and Retrofitted Buildings by NLTH Analyses

In this section, comparative performance evaluation of the original and seismically retrofitted buildings is performed using the NLTH analyses results. The analyses results in terms of the maximum interstory drift, roof displacement and damage indices are presented for each earthquake as well as, using the average of the analyses results from the seven earthquakes.

### 8.5.1 NLTH Analyses Results in the X Direction of the Office Building

Tables 8.5, 8.6 and 8.7 compare the average of the interstory drift demands from the seven earthquakes with the interstory drift capacities respectively for the original building as well as the building retrofitted with the proposed and conventional methods. In the tables, the analyses results are presented for the three performance levels (IO, LS, CP) considered in the retrofitting design of the building. As observed from the tables, for the original building, the interstory drift

demands severely exceed (especially for the fifth and the sixth stories) the interstory drift capacities for all the performance levels considered in the analyses. For the building retrofitted with the proposed method however, the interstory drift demands are nearly equal to the corresponding capacities for all the performance levels considered in the retrofitting design. Nevertheless, this is not the case for the building retrofitted with the conventional method. For this case, while the interstory drift demands for the IO performance level is completely satisfied, the interstory drift demands at the LS and CP performance levels for the fifth and sixth stories are extremely larger than the corresponding capacities. This may be attributed to the heavy weight and pinching in the hysteresis loops of the squat infill shear panels resulting in smaller energy dissipation throughout the earthquake compared to the case associated with proposed retrofitting system.

Figure 8.7 displays the maximum interstory drifts and maximum roof displacements of the original and seismically retrofitted buildings as a function of the earthquakes used in the analyses for each one of the seismic performance levels (IO, LS, CP) considered in the retrofitting design. Figure 8.8 displays the same information for the average of the maximum interstory drifts and maximum roof displacements from the seven earthquakes used in the analyses. For the IO, performance level, Figures 8.7 and 8.8 show that the lateral drift responses of the original building and the building retrofitted with the proposed and conventional techniques are comparable. For the LS and CP performance levels however, there is a considerable increase in the value of the lateral drifts of the original office building. Furthermore, Figure 8.8 shows that the story drift demands in the case of the building retrofitted with the proposed method are lower than the building retrofitted with the conventional technique.

In summary, both seismic retrofitting techniques display a more desirable response than that of unretrofitted building for the IO performance level. However, for the LS and CP performance levels, the response of the building retrofitted with the conventional technique becomes unsatisfactory due to the

extremely large drift demands ( Table 8.6 and 8.7) due to the soft story formation, at the upper three story levels of the office building.

**Table 8.5** Comparison of the average of the maximum interstory drifts from the seven earthquakes with the interstory drift capacity for the original building in the x direction

| Story | Performance Level | | | | | |
|---|---|---|---|---|---|---|
| | IO | | LS | | CP | |
| | Demand (mm) | Capacity (mm) | Demand (mm) | Capacity (mm) | Demand (mm) | Capacity (mm) |
| 2 | 13 | 25 | 19 | 28 | 26 | 31 |
| 3 | 14 | 15 | 29 | 18 | 34 | 20 |
| 4 | 17 | 14 | 30 | 16 | 101 | 18 |
| 5 | 17 | 12 | 222 | 15 | 521 | 16 |
| 6 | 11 | 13 | 38 | 15 | 261 | 16 |

**Table 8.6** Comparison of the average of the maximum interstory drifts from the seven earthquakes with the interstory drift capacity for the building retrofitted with the proposed method in the x direction

| Story | Performance Level | | | | | |
|---|---|---|---|---|---|---|
| | IO | | LS | | CP | |
| | Demand (mm) | Capacity (mm) | Demand (mm) | Capacity (mm) | Demand (mm) | Capacity (mm) |
| 2 | 15 | 22 | 24 | 25 | 30 | 32 |
| 3 | 12 | 14 | 19 | 17 | 26 | 23 |
| 4 | 11 | 11 | 19 | 15 | 25 | 20 |
| 5 | 10 | 10 | 18 | 15 | 24 | 19 |
| 6 | 9 | 10 | 16 | 13 | 21 | 18 |

**Table 8.7** Comparison of the average of the maximum interstory drifts from the seven earthquakes with the interstory drift capacity for the building retrofitted with the conventional method in the x direction

| Story | Performance Level | | | | | |
|---|---|---|---|---|---|---|
| | IO | | LS | | CP | |
| | Demand (mm) | Capacity (mm) | Demand (mm) | Capacity (mm) | Demand (mm) | Capacity (mm) |
| 2 | 11 | 23 | 17 | 27 | 20 | 32 |
| 3 | 10 | 17 | 16 | 19 | 19 | 20 |
| 4 | 12 | 14 | 22 | 16 | 29 | 18 |
| 5 | 12 | 13 | 23 | 15 | 34 | 18 |
| 6 | 11 | 13 | 27 | 15 | 44 | 18 |

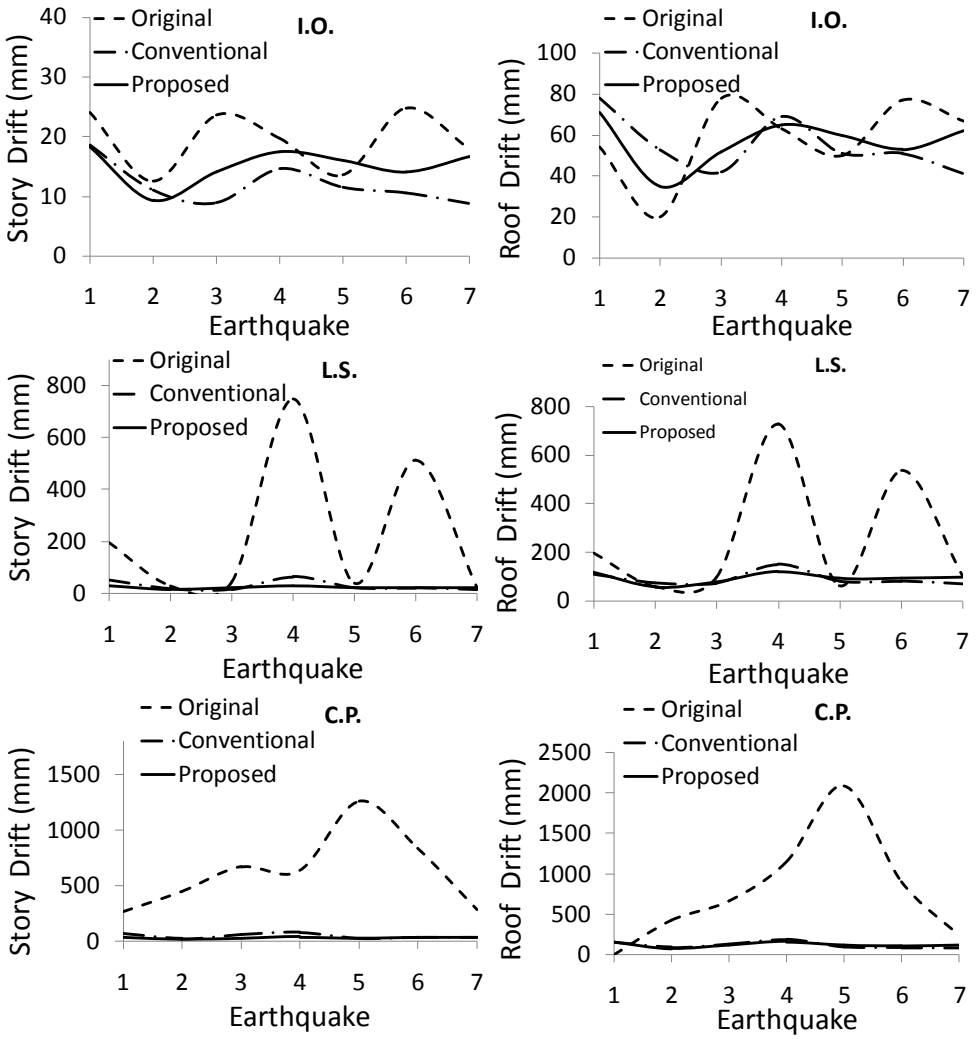


**Figure 8.7** Maximum interstory and roof drifts for the office building in x direction

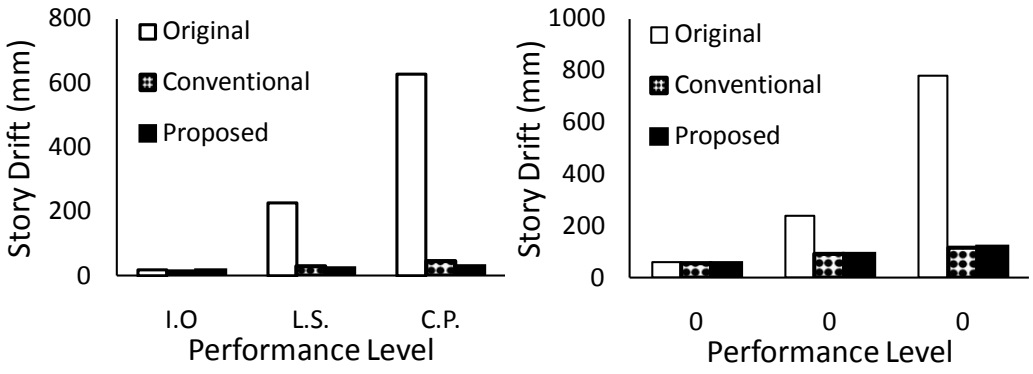


**Figure 8.8** Average interstory and roof drifts for the office building in x direction

### 8.5.2 NLTH Analyses Results in the Y Direction of the Office Building

The NLTH analyses results of the office building in the y direction for the original and retrofitted conditions are tabulated in Tables 8.8, 8.9 and 8.10 and shown in Figures 8.13 and 8.14. As observed from the tables and figures, the performance of the building in the y direction is nearly identical to that in the x direction for the unretrofitted case of the building. However, for both of the retrofitted cases of the office building, the behavior of the office building for IO, LS and CP performance levels is satisfactory where the building retrofitted with the proposed method exhibits a slightly better performance.

**Table 8.8** Comparison of the average of the maximum interstory drifts from the seven earthquakes with the interstory drift capacity for the original building in the y direction

| Story | Performance Level | | | | | |
|---|---|---|---|---|---|---|
| | IO | | LS | | CP | |
| | Demand (mm) | Capacity (mm) | Demand (mm) | Capacity (mm) | Demand (mm) | Capacity (mm) |
| 2 | 11 | 26 | 15 | 29 | 21 | 30 |
| 3 | 12 | 17 | 18 | 18 | 27 | 19 |
| 4 | 15 | 16 | 26 | 17 | 39 | 19 |
| 5 | 16 | 15 | 107 | 16 | 280 | 17 |
| 6 | 19 | 15 | 171 | 16 | 310 | 17 |

**Table 8.9** Comparison of the average of the maximum interstory drifts from the seven earthquakes with the interstory drift capacity for the building retrofitted with the proposed method in the y direction

| Story | Performance Level | | | | | |
|---|---|---|---|---|---|---|
| | IO | | LS | | CP | |
| | Demand (mm) | Capacity (mm) | Demand (mm) | Capacity (mm) | Demand (mm) | Capacity (mm) |
| 2 | 11 | 25 | 19 | 27 | 26 | 30 |
| 3 | 12 | 15 | 19 | 17 | 25 | 20 |
| 4 | 11 | 16 | 16 | 17 | 23 | 20 |
| 5 | 7 | 12 | 10 | 15 | 12 | 18 |
| 6 | 6 | 8 | 9 | 12 | 11 | 15 |

**Table 8.10** Comparison of the average of the maximum interstory drifts from the seven earthquakes with the interstory drift capacity for the building retrofitted with the conventional method in the y direction

| Story | Performance Level | | | | | |
|---|---|---|---|---|---|---|
| | IO | | LS | | CP | |
| | Demand (mm) | Capacity (mm) | Demand (mm) | Capacity (mm) | Demand (mm) | Capacity (mm) |
| 2 | 11 | 24 | 18 | 26 | 24 | 30 |
| 3 | 9 | 17 | 16 | 18 | 24 | 20 |
| 4 | 10 | 14 | 16 | 15 | 22 | 18 |
| 5 | 10 | 13 | 15 | 15 | 19 | 17 |
| 6 | 9 | 13 | 14 | 15 | 16 | 17 |

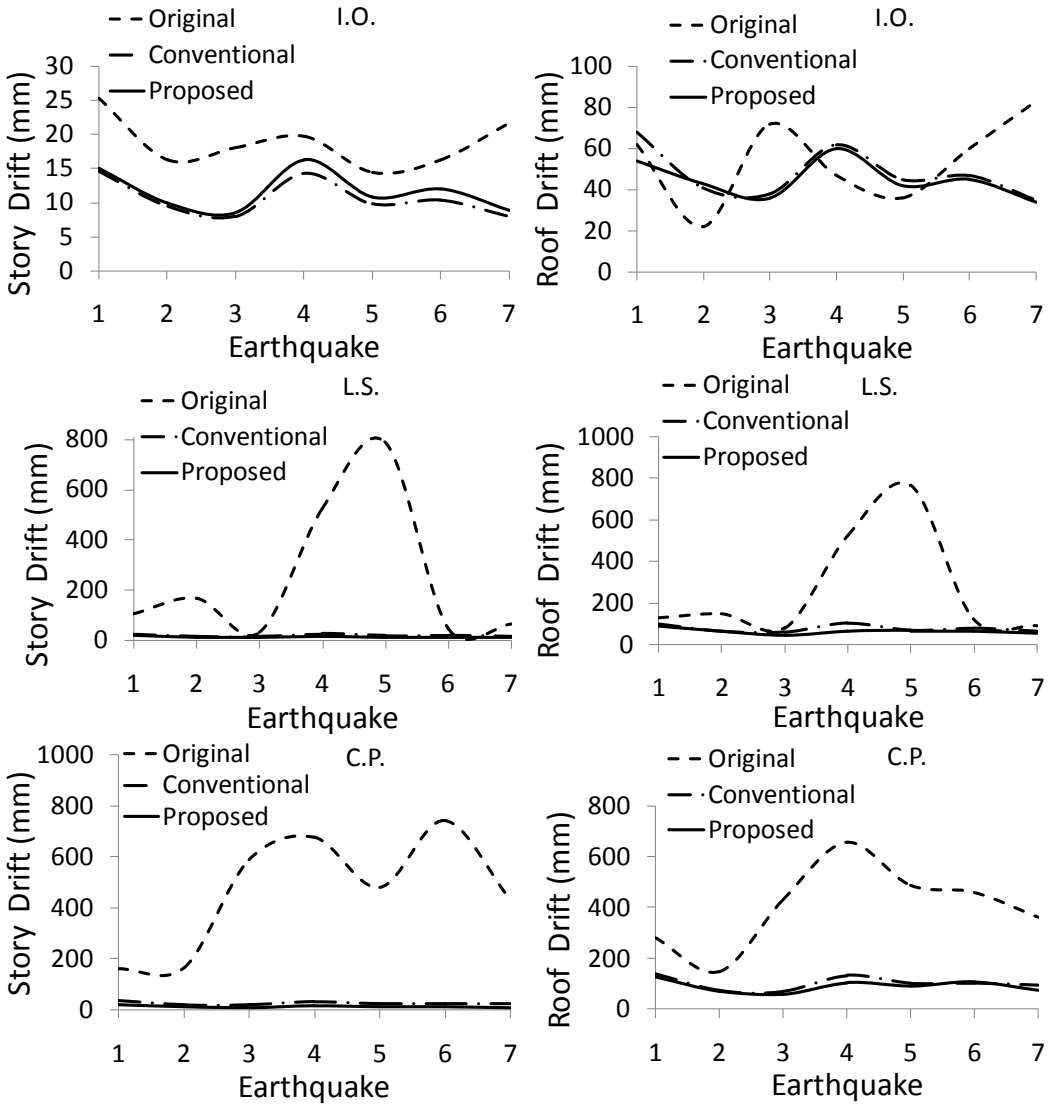


**Figure 8.9** Maximum roof and story drifts for the office building in y direction

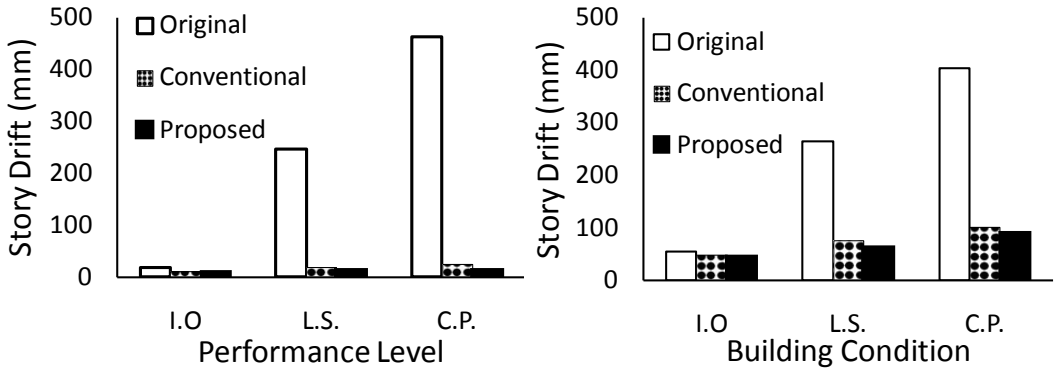


**Figure 8.10** Average roof and story drifts for the office building in y direction

## 8.6 Shear Link Rotations for the Proposed Retrofitting System of the Office building

The rotation values of the most critical shear links in the most critical performance level (CP) are presented for x and y directions of the office building in Figure 8.11. Table 8.11 gives the locations and ID numbers of the links used in the NLTH analyses. As observed from Figure 8.11, the link rotations are smaller than the 0.1 radian limit proposed by Kasai and Popov (1986a, 1986b). Thus, the shear links used as part of the proposed retrofitting system are expected to function as intended.

**Table 8.11** Shear link locations and ID numbers

| X Direction | | Y Direction | |
|---|---|---|---|
| **Location** | **Link ID** | **Location** | **Link ID** |
| 6-A(3-5) | 1 | 6-6(B-C) | 1 |
| 5-A(3-5) | 2 | 5-6(B-C) | 2 |
| 4-A(3-5) | 3 | 4-6(B-C) | 3 |
| 3-A(3-5) | 4 | 3-6(C-D) | 4 |
| 2-A(3-5) | 5 | 2-6(B-C) | 5 |

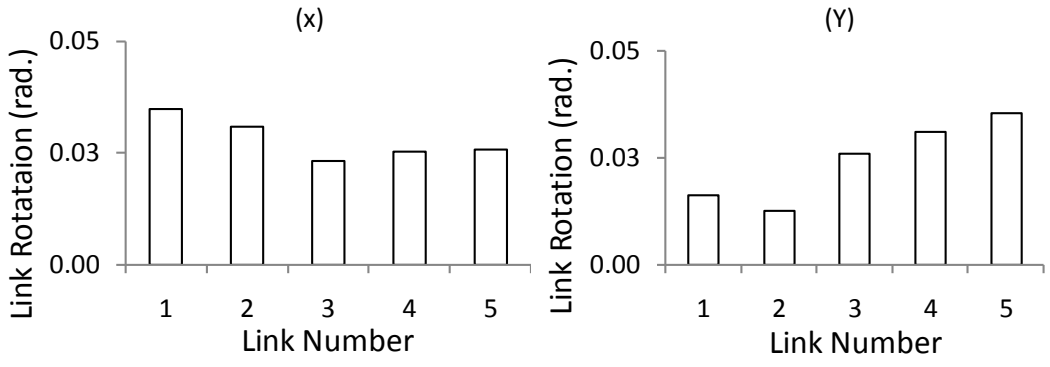


**Figure 8.11** Shear link rotations for the proposed retrofitting system of the office building in the x and y directions

## 8.7. Evaluation of the Story Drifts Along the Height of the Office Building.

Maximum story drift levels along the height of the office building is shown to further assess the performance of the proposed seismic retrofitting system in relation to original and conventional seismically retrofitted cases of the office building.

### 8.7.1. Evaluation of the Story Drifts in X Direction

Maximum story drift levels along the height of the office building in the x-direction are given in this section. The deformed shapes of the buildings are obtained at the instant when the maximum interstory drift occurs. Figure 8.12 compares the deformed shapes of the original building as well as the building retrofitted with the proposed and conventional methods for the average of the seven ground motions for IO, LS and CP performance levels.

For the IO performance level, the figure reveals that both the building retrofitted with the proposed and conventional method display similar deformed shapes. However, for the LS and CP performance levels, the original building and the building retrofitted with the conventional method display a less uniform distribution of interstory drifts along the height of the building compared to that of the building retrofitted with the proposed method. In the case of the original building a severe soft story formation at the fifth story level is observed. The deformation of the building retrofitted with the conventional technique is mostly concentrated at the fifth and sixth -story levels with the deformation at the lower story levels being relatively modest. This resulted in slight soft-story formations at the fifth and sixth story levels, as observed from Figure 8.12, and the concentration of the energy dissipation at the fifth and sixth story levels. Compared to the original and conventionally retrofitted building, the building retrofitted with the proposed technique exhibit smaller interstory drifts, a better lateral deformation pattern, and hence a more even distribution of energy

dissipation along the height of the building. This is indicative of less damage in the case of a potential earthquake.

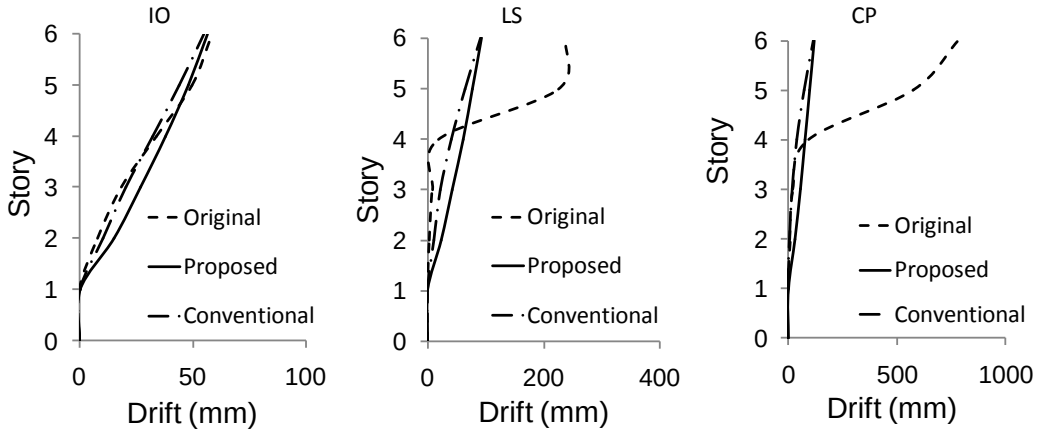


**Figure 8.12** Maximum story drifts along the height of the building for x direction

### 8.7.2. Evaluation of the Story Drifts in Y Direction

Maximum story drift levels along the height of the office building in the y direction for the original and retrofitted conditions are shown in Figure 8.17. As observed from the figure, the performance of the building in the y direction is nearly identical to that in the x direction for the unretrofitted case of the building. However, for both of the retrofitted cases of the office building, the behavior of the office building for IO, LS and CP performance levels are nearly identical and satisfactory.

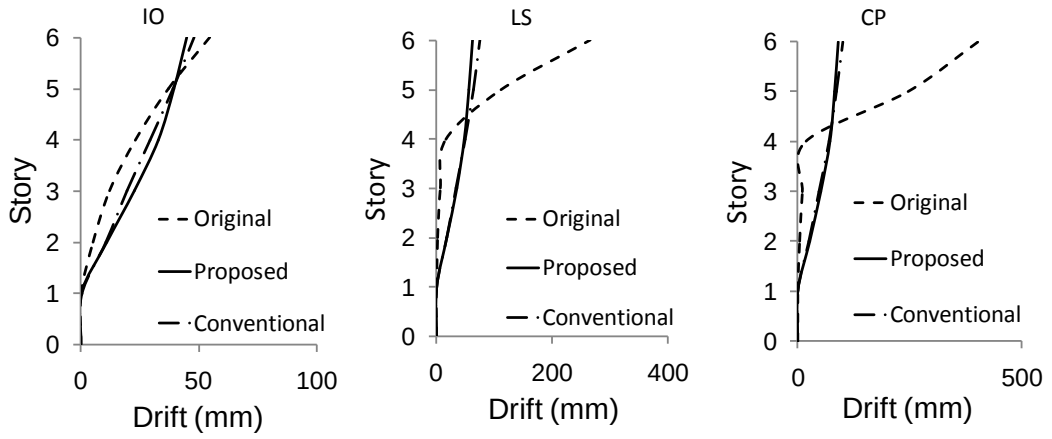


**Figure 8.13** Maximum story drifts along the height of the building for y direction

## 8.8 Comparative Damage Analyses of the Original and Retrofitted Buildings

The results of the damage analyses of the office building for the x and y directions are presented in Figure 8.19. In the figure, the averages of the damage indices from the seven earthquakes used in the analyses are plotted as a function of the performance level. It is observed from the figure that for the IO performance level a severe damage ($D_n$=0.68) to the original building is observed while the damage indices for the buildings retrofitted with the proposed and conventional methods are quite low and comparable. For the LS and CP performance levels in the y direction the building retrofitted with both methods have similar damage indices. However, in the x direction, the building retrofitted with the proposed method experiences significantly less damage than the one retrofitted with the conventional method. This indicates a greater reserve energy dissipation capacity, less damage, and smaller rehabilitation cost after a major seismic activity in the case of the building retrofitted with the proposed method. Thus, the damage analyses further reinforce the more desirable behavior of the building retrofitted with the proposed technique, as compared to that retrofitted with the conventional technique.

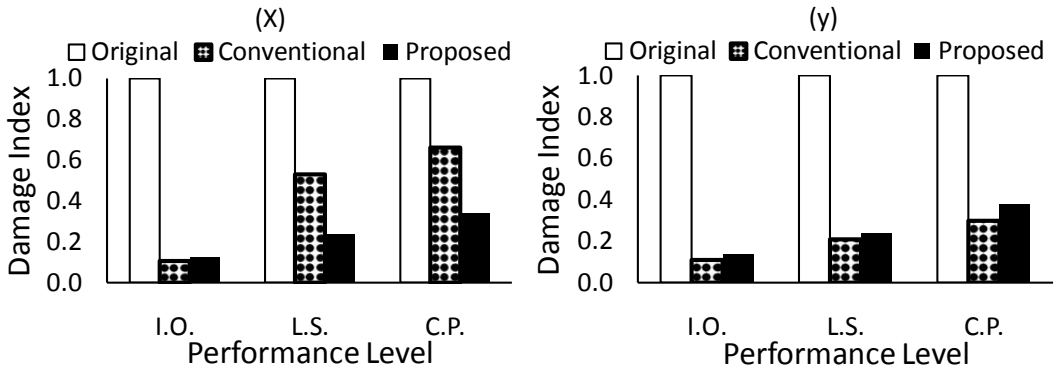


**Figure 8.19** Damage analyses results of the office building in the x and y directions

# CHAPTER 9

## SUMMARY AND CONSLUSIONS

This thesis presents a proposed seismic retrofitting system configured to improve the performance of seismically vulnerable reinforced concrete buildings by combining the advantages and eliminating most of the disadvantages of conventional and modern response modification retrofitting techniques. The proposed system is composed of a rigid steel frame with chevron braces and a conventional energy dissipating shear link connected between the braces and the frame. The retrofitting system is installed within the bays of a reinforced concrete building frame to enhance the stiffness, strength and ductility of the structure. The proposed system can be applied in various configurations where (i) the link and the braces are directly connected to the reinforced concrete members, (ii) the link is connected to a collector steel beam attached to the concrete beam and the rest of the members are connected to the reinforced concrete members via steel plates (iii) the link and the braces are encased in a steel frame system (steel panel) where the steel frame is connected to the reinforced concrete members via bolts and epoxy grouting. In order to select the configuration with the most benefits, comparative finite element analyses of a sample, two stories, one bay reinforced concrete frame retrofitted with various configurations of the proposed retrofitting system are conducted. A retrofitting design procedure using the proposed seismic retrofitting system is also developed as part of this study. The developed design methodology is based on performance-based design procedure. The retrofitting design procedure is configured to provide a uniform dissipation of earthquake input energy along the height of the reinforced concrete building. In addition to that, the performance of two existing reinforced concrete buildings retrofitted using the proposed methodology and a conventional technique involving reinforced concrete shear panels (squat infill shear walls) is also compared as part of this study. Followings are the conclusions deduced from this study.

From the 2-D and 3-D finite element analyses results of a sample reinforced concrete frame, the third configuration of the proposed seismic retrofitting method, where the link and the braces are encased in a steel frame system, was observed to increase the stiffness and strength of the frame while decreasing the stress concentrations within the reinforced concrete members of the frame and providing support to the reinforced concrete structure to prevent potential collapse due to gravitational effects after a potential damaging earthquake. Accordingly, the third configuration is selected for the retrofitting of the buildings used in this study.

The NLP and NLTH analyses results revealed that the proposed seismic retrofitting system can efficiently alleviate the detrimental effects of earthquakes on the buildings. The building retrofitted with the proposed seismic retrofitting system has a more stable lateral force-deformation behavior with enhanced energy dissipation capability than that of the one retrofitted with squat infill shear panels. For IO performance level (small intensity ground motions), the maximum inter-story drift of the building retrofitted with the proposed seismic retrofitting system is comparable to that of the one retrofitted with squat infill shear panels. But, for LS and CP performance levels (moderate to high intensity ground motions), the maximum inter-story drift of the building retrofitted with the proposed seismic retrofitting system is considerably smaller than that of the one retrofitted with squat infill shear panels. Furthermore, compared with the building retrofitted with squat infill shear panels, for LS and CP performance levels (medium to large intensity ground motions), the building retrofitted with the proposed method experiences significantly less damage due to the more ductile behavior of the system.

# REFERENCES


Abdullah and Takiguchi, K. (2003), "An Investigation into the Behavior and Strength of Reinforced Concrete Columns Strengthened with Ferrocement Jackets", Cement & Concrete Composites, 25, pp.233-242.

Aboutaha, R.S. (2001), "Ductility of CFRP Strengthened Concrete Flexural Members", Rehabilitating and Repairing the Buildings and Bridges of Americas: Hemispheric Workshop on Future Directions Proceedings of the Rehabilitating and Repairing the Buildings and Bridges of the Americas 2001 Conference.

Aboutaha, R.S., Engelhardt, M.D., Jirsa, J.O. and Kreger, M.E. (1999), "Rehabilitation of Shear Critical Concrete Columns by Use of Rectangular Steel Jackets", American Concrete Institute, ACI Structural Journal, Vol. 96, No.1, pp.68-78.

Ahmad,S., Ghani, F., Adil, R. (2009) "Seismic friction base isolation performance using demolished waste in masonry housing" Construction and Building Materials, Volume 23, Issue 1, January 2009, Pages 146-152

Alcocer and Sergio, M. (1993), "RC Frame Connections Rehabilitated by Jacketing**",** Journal of Structural Engineering New York, N.Y. 119 (5), pp. 1413-1431.

Amin, N. and Mokha, A.S. (1995), "Base Isolation Gets its Day in Court" Civil Engineering, 65 (2), pp. 44-47.

Andrews, B.M., Fahnestock, L.A., Song, J.( 2009) Ductility capacity models for buckling-restrained braces . *Journal of Constructional Steel Research* 65 (8-9), pp. 1712-1720

Anil, Ö. and Altin, S. (2007), "An Experimental Study on Reinforced Concrete Partially Infilled Frames", Elsevier Science, Engineering Structures Vol. 29, No, 3, pp.449-460.

ANSYS (2009). *Structural Simulation Software*, SAS IP Inc., Canonsburg, PA, USA.

Aoyama H, Kato D, Katsumata H, Hosokawa Y. (1984) "Strength and behavior of postcast shear walls for strengthening of existing R/C buildings", in: Proc of Eight World Conference on Earthquake Engineering, San Francisco CA, 1984, vol. 1, p. 485–92.

ATC-17 (1986), " Proceedings, Seminar on Workshop on Base İsolation and Passive Energy Dissipation", Applied Technology Council, San Francisco, California

Badoux, Marc, Jirsa and James, O. (1990), "Steel Bracing of RC Frames for Seismic Retrofitting"**,** Journal of Structural Engineering New York, N.Y. 116 (1), pp. 55-74.

Balazic, J., Guruswamy, G., Elliot, J., Rashmi, T.P. and Pall, A. (2000), "Seismic Rehabilitation of Justice Headquarters Building", Ottawa, Canada. www.palldynamics.com/pdf/5Seismic.pdf. Last access date: 20.07.2009

Bass, Robert, A., Carrasquillo, Ramon, L., Jirsa and James, O. (1989), "Shear Transfer Across New and Existing Concrete Interfaces", ACI Structural Journal 86 (4), pp. 383-393.

Besing, C. (2004), "The Retrofitting of Existing Buildings for Seismic Criteria." Massachusetts Institute of Technology.

Bett, John, B., Klingner, Richard, E., Jirsa and James, O. (1988), " Lateral Load Response of Strengthened and Repaıred Reınforced Concrete Columns**",** ACI Structural Journal 85 (5), pp. 499-508.

Binici, B. and Ozcebe, G. (2005), "Analysis of Infilled Reinforced Concrete Frames Strengthened with Frps", NATO Int. Workshop on Advances in Earthquake Engineering..- Keynote Address and Abstracts of Papers, p.15-18.

Bracci, J.M., Hueste, M.B.D. and Roesset, J.M. (2001), "Requirements for Performance-Based Design of Buildings", Advances in Earthquake Engineering 9, pp. 293-302.

Bruneau, M., Uang, C.M. and Whittaker, A. (1998) "Ductile Design of Steel Structures" (McGraw-Hill, New York, 1998).

BS 8110 (1985), "Structural use of concrete" British Standards Institution , London, p.3/49.

Chagnon, N. and Massicotte, B. (2005), "Seismic Retrofitting of Rectangular Bridge Piers with CFRP", ConMat'05 Third International Conference on Construction Material: Performance, Innovations and Structural Implications (Vancouver, B.C. August 22, 2005), pp. 1-10, August 01, 2005.

Chai, Y. H., Priestley, M. J. N., and Seible, F. (1990) "Seismic retrofit of circular bridge columns for enhanced flexural performance", ACI Struct. J. 88, 572–584.

Chang, S., Li, Y. and Loh, C. (2004), "Experimental Study of Seismic Behaviors of As-Built and Carbon Fiber Reinforced Plastics Repaired Reinforced Concrete Bridge Columns", Journal of Bridge Engineering, ASCE, Vol. 9, No. 4, 391-402.

Chen, W.F. and Lui, E.M. (2006), "Earthquake Engineering for Structural Design".

Chopra, A. (2001), “Dynamics of Structures; Theory and Applications to Earthquake Engineering” Second edition, Prentice Hall, Newyork.

Clarke, J. (1998), “Concrete Reinforced with Fibre Reinforced Plastic”, Materials World vol. 6 no. 2 pp. 78-80 February 1998. Institute of Materials, London, UK.

Clough, R.W. (1966) “Effect of stiffness degradation on earthquake ductility requirements”. Report No. 66-16, Dept. of Civil Engineering, University of California, Berkeley, CA, 1966.

Corley, W. G., Fiorato**,** A. E., Oesterle, R. G. and Scanlon,A. (1981) “Evaluation, repair and strengthening of reinforced concrete buildings” Procedings of the US/PRC workshop on Seismic Analyses and Design of Structures, p. 227-251, Ann Harbor, Michigan, May, 1981

Dicleli, M. and Mehta, A. (2009), “Seismic Retrofitting of Chevron-Braced Steel Frames Based on Preventing Buckling Instability of Braces” International Journal of Structural Stability and Dynamics 9 (2), pp. 333-356.

Dicleli, M., Constantinou, M. C., Buckle, I. G., Ghasemi, H. (2004) “Seismic Isolation Design of Highway Bridges”, TRB Seismic Committee AFF50, US Department of Transportation, Federal Highway Administration, Washington D.C.

Dipti, R.S. and Durgesh, C.R. (2009), “A Novel Technique of Seismic Strengthening of Nonductile RC Frame Using Steel Caging and Aluminum Shear Yielding Damper”, Earthquake Spectra Volume 25, Issue 2, pp. 415-437.

Eberhard, M.O. and Sozen, M.A. (1993), “A Behavior-Based Method to Determine Design Shear in Earthquake-Resistant Walls”, Journal of Structural Engineering, ASCE, February 1993, Vol. 119, No. 2, pp. 619-640.(Received 1994 ASCE Raymond C. Reese Research Prize).

Ehsani, M.R. and Saadatmanesh, H. (1997), “Fiber Composites: An Economical Alternative for Retrofitting Earthquake – Damaged Precast-Concrete Walls”, Earthquake Spectra 13 (1997) (2), pp. 225–241.

El-Dakhakhni, W.W., Elgaaly, M. and Hamid, A.A. (2003), “Three Strut Model for Concrete Masonry-Infilled Steel Frames”, ASCE Journal of Structural Engineering, Vol. 129, No. 2, 2003, pp.177–185.

Endo, T., Okifuji, A., Sugano, S., Ayashi, T., Shimizu, T., Takahara, K., Saito, H., and Yoneyama, Y. (1984) “Practices of seismic retrofit of existing concrete structures in Japan”, in *Proc. of 8th World Conference on Earthquake Engineering*, vol. 1, San Francisco (CA), pp. 469–476.

Fajfar, P. and Fischinger, M. (1984), Dynamıc Analysıs of Rc Buıldıngs - How Much Sophistication is Justified? ,

FEMA 306, (1998), “Evaluation Of Earthquake Damaged Concrete and Masonry Wall Buildings”, Basic Procedures Manual, Applied Technology Council (ATC), Washington D.C

FEMA-273 (1997), “NEHRP Guidelines for the Seismic Rehabilitation of Buildings”, Federal Emergency Management Agency Washington, D.C.

FEMA368 (2000), “NEHRP Recommended Provisions for Seismic Regulations for New Buildings and Other Structures”, Part1-Provisions, Federal Emergency Management Agency, Washington, DC.

Foo, S., Naumoski, N. and Cheung, M. (1996), “Research and Application of Seismic Retrofit Technologies in Canada”, RPS/AES/Technology Directorate Public Works & Government Services Canada 11 Laurier Street Hull, Quebec, Canada.

Frosch, R.J. (2005), “Seismic Rehabilitation Usıng Infill Wall Systems”, Advances in Earthquake Engineering for Urban Risk Reduction, NATO SfP977231, Seismic Assessment and Rehabilitation of Existing Buildings. International Closing Workshop, Istanbul-Turkey June 1, 2005.

Gaynor, P. J.,(1988) “The Effect of Openings on the Cyclic Behavior of Reinforced Concrete Infilled Shear Walls” Master of Science thesis, The University of Texas at Austin, May, 1988.

Ghobarah, A. (2001), “Performance-Based Design in Earthquake Engineering: State of Development”, Engineering Structures, 23(8), 878-884.

Greifenhagen, C., Lestuzzi, P. and Papas, D. (2005), Static-Cyclic Tests on Reinforced Concrete Shear Walls with Low Reinforcement Ratios. Rapport IMAC Nr. 4. Lausanne: Ecole Polytechnique Fédérale; 2005.

Hayashi T, Niwa H, Fukuhara M. (1980) “Strengthening methods of the existing reinforced concrete buildings”. In: Proceedings of the seventh world conference on earthquake engineering, vol. 4, Istanbul, 1980. p. 89–97.

Heninger, R.B., Larsen, R.C. and Simmons, R.R. (2003), “Seismic Retrofit Strategy, Design, and Construction of the San Francisco Oakland Bay Bridge West Crossing”, Proceedings Second MIT Conference on Compurational Fluid and Solid Mechanics June 17–20, 2003 Copyright © 2003 Elsevier Ltd. All Rights Reserved.

Hindi, R.A. and Sexsmıth, R.G. (2001), “A Proposed Damage Model for RC Bridge Columns under Cyclic Loading”, Earthquake Engineering Research Institute, Oakland, Ca, Etats-Unıs , vol. 17, no2, pp. 261-290.

Higashi, Y., Endo, T., Ohkubo, M. and Shimizu, Y. (1980) "Experimental Study on ... 7th WCEE, Istanbuhl, Turkey, September, 1980

Hognestad, E. (1951), “A Study of Combined Bending and Axial Loads in Reinforced Concrete Members”, University of Illinois Engineering Experimental Station, Bulletin Series No. 399, November.

Hsu, T.T.C. and Mo, Y.L. (1985), “Softening of Concrete in Torsional Members - Theory and Tests”, Journal of the American Concrete Institute, Proc., Vol. 82, No. 3, May-June, 1985, pp. 290-303.

IBC (2000), Structural/Seismic Design Manual - Volumes 1,2,&3 IBC , Structural Engineers Association Of California, Sacramento, CA

Ilki, A. and Kumbasar, N. (2000), “Hysteresis Model for Reinforced Concrete Members”, Proc. ASCE 14th Engineering Mechanics Conference, Austin, on CD, University of Texas, Austin, 2000.

Inel, M., Aschheim, M.A. and T.Tjhin (2003), “The Significance of Lateral Load Pattern in Pushover Analysis”.

Julio, E.S, Branco, F, Silva, V.D. (2003) “Structural rehabilitation of columns using reinforced concrete jacketing”. Prog Struct Engng Mater 2003;5:29–37.

Julio, E.S., Branco, F., Silva, V.D. (2004) “Concrete-to-Concrete Bond Strength. Influence of the Roughness of the Substrate Surface”, Elsevier, Construction and Building Materials 18 (9): 675-681 NOV 2004.

Kahn, L.F. (1976.) "Reinforced Concrete Infilled Shear Walls for Aseismic Strengthening", Ph.D. Thesis, , University of Michigan, Ann Arbor, Michigan

Kawamata, Shigeya, Ohnuma and Masaaki (1980), **“**Strengthenıng Effect of Eccentrıc Steel Braces to Exıstıng Reınforced Concrete Frames” .

Kelly, J.M. (1986), "Aseismic Base Isolation: Review and Bibliography", Soil Dynamics and Earthquake Engineering 5 (4), pp. 202-216.

Khatib, I.F., Mahin, S.A. and Pister, K.S. (1988) "Seismic behavior of concentrically braced steel frames". Earthquake Engineering Research Centre, Report No. UCB/EERC- 88/01 (1988).

Kim, T.-H., Lee, K.-M., Chung, Y.-S. and Shin, H.M.(2005), "Seismic Damage Assessment of Reinforced Concrete Bridge Columns", Engineering Structures 27 (2005) (4), pp. 57

Madan, A., Reinhorn, A.M., Mander, J.B. and Valles, R.E. (1997), "Modeling of Masonry Infill Panels for Structural Analysis", Journal of Structural Engineering 123 (10), pp. 1295-1302.

Maheri, M.R. and Sahebi, A. (1997), "Use of Steel Bracing in Reinforced Concrete Frames", Engineering Structures 19 (12), pp. 1018-1024.

Mansour, M. and Hsu, T.T.C. (2005), "Behavior of Reinforced Concrete Elements Under Cyclic Shear: Part I – Experiments", Journal of Structural Engineering, ASCE, Vol. 131, No. 1, pp. 44 – 53.

Mau, S.T. (1990) "Effect of tie spacing on inelastic buckling of reinforcing bars". ACI Structural Journal 1990;87(6):671-7.

Mau, S.T., El-Mabsout, M. (1989) "Inelastic buckling of reinforcing bars". ASCE Journal of Engineering Mechanics 1989; 115(1):1-17.

Meftah, S.A., Yeghnem, R., Tounsi, A. and Adda Bedia, E.A. (2007), "Seismic Behavior of RC Coupled Shear Walls Repaired with CFRP Laminates Having Variable Fibers Spacing", Construction and Building Materials 21 (8), pp. 1661-1671.

Mehrabı, A.B. and Shıng, P.B. (1997), “Finite Element Modelling of Masonry-Infilled RC Frames”, Journal of the Structural Division, Proceedings of ASCE, Vol. 123, No. 5, pp.604-613.

Meier, U. (1995), “Strengthening of Structures Using Carbon Fibre/Epoxy Composites”, Constr Build Mater 1995;9(6):341–51.

Mo, Y.L. and Kuo, C.J. (1998), “Structural Behavior of Reinforced Concrete Frame-Wall Components”, Materials and Structures, RILEM, Vol.31, November, pp.609-615.

Moon, B.Y., Kang, G.J., Kang, B.S. and Kelly, J.M. (2002), “Design and Manufacturing of Fiber Reinforced Elastomeric Isolator for Seismic Isolation”, Journal of Materials Processing Technology Volumes 130-131, Pages 145-150.

Mosalam, K.M. (1996), “Modeling of the Nonlinear Seismic Behavior of Gravity Load Designed Frames”, Earthquake Spectra 12 (3), pp. 479-492.

Naderzadeh, A. and Moinfar, A.A. (2004), “Earthquake Resistance Diagnosis and Strengthening Techniques for Existing Buildings in Tehran”, Proceedings, 13th World Conference in Earthquake Engineering (13WCEE), Aug. 2004, Ontario, Canada.

Ogata, K., and T. Kabeyasawa, (1984)"Experimental Study on the Hysteretic Behavior of. Reinforced Concrete Shear Walls Under the Loading of Different Moment-to-Shear Ratios” Transections of the Japan Concrete Institute, Volume 6, p. 717-727

Pall, A., Pall, R. (2004) "Performance Based Design Using Pall Friction Dampers - An Economical Design Solution", Proceedings, Thirteenth World Conference on Earthquake Engineering, Vancouver, 2004. Paper #1955

Paterson, J. and Mitchell, D. (2003), “Seismic Retrofit of Shear Walls with Headed Bars and Carbon Fiber Wrap”, Journal of Structural Engineering, ASCE, May 2003, pp. 606-614.

Paulay, T. and Priestley, M.J.N. (1992), Seismic Design of Reinforced Concrete and Masonry Buildings, New York: J. Wiley, 1992.

Paz M, (1994) editor. “International handbook of earthquake engineering. Codes, programs, and examples”. New York: Chapman and Hall

Phan and Douglas, D.H. (1993), “Applying Constraint Satisfaction Neural Networks to Multiple Views' Data Partitioning in Building Engineering”, Computing in Civil and Building Engineering, pp. 965-968.

Pincheira J. A. and Jirsa J. O. (1995), “ Seismic Response of RC Frames Retrofitted with Steel Braces or Walls”, Journal of Structural Engineering, Vol. 121, No. 8, pp 1225-1335.

Pollino, M. and Bruneau, M. (2007), “Seismic Retrofit of Bridge Steel Truss Piers Using a Controlled Rocking Approach.” ASCE Journal of Bridge Engineering, Vol.12, No.5, pp.600-610.

Priestley, M.J.N. and Benzoni, G. (1996), “Seismic Performance of Circular Columns with Low Longitudinal Reinforcement Ratios”, ACI Structural Journal 93 (4), pp. 474-485.

Rocha, P., Delgado, P., Costa, A. and Delgado, R. (2004), “Seismic Retrofit of RC Frames. Comput Struct”, 82(17–19): 1523–1534.

Rodriguez, M. and Park, R. (1994), “Seismic Load Tests on Reinforced Concrete Columns Strengthened by Jacketing”, Structural Journal 91 (2), pp. 150-159.

Saatcıoglu, M. and Ozcebe,G. (1989), “Response of Reinforced Concrete Columns to Simulated Seismic Loading”, Acı Structural Journal, Vol.86, No.1, Jan.- Feb.,1989, pp.3 - 12.

Saatcioglu, M. and. Humar, J.M (2003) ”Dynamic analysis of buildings for earthquake-resistant design,” Journal of Civil Engineering Canada 30 (2003), pp. 338–359

Saatcioglu, M. and Razvi, S. (1992), “Strength and Ductility of Confinde Concrete.” Journal of Struct. Div., ASCE, Vol. 118(6), pp.1590-1607.

Sakino, K. and Ishibashi, H. (1985), “Experimental Studies on Concrete Filled Square Steel Tubular Short Columns Subjected to Cyclic Shearing Force and Constant Axial Force”, Transactions of the Architectural Institute of Japan 353, pp. 81–89.

Saneinejad, A. and Hobbs, B. (1995), “Inelastic Design of Infilled Frames”, Journal of Structural Engineering. ASCE, 121 (4): 634-650.

SAP2000 (2006). Integrated Finite Element Analysis and Design of Structures, Computers and Structures Inc., Berkeley, CA, USA.

Shah, S. 1988. "Evaluation of Infill Wall Strengthening Schemes for Non-Ductile Reinforced Concrete Buildings, " Master of Science thesis, The University of Texas at Austin, May, 1989.

Sokolov, V. Y. (2000) ‘‘Site & region-specific response spectra: a probabilistic approach,’’ Soil Dynamic and Earthquake Engineering 20 (5), 273–281.

Soong, T.T. and Dargush, G.F. (1997), “Passive Energy Dissipation Systems in Structural Engineering”, John Wiley & Sons, New York.

Stafford-Smith, B. and Carter, C. (1969), "A Method for the Analysis of Infilled Frames", Proceedings of the Institution of Civil Engineers, London, England, 44, 31-38.

Sugano, Shunsuke, Fujimura and Masaru, (1980), "Aseismic Strengthening of Exıstıng Reınforced Concrete Buıldıngs".

Takeda, T., Sözen, M.A., Nielsen, N.N., (1970). "Reinforced Concrete Response to Simulated Earthquakes", Journal of the Structural Division-ASCE, 96, ST12, 2557-2573.

Tankut, T. (2008), **"**Türkiye'deki Bina Yapıları İçin Güçlendirme Stratejisi", İMO-www.e-kutuphane.imo.org.tr/pdf/11056.pdf Last access date: 20.07.2009

Taylor, D.P. (2002), "History, Design, and Applications of Fluid Dampers in Structural Engineering" www.taylordevices.com/papers/history/design.htm (20.07.2009)

Tezcan, S.S. and Cimilli, S. (2002), "Seismic Base Isolation." Yüksek Öğrenim ve Araştırma Vakfı Yayınları, İstanbul, June.

Tezcan, S.S. and Erkal, A. (2002), "Seismic Base Isolation and Energy Absorbing Devices", Yüksek Öğrenim ve Araştırma Vakfı Yayınları, İstanbul, June.

Thermou, G., E. and Elnashai, A., S. (2005), "Seismic Retrofit Schemes for RC Structures and Local-Global Consequences", *Journal of Progress in Structural Engineering and Materials,* Vol. 8, Issue 1, pp. 1-15, 2006.

Tremblay, R. and Filiatrault, A. (1996), "Seismic Impact Loading in Inelastic Tension-Only Concentrically Braced Steel Frames: Myth or Reality?", Earthquake Engineering and Structural Dynamics 25 (12), pp. 1373-1389.

Vecchio, F.J. and Collins, M.P. (1993), “Compression Response of Cracked Reinforced Concrete”, ASCE Journal of Structural Engineer, Dicembre, pp. 3590-3610.

Victoria R., Wigle, L. Fahnestock , A. (2009), “Buckling-restrained braced frame connection performance” Journal of Constructional Steel Research, In Press, Corrected Proof, Available online 18 August 2009

Yalcin, C. and Saatcioglu, M., (2000) "Inelastic Analysis of Reinforced Concrete Columns," *Computers and Structures* , Pergamon Press, Vol. 77 (2000), pp. 539-555.

## APPENDIX

**Table A1** Dimensions of reinforced column and beams of the school building

| Column-Name | Dimension(x)(cm) | Dimension(y)(cm) |
|---|---|---|
| C-1-A1 | 30 | 50 |
| C-1-A2 | 30 | 50 |
| C-1-A3 | 30 | 50 |
| C-1-A4 | 30 | 50 |
| C-1-A5 | 30 | 60 |
| C-1-A6 | 30 | 50 |
| C-1-A7 | 30 | 50 |
| C-1-A8 | 30 | 50 |
| C-1-A9 | 30 | 50 |
| C-1-B2 | 30 | 50 |
| C-1-B3 | 30 | 50 |
| C-1-B4 | 30 | 50 |
| C-1-B6 | 30 | 50 |
| C-1-B7 | 30 | 50 |
| C-1-B8 | 30 | 50 |
| C-1-C1 | 50 | 40 |
| C-1-C2 | 50 | 40 |
| C-1-C4 | 50 | 40 |
| C-1-C5 | 55 | 50 |
| C-1-C6 | 50 | 40 |
| C-1-C8 | 50 | 40 |
| C-1-C9 | 50 | 40 |
| C-1-D2 | 30 | 50 |
| C-1-D3 | 30 | 50 |
| C-1-D4 | 30 | 50 |
| C-1-D6 | 30 | 50 |
| C-1-D7 | 30 | 50 |
| C-1-D8 | 30 | 50 |
| C-1-E1 | 30 | 50 |
| C-1-E2 | 30 | 50 |
| C-1-E3 | 30 | 50 |
| C-1-E4 | 30 | 50 |
| C-1-E5 | 30 | 60 |
| C-1-E6 | 30 | 50 |
| C-1-E7 | 30 | 50 |

**Table A1** (cont'd)

| | | |
|---|---|---|
| C-1-E8 | 30 | 50 |
| C-1-E9 | 30 | 50 |
| C-2-A1 | 30 | 50 |
| C-2-A2 | 30 | 50 |
| C-2-A3 | 30 | 50 |
| C-2-A4 | 30 | 50 |
| C-2-A5 | 30 | 60 |
| C-2-A6 | 30 | 50 |
| C-2-A7 | 30 | 50 |
| C-2-A8 | 30 | 50 |
| C-2-A9 | 30 | 50 |
| C-2-B2 | 30 | 50 |
| C-2-B3 | 30 | 50 |
| C-2-B4 | 30 | 50 |
| C-2-B6 | 30 | 50 |
| C-2-B7 | 30 | 50 |
| C-2-B8 | 30 | 50 |
| C-2-C1 | 50 | 40 |
| C-2-C2 | 50 | 40 |
| C-2-C4 | 50 | 40 |
| C-2-C5 | 50 | 40 |
| C-2-C6 | 50 | 40 |
| C-2-C8 | 50 | 40 |
| C-2-C9 | 50 | 40 |
| C-2-D2 | 30 | 50 |
| C-2-D4 | 30 | 50 |
| C-2-D6 | 30 | 50 |
| C-2-D8 | 30 | 50 |
| C-2-E1 | 30 | 50 |
| C-2-E2 | 30 | 50 |
| C-2-E3 | 30 | 50 |
| C-2-E4 | 30 | 50 |
| C-2-E5 | 30 | 60 |
| C-2-E6 | 30 | 50 |
| C-2-E7 | 30 | 50 |
| C-2-E8 | 30 | 50 |
| C-2-E9 | 30 | 50 |
| **Beam-Name** | **Width(cm)** | **Height(cm)** |
| B-1-A(1-2) | 30 | 70 |
| B-1-A(2-3) | 30 | 70 |

**Table A1** (cont'd)

| | | |
|---|---|---|
| B-1-A(3-4) | 30 | 60 |
| B-1-A(4-5) | 30 | 70 |
| B-1-A(5-6) | 30 | 70 |
| B-1-A(6-7) | 30 | 60 |
| B-1-A(7-8) | 30 | 70 |
| B-1-A(8-9) | 30 | 70 |
| B-1-B(2-3) | 30 | 50 |
| B-1-B(3-4) | 30 | 50 |
| B-1-B(6-7) | 30 | 50 |
| B-1-B(7-8) | 30 | 50 |
| B-1-C(1-2) | 40 | 70 |
| B-1-C(4-5) | 40 | 70 |
| B-1-C(5-6) | 40 | 70 |
| B-1-C(8-9) | 40 | 70 |
| B-1-D(2-3) | 30 | 70 |
| B-1-D(3-4) | 30 | 70 |
| B-1-D(6-7) | 30 | 70 |
| B-1-D(7-8) | 30 | 70 |
| B-1-E(1-2) | 30 | 70 |
| B-1-E(2-3) | 30 | 70 |
| B-1-E(3-4) | 30 | 70 |
| B-1-E(4-5) | 30 | 70 |
| B-1-E(5-6) | 30 | 70 |
| B-1-E(6-7) | 30 | 70 |
| B-1-E(7-8) | 30 | 70 |
| B-1-E(8-9) | 30 | 70 |
| B-1-1(A-C) | 30 | 70 |
| B-1-1(C-E) | 30 | 70 |
| B-1-2(A-B) | 30 | 50 |
| B-1-2(B-C) | 30 | 50 |
| B-1-2(C-D) | 30 | 50 |
| B-1-2(D-E) | 30 | 50 |
| B-1-3(A-B) | 30 | 50 |
| B-1-3(D-E) | 30 | 70 |
| B-1-4(A-B) | 30 | 50 |
| B-1-4(B-C) | 30 | 50 |
| B-1-4(C-D) | 30 | 50 |
| B-1-4(D-E) | 30 | 70 |
| B-1-5(A-C) | 40 | 70 |
| B-1-5(C-E) | 40 | 70 |

**Table A1** (cont'd)

| | | |
|---|---|---|
| B-1-6(A-B) | 30 | 50 |
| B-1-6(B-C) | 30 | 50 |
| B-1-6(C-D) | 30 | 50 |
| B-1-6(D-E) | 30 | 70 |
| B-1-7(A-B) | 30 | 50 |
| B-1-7(D-E) | 30 | 70 |
| B-1-8(A-B) | 30 | 50 |
| B-1-8(B-C) | 30 | 50 |
| B-1-8(C-D) | 30 | 50 |
| B-1-8(D-E) | 30 | 50 |
| B-1-9(A-C) | 30 | 70 |
| B-1-9(C-E) | 30 | 70 |
| B-2-A(1-2) | 30 | 70 |
| B-2-A(2-3) | 30 | 70 |
| B-2-A(3-4) | 30 | 70 |
| B-2-A(4-5) | 30 | 70 |
| B-2-A(5-6) | 30 | 70 |
| B-2-A(6-7) | 30 | 70 |
| B-2-A(7-8) | 30 | 70 |
| B-2-A(8-9) | 30 | 70 |
| B-2-B(2-3) | 40 | 70 |
| B-2-B(3-4) | 40 | 70 |
| B-2-B(6-7) | 40 | 70 |
| B-2-B(7-8) | 40 | 70 |
| B-2-C(1-2) | 40 | 70 |
| B-2-C(4-5) | 40 | 70 |
| B-2-C(5-6) | 40 | 70 |
| B-2-C(8-9) | 40 | 70 |
| B-2-D(2-4) | 40 | 70 |
| B-2-D(6-8) | 40 | 70 |
| B-2-E(1-2) | 30 | 70 |
| B-2-E(2-3) | 30 | 70 |
| B-2-E(3-4) | 30 | 70 |
| B-2-E(4-5) | 30 | 70 |
| B-2-E(5-6) | 30 | 70 |
| B-2-E(6-7) | 30 | 70 |
| B-2-E(7-8) | 30 | 70 |
| B-2-E(8-9) | 30 | 70 |
| B-2-1(A-C) | 30 | 70 |
| B-2-1(C-E) | 30 | 70 |

**Table A1** (cont'd)

| | | |
|---|---|---|
| B-2-2(A-B) | 30 | 50 |
| B-2-2(B-C) | 30 | 50 |
| B-2-2(C-D) | 30 | 50 |
| B-2-2(D-E) | 30 | 50 |
| B-2-4(A-B) | 30 | 50 |
| B-2-4(B-C) | 30 | 50 |
| B-2-4(C-D) | 30 | 50 |
| B-2-4(D-E) | 30 | 50 |
| B-2-5(A-C) | 30 | 70 |
| B-2-5(C-E) | 30 | 70 |
| B-2-6(A-B) | 30 | 50 |
| B-2-6(B-C) | 30 | 50 |
| B-2-6(C-D) | 30 | 50 |
| B-2-6(D-E) | 30 | 50 |
| B-2-8(A-B) | 30 | 50 |
| B-2-8(B-C) | 30 | 50 |
| B-2-8(C-D) | 30 | 50 |
| B-2-8(D-E) | 30 | 50 |
| B-2-9(A-C) | 30 | 70 |
| B-2-9(C-E) | 30 | 70 |

**Table A2** Dimensions of reinforced column and beams of the office building

| Column Name | Dimension(x)(cm) | Dimension(y)(cm) |
|---|---|---|
| C-1-A1 | 30 | 60 |
| C-1-A3 | 40 | 25 |
| C-1-A5 | 40 | 40 |
| C-1-A6 | 40 | 40 |
| C-1-B1 | 65 | 35 |
| C-1-B3 | 40 | 40 |
| C-1-B5 | 40 | 45 |
| C-1-B6 | 45 | 60 |
| C-1-C1 | 35 | 65 |
| C-1-C5 | 55 | 45 |
| C-1-C6 | 25 | 50 |
| C-1-D1 | 35 | 65 |
| C-1-D3 | 60 | 60 |
| C-1-D5 | 25 | 60 |
| C-1-D6 | 25 | 65 |
| C-1-E1 | 35 | 90 |
| C-1-E2 | 60 | 60 |
| C-1-E4 | 60 | 60 |
| C-1-E5 | 60 | 65 |
| C-1-E6 | 45 | 60 |
| C-2-A1 | 30 | 60 |
| C-2-A3 | 40 | 25 |
| C-2-A5 | 40 | 40 |
| C-2-A6 | 40 | 40 |
| C-2-B1 | 65 | 35 |
| C-2-B3 | 40 | 40 |
| C-2-B5 | 40 | 45 |
| C-2-B6 | 45 | 60 |
| C-2-C1 | 35 | 65 |
| C-2-C5 | 55 | 45 |
| C-2-C6 | 25 | 50 |
| C-2-D1 | 35 | 65 |
| C-2-D3 | 40 | 40 |
| C-2-D5 | 25 | 60 |
| C-2-D6 | 25 | 65 |

**Table A2** (cont'd)

| | | |
|---|---|---|
| C-2-E1 | 35 | 90 |
| C-2-E2 | 40 | 60 |
| C-2-E4 | 40 | 60 |
| C-2-E5 | 40 | 65 |
| C-2-E6 | 45 | 45 |
| C-3-A1 | 25 | 40 |
| C-3-A3 | 40 | 25 |
| C-3-A5 | 35 | 35 |
| C-3-A6 | 35 | 35 |
| C-3-B1 | 65 | 25 |
| C-3-B3 | 40 | 40 |
| C-3-B5 | 35 | 35 |
| C-3-B6 | 25 | 30 |
| C-3-C1 | 30 | 30 |
| C-3-C5 | 25 | 40 |
| C-3-C6 | 25 | 30 |
| C-3-D1 | 25 | 65 |
| C-3-D3 | 35 | 35 |
| C-3-D5 | 25 | 55 |
| C-3-D6 | 30 | 60 |
| C-3-E1 | 30 | 60 |
| C-3-E2 | 30 | 60 |
| C-3-E4 | 30 | 35 |
| C-3-E5 | 30 | 65 |
| C-3-E6 | 25 | 30 |
| C-4-A1 | 25 | 30 |
| C-4-A3 | 30 | 25 |
| C-4-A5 | 25 | 30 |
| C-4-A6 | 30 | 25 |
| C-4-B1 | 25 | 25 |
| C-4-B3 | 35 | 35 |
| C-4-B5 | 25 | 35 |
| C-4-B6 | 25 | 30 |
| C-4-C1 | 25 | 25 |
| C-4-C5 | 25 | 25 |
| C-4-C6 | 25 | 30 |
| C-4-D1 | 25 | 30 |
| C-4-D3 | 35 | 35 |
| C-4-D5 | 25 | 40 |

**Table A2** (cont'd)

| | | |
|---|---|---|
| C-4-D6 | 25 | 40 |
| C-4-E1 | 25 | 30 |
| C-4-E2 | 25 | 45 |
| C-4-E4 | 25 | 25 |
| C-4-E5 | 25 | 50 |
| C-4-E6 | 25 | 30 |
| C-5-A1 | 20 | 30 |
| C-5-A3 | 30 | 25 |
| C-5-A5 | 25 | 30 |
| C-5-A6 | 25 | 30 |
| C-5-B1 | 20 | 25 |
| C-5-B3 | 35 | 35 |
| C-5-B5 | 25 | 35 |
| C-5-B6 | 25 | 30 |
| C-5-C1 | 20 | 25 |
| C-5-C5 | 25 | 25 |
| C-5-C6 | 25 | 30 |
| C-5-D1 | 20 | 30 |
| C-5-D3 | 35 | 35 |
| C-5-D5 | 25 | 30 |
| C-5-D6 | 25 | 30 |
| C-5-E1 | 20 | 30 |
| C-5-E2 | 25 | 35 |
| C-5-E4 | 25 | 20 |
| C-5-E5 | 25 | 30 |
| C-5-E6 | 25 | 30 |
| C-6-A1 | 15 | 30 |
| C-6-A3 | 20 | 20 |
| C-6-A5 | 20 | 20 |
| C-6-A6 | 20 | 20 |
| C-6-B1 | 20 | 20 |
| C-6-B3 | 30 | 30 |
| C-6-B5 | 20 | 20 |
| C-6-B6 | 20 | 20 |
| C-6-C1 | 20 | 20 |
| C-6-C5 | 20 | 20 |
| C-6-C6 | 20 | 20 |
| C-6-D1 | 20 | 20 |
| C-6-D3 | 30 | 30 |

**Table A2** (cont'd)

| | | |
|---|---|---|
| C-6-D5 | 20 | 20 |
| C-6-D6 | 20 | 20 |
| C-6-E1 | 15 | 30 |
| C-6-E2 | 20 | 25 |
| C-6-E4 | 20 | 20 |
| C-6-E5 | 20 | 20 |
| C-6-E6 | 20 | 20 |
| **Beam Name** | **Width(cm)** | **Height(cm)** |
| B-1-B(1-3) | 10 | 60 |
| B-1-B(3-5) | 10 | 60 |
| B-1-C(1-3) | 10 | 55 |
| B-1-D(1-3) | 10 | 65 |
| B-1-D(3-5) | 10 | 65 |
| B-1-D(5-6) | 10 | 65 |
| B-2-A(1-3) | 10 | 50 |
| B-2-A(3-5) | 10 | 50 |
| B-2-A(5-6) | 10 | 50 |
| B-2-B(1-3) | 10 | 60 |
| B-2-B(3-5) | 10 | 60 |
| B-2-C(1-3) | 10 | 55 |
| B-2-D(1-3) | 10 | 65 |
| B-2-D(3-5) | 10 | 65 |
| B-2-D(5-6) | 10 | 65 |
| B-2-E(1-2) | 10 | 50 |
| B-2-E(5-6) | 10 | 50 |
| B-3-A(1-3) | 10 | 50 |
| B-3-A(3-5) | 10 | 50 |
| B-3-A(5-6) | 10 | 50 |
| B-3-B(1-3) | 10 | 60 |
| B-3-B(3-5) | 10 | 60 |
| B-3-C(1-3) | 10 | 55 |
| B-3-D(1-3) | 10 | 65 |
| B-3-D(3-5) | 10 | 65 |
| B-3-D(5-6) | 10 | 65 |
| B-3-E(1-2) | 10 | 50 |
| B-3-E(5-6) | 10 | 50 |
| B-4-A(1-3) | 10 | 50 |
| B-4-A(3-5) | 10 | 50 |
| B-4-A(5-6) | 10 | 50 |

**Table A2** (cont'd)

| | | |
|---|---|---|
| B-4-B(1-3) | 10 | 60 |
| B-4-B(3-5) | 10 | 60 |
| B-4-C(1-3) | 10 | 55 |
| B-4-D(1-3) | 10 | 65 |
| B-4-D(3-5) | 10 | 65 |
| B-4-D(5-6) | 10 | 65 |
| B-4-E(1-2) | 10 | 50 |
| B-4-E(5-6) | 10 | 50 |
| B-5-A(1-3) | 10 | 50 |
| B-5-A(3-5) | 10 | 50 |
| B-5-A(5-6) | 10 | 50 |
| B-5-B(1-3) | 10 | 60 |
| B-5-B(3-5) | 10 | 60 |
| B-5-C(1-3) | 10 | 55 |
| B-5-D(1-3) | 10 | 65 |
| B-5-D(3-5) | 10 | 65 |
| B-5-D(5-6) | 10 | 65 |
| B-5-E(1-2) | 10 | 50 |
| B-5-E(5-6) | 10 | 50 |
| B-6-A(1-3) | 10 | 50 |
| B-6-A(3-5) | 10 | 50 |
| B-6-A(5-6) | 10 | 50 |
| B-6-B(1-3) | 10 | 60 |
| B-6-B(3-5) | 10 | 60 |
| B-6-C(1-3) | 10 | 55 |
| B-6-D(1-3) | 10 | 65 |
| B-6-D(3-5) | 10 | 65 |
| B-6-D(5-6) | 10 | 65 |
| B-6-E(1-2) | 10 | 50 |
| B-6-E(5-6) | 10 | 50 |
| B-1-3(B-D) | 20 | 55 |
| B-1-4(D-E) | 10 | 55 |
| B-1-5(A-B) | 10 | 40 |
| B-1-5(B-C) | 10 | 40 |
| B-1-5(C-D) | 10 | 40 |
| B-1-5(D-E) | 10 | 40 |
| B-1-6(A-B) | 10 | 50 |
| B-1-6(B-C) | 10 | 50 |
| B-1-6(C-D) | 10 | 50 |

**Table A2** (cont'd)

| | | |
|---|---|---|
| B-1-6(D-E) | 10 | 50 |
| B-2-1(A-B) | 10 | 50 |
| B-2-1(D-E) | 10 | 50 |
| B-2-3(B-D) | 20 | 55 |
| B-2-4(D-E) | 10 | 55 |
| B-2-5(A-B) | 10 | 40 |
| B-2-5(B-C) | 10 | 40 |
| B-2-5(C-D) | 10 | 40 |
| B-2-5(D-E) | 10 | 40 |
| B-2-6(A-B) | 10 | 50 |
| B-2-6(B-C) | 10 | 50 |
| B-2-6(C-D) | 10 | 50 |
| B-2-6(D-E) | 10 | 50 |
| B-3-1(A-B) | 10 | 50 |
| B-3-1(D-E) | 10 | 50 |
| B-3-3(B-D) | 20 | 55 |
| B-3-4(D-E) | 10 | 55 |
| B-3-5(A-B) | 10 | 40 |
| B-3-5(B-C) | 10 | 40 |
| B-3-5(C-D) | 10 | 40 |
| B-3-5(D-E) | 10 | 40 |
| B-3-6(A-B) | 10 | 50 |
| B-3-6(B-C) | 10 | 50 |
| B-3-6(C-D) | 10 | 50 |
| B-3-6(D-E) | 10 | 50 |
| B-4-1(A-B) | 10 | 50 |
| B-4-1(D-E) | 10 | 50 |
| B-4-3(B-D) | 20 | 55 |
| B-4-4(D-E) | 10 | 55 |
| B-4-5(A-B) | 10 | 40 |
| B-4-5(B-C) | 10 | 40 |
| B-4-5(C-D) | 10 | 40 |
| B-4-5(D-E) | 10 | 40 |
| B-4-6(A-B) | 10 | 50 |
| B-4-6(B-C) | 10 | 50 |
| B-4-6(C-D) | 10 | 50 |
| B-4-6(D-E) | 10 | 50 |
| B-5-1(A-B) | 10 | 50 |
| B-5-1(D-E) | 10 | 50 |

**Table A2** (cont'd)

| | | |
|---|---|---|
| B-5-3(B-D) | 20 | 55 |
| B-5-4(D-E) | 10 | 55 |
| B-5-5(A-B) | 10 | 40 |
| B-5-5(B-C) | 10 | 40 |
| B-5-5(C-D) | 10 | 40 |
| B-5-5(D-E) | 10 | 40 |
| B-5-6(A-B) | 10 | 50 |
| B-5-6(B-C) | 10 | 50 |
| B-5-6(C-D) | 10 | 50 |
| B-5-6(D-E) | 10 | 50 |
| B-6-1(A-B) | 10 | 50 |
| B-6-1(D-E) | 10 | 50 |
| B-6-3(B-D) | 20 | 55 |
| B-6-4(D-E) | 10 | 55 |
| B-6-5(A-B) | 10 | 40 |
| B-6-5(B-C) | 10 | 40 |
| B-6-5(C-D) | 10 | 40 |
| B-6-5(D-E) | 10 | 40 |
| B-6-6(A-B) | 10 | 50 |
| B-6-6(B-C) | 10 | 50 |
| B-6-6(C-D) | 10 | 50 |
| B-6-6(D-E) | 10 | 50 |